Transport and degradation of contaminants in the vadose zone

Dieuwke Schotanus

Transport and degradation of contaminants in the vadose zone

Dieuwke Schotanus

Foar heit
en ek foar mem fansels

Dichtbij de dovenetel, die niet steekt of geurt,
- op de blaadjes fijne haren als op een mensenoor -
daar ging ik liggen en ik rook mijn eigen haren
en sterker gras en sterker nog de grond,
en merkte met gesloten ogen in de zon, dat ik bestond.

Fragment uit: Waterkant. Vroeger
M. Vasalis

Voorwoord

Thanks, tusen takk, bedankt, dankewol!

Het is af! Zonder de hulp van een aantal mensen zou dit boekje er heel anders uit hebben gezien. Daarom wil ik deze mensen hier graag bedanken:

Allereerst wil ik mijn promotor en begeleider Sjoerd van der Zee bedanken. Je liet mij mijn eigenwijze gang gaan, wat ik als een voorrecht beschouw. Bovendien had jij op bepaalde momenten meer vertrouwen in mij dan ikzelf. Bedankt daarvoor. Tineke van der Ploeg, van collega-aio, via projectgenoot naar co-promotor. Zonder jou was ik nu waarschijnlijk nog aan het worstelen met veel te ingewikkelde zinsconstructies. Ook wil ik je bedanken voor je aandacht voor de persoon achter de artikelen. Hans Meeussen, bedankt voor je snelle reacties op al mijn vragen over ORCHESTRA. Ik vond het hartstikke leuk om met jou te kunnen praten over het kleinste detail van het model, en over de praktische kant van onderzoek. Toon Leijnse was altijd betrokken vanaf de zijlijn. Bedankt. Ik wil Ed Veling bedanken voor zijn enthousiaste hulp bij de semi-analytische oplossing. Dit was precies de zijweg die ik nodig had om weer de goede richting te vinden.

Fortunately, I was not the only one who had to spend some time in the field, a big thank you to the entire Moreppen crew! Thanks to you I have some pleasant memories about holy mice, adventures with snakes, unidentifiable food, shovelling tons of snow and much more. Especially I want to mention Helen French and Esther Bloem. Thank you for facilitating that I could work at Moreppen. Furthermore, I want to thank Kyle Elkin, Gro Eggen and Oddvar Vigdal for assistance in the lab and field, and for the nice time. Heidi Lissner, it was a pleasure to share the field site, the "hostel" and our thoughts on the excitement and dullness of the life of a PhD. Pieter Hazenberg, bedankt voor het opknappen van de mcs, en dat ik altijd kon bellen als er weer eens een pomp overuren draaide. Harm Gooren, dank voor de hulp met de tensiometers.

Abstract

Leaching of contaminants from the vadose zone to the groundwater depends on the soil properties and the infiltration rate. In this thesis, organic degradable contaminants were studied, such as de-icing chemicals (consisting of propylene glycol, PG) and pesticides. Heterogeneous soil properties lead to spatial variability in leaching, which is particularly important for degradable contaminants. The infiltration rate determines the travel time in the vadose zone, and thus the time available for degradation.

Two field experiments were performed with a multi-compartment sampler (consisting of 10×10 cells of $3.15 \times 3.15 \, \text{cm}^2$ each) to examine the dependence of spatial variability in contaminant leaching on the infiltration rate. The first experiment was carried out during the snowmelt period, characterized by high infiltration rates from snowmelt. The second experiment was carried out with irrigation to mimic homogeneous rainfall. The preferential flow paths were similar for both experiments. With a high infiltration rate during the snowmelt experiment, the leaching was distributed more homogeneous than during the irrigation experiment. Therefore, it is concluded that the soil heterogeneity is mainly caused by spatial differences in the soil hydraulic properties, and not by macropores. The leached masses of the degradable PG and a nondegradable tracer were highly correlated. At the scale of the experiment, heterogeneous infiltration resulting from spatial differences in snowmelt did not have much influence on the flow and solute paths.

The results from the field experiment were used to parameterize a random field for the scaling factor of the retention curve. As a criterion to compare the results from simulations and observations, the sorted and cumulative total drainage in a cell was used. The effect of the ratio of the infiltration rate over the degradation rate on leaching of degradable solutes was investigated. Furthermore, the spatial distribution of the leaching of degradable and non-degradable solutes was compared. The infiltration rate influences contaminant leaching in two ways. Firstly, the travel time of the contaminant in the vadose zone depends on the infiltration rate. Secondly, the fraction of the soil which is

active in transport is influenced by the infiltration rate. As a result, the spatial distribution of contaminant leaching, and therefore the leached fraction, depends on the infiltration rate.

The leached fraction of a degradable contaminant is often estimated from average soil properties and stationary weather series. For contaminants that degrade in both the adsorbed and aqueous phase, it is known how these averaged properties should be derived from heterogeneous properties. However, for contaminants that only degrade in the aqueous phase, this is not well known. In soils that are layered with respect to the adsorption constant, the propagation of the contaminant plume, and thus the travel time in the vadose zone, depends on the adsorption constant, degradation rate, and dispersivity. Regarding variable weather series, seasonal fluctuations in precipitation lead to large differences in travel times in a dry climate, and thus large differences in the leached fraction, especially for contaminants with little adsorption. In a wet climate, the effect of such seasonal fluctuations is diminished.

In the vadose zone, PG can be degraded by micro-organisms, for which electron-acceptors are needed. A field experiment showed that aerobic as well as anaerobic degradation occurs in the vadose zone. For anaerobic degradation, manganese-oxides (which are present in the soil) or nitrate (applied to enhance biodegradation) can be used as electron-acceptors. Reduced forms of manganese can be transported to the groundwater, and thus the soil could be depleted from manganese-oxides. A model was developed in which both types of degradation were included. The application of nitrate did not lead to a lower PG leaching, or in a slower depletion of manganese-oxides. The leached fraction is higher with a thick snowcover and high meltrate, as then PG is transported rapidly in the soil. Snowmelt did not result in anaerobic soil, despite the high soil moisture content, and thus low oxygen diffusion.

Samenvatting

Uitspoeling van verontreinigingen van de onverzadigde zone naar het grondwater is afhankelijk van bodemeigenschappen en de infiltratiesnelheid. In dit proefschrift worden organische afbreekbare verontreinigingen bestudeerd, zoals antivriesmiddelen (bestaande uit propyleenglycol, PG) en pesticiden. Heterogene bodemeigenschappen leiden tot ruimtelijke variabiliteit in uitspoeling, wat vooral belangrijk is voor afbreekbare verontreinigingen. De infiltratiesnelheid bepaalt de reistijd in de onverzadigde zone en daardoor the beschikbare tijd voor afbraak.

Twee veldexperimenten zijn uitgevoerd met een multi-compartment sampler (bestaande uit 10×10 cellen van elk 3.15×3.15 cm^2), om te onderzoeken hoe de ruimtelijke variabiliteit in uitspoeling van verontreinigingen afhangt van de infiltratiesnelheid. Het eerste experiment werd uitgevoerd tijdens sneeuwsmelt, gekenmerkt door een hoge infiltratiesnelheid. In het tweede experiment werd geïrrigeerd om homogene neerslag na te bootsen. De preferente stroombanen waren vergelijkbaar voor beide experimenten. Tijdens het sneeuwsmeltexperiment, met een hoge infiltratiesnelheid, was de uitspoeling homogener dan tijdens het irrigatie-experiment. Daaruit is afgeleid dat de bodemheterogeniteit waarschijnlijk wordt veroorzaakt door kleinschalige ruimtelijke verschillen in the hydraulische bodemeigenschappen, en niet door macroporiën. De correlatie van de uitgespoelde massa's van het afbreekbare PG en een onafbreekbare tracer was hoog. Op de ruimtelijke schaal van de experimenten had de mogelijk heterogene infiltratie van smeltende sneeuw weinig invloed op de stroming van water en stoffen.

De resultaten van de experimenten zijn gebruikt om een random veld voor de schalingsfactor van de retentiecurve te parameteriseren. Om te bepalen in welke mate de resultaten van simulaties en veldwaarnemingen overeenkomen, werd de gesorteerde en gesommeerde drainage gebruikt. Het effect van de verhouding van de infiltratiesnelheid en de afbraaksnelheid op de uitspoeling van afbreekbare stoffen werd bestudeerd met dit model. Bovendien is de ruimtelijke verdeling van een afbreekbare stof vergeleken met die

van een onafbreekbare stof. De infiltratiesnelheid bepaalt de uitspoeling van de verontreiniging op twee manieren: de reistijd van de verontreiniging en het deel van de bodem waarin transport voor komt. Door dit laatste wordt de ruimtelijke verdeling van de uitspoeling van de verontreiniging bepaald door de infiltratiesnelheid, en daardoor ook de uitgespoelde fractie.

De uitgespoelde fractie van een afbreekbare verontreiniging wordt vaak geschat met behulp van gemiddelde bodemeigenschappen en stationaire weerreeksen. Voor verontreinigingen die afbreken in zowel de geadsorbeerde als opgeloste fase, is bekend hoe deze gemiddelde eigenschappen kunnen worden bepaald uit de heterogene eigenschappen. Maar, voor verontreinigingen die alleen in de opgeloste fase afbreken, dit is niet bekend. In bodems die bestaan uit lagen met verschillende adsorptieconstanten is de beweging van de verontreiniging, en dus ook de reistijd in de onverzadigde zone, afhankelijk van de adsorptieconstante, de afbraaksnelheid en dispersiviteit. In een droog klimaat leiden seizoenseffecten in variabele weerreeksen tot grote verschillen in de reistijd, en daardoor in grote verschillen in de uitgespoelde fractie, vooral voor verontreinigingen die weinig adsorberen. In een nat klimaat is dit seizoenseffect zwakker.

In de onverzadigde zone kan PG worden afgebroken door micro-organismen, die daarvoor elektronacceptoren nodig hebben. Een veldexperiment liet zien dat zowel aerobe als anaerobe afbraak voorkomt in de onverzadigde zone. Bij anaerobe afbraak kan mangaanoxide (voorkomend in de bodem) of nitraat (toegevoegd aan de bodem om afbraak te versnellen) worden gebruikt als elektronacceptor. Gereduceerde vormen van mangaan zijn mobiel en kunnen richting grondwater worden getransporteerd, waardoor het gehalte mangaanoxide in de bodem daalt. Er is een model ontwikkeld waarin beide soorten afbraak tegelijk voor kunnen komen. De toevoeging van nitraat leidt niet tot lagere uitspoeling van PG, en ook niet in een langzamere afname van mangaanoxiden in de bodem. De uitgespoelde fractie is hoger bij een grotere sneeuwdikte en een grotere smeltsnelheid, omdat PG dan sneller getransporteerd wordt naar diepere bodemlagen. Sneeuwsmelt leidt niet tot een anaerobe bodem, hoewel het bodemvochtgehalte dan hoog is, en daardoor diffusie van zuurstof in de bodem laag.

Contents

1

Introduction

1.1 Contamination of soil and groundwater

Contamination of the environment is a problem that gains much attention. By intensification of agriculture and industrialisation, the application of contaminants to the soil surface increased. In the soil, contaminants may be adsorbed, degraded or leached to the groundwater. Once contaminants reach the groundwater, they can spread relatively fast horizontally, such that they spread over a large area. This may be hazardous for humans and nature. For instance, when the contaminant concentration exceeds a critical value, groundwater cannot be used to produce drinking water.

To investigate the risk of groundwater contamination, information on transport of contaminants through the soil is acquired with measurements and models. Tracer experiments with suction cups show how fast contaminants are transported in the soil. From batch experiments in laboratory the degradation rate and adsorption of contaminants in a particular soil can be estimated. This information is then applied in models, to predict the transport and degradation under certain circumstances. Soil heterogeneity can be included by random distributions of parameters for transport and degradation, in a one, two or three dimensional field.

This thesis focusses on transport and degradation of degradable contaminants, with and without adsorption. De-icing chemicals, which are used in large amounts at airports during winter time, belong to degradable contaminants. Particularly, the effects of heterogeneous soil parameters and the infiltration rate on contaminant transport and degradation are studied.

1.2 De-icing chemicals at Oslo airport

At Oslo airport in Norway, de-icing chemicals are used to remove snow and ice from airplanes before departure during winter time. This is done on a platform, such that about 80% of the de-icing chemicals is collected, but the remaining is spread along the runways or carried further by the aircraft (OSL Airport, 2013). This results in an annual contaminant load of 100–200 tons along the runways (Øvstedal and Wejden, 2007). During snowmelt, the infiltration rates are high, and the de-icing chemicals can be transported rapidly through the coarse textured soil on which the airport is located (French et al., 2001). Groundwater contamination with the de-icing chemicals should be avoided, as the airport is located on a large unconfined aquifer.

Previous studies at the experimental site at Oslo airport revealed that meltwater from the snow is redistributed spatially, caused by microtopography, thus snowmelt increases the spatial variability in the leaching of de-icing chemical (French and Van der Zee, 1999). The contaminant plume can move to a depth of around 2 m before summer (French et al., 2001). During summer, the evaporation equals the precipitation, therefore the contaminant plume does not move. The de-icing chemical consists mainly of propylene glycol (PG). PG is degradable by micro-organisms, and non-adsorbing to soil particles. Simultaneously with PG degradation, an increase in the concentration of reduced manganese was found by French et al. (2001). This may be caused by anaerobic degradation. In the

3

Figure 1.1: Spraying of de-icing chemical (picture: OSL).

absence of oxygen, other electron acceptors such as manganese can be used by microorganisms in the process of PG degradation.

The degradation rate of PG is often approximated as a first order rate (Bausmith and Neufeld, 1999; French et al., 2001). With frequent PG application, the degradation rate increases (Bausmith and Neufeld, 1999; Jia et al., 2007), but when the PG concentration in the soil water is too high, degradation is inhibited (Bausmith and Neufeld, 1999; Jaesche et al., 2006). The degradation rate also depends on temperature (Revitt and Worrall, 2003; Jaesche et al., 2006), and vegetation (Shupack and Anderson, 2000).

The amount of PG leaching mainly depends on the infiltration rate and the degradation rate. The infiltration rate influences the leached fraction in two ways. Firstly, the infiltration rate determines the extent of spatial variability in leaching. Secondly, a higher infiltration rate results in a lower travel time to the groundwater, thus in less time for degradation. Both will be discussed in the following sections.

1.3 Spatial variability of leaching

Heterogeneous soil properties will lead to spatial variability in contaminant leaching. This is particularly important for the leaching of degradable contaminants (Pot et al., 2005). Due to heterogeneous water flow, the travel time of contaminants to the groundwater is variable in space, and therefore the time that is available for degradation varies. For degradable contaminants, the leached fraction of these contaminants is higher in a heterogeneous medium than in a homogeneous medium with the same average properties (Allaire et al., 2009). Soil can be heterogeneous due to for example macropores (Jarvis, 2007), hydrophobicity, small scale differences in the soil hydraulic properties (Roth, 1995).

The spatial variability in contaminant leaching depends on the infiltration rate, among others. When heterogeneous leaching is caused by macropores, the heterogeneity increases with an increasing infiltration rate (Quisenberry et al., 1994; Williams et al., 2003). Macropores are active when the infiltration rate is high compared to the mean hydraulic conductivity of the soil. When small scale differences in the soil hydraulic properties cause heterogeneous leaching, the heterogeneity may decrease with an increasing infiltration rate, as then a larger part of the soil contributes to contaminant leaching and thus the leaching is more homogeneous (Roth, 1995; Lennartz et al., 2008).

Transport of contaminants in heterogeneous soil can be modelled with stream tubes that each have a different velocity and dispersion coefficient (Vanderborght et al., 2006; Russo and Fiori, 2009), or with a random field for parameters like the soil hydraulic conductivity. For the latter case, the distribution for this field can be based on many soil samples (Rockhold et al., 1996; Hammel et al., 1999). The spatial variability in contaminant leaching can be measured with a multi-compartment sampler (Poletika and Jury, 1994; Buchter et al., 1995; Bloem et al., 2009, 2010)).

1.4 Seasonal variation and layered soil properties

The infiltration rate determines the extent of the spatial variability of leaching, when this is studied in two dimensions, like was discussed in section 1.3. Also in a one dimensional approach, the infiltration rate determines the leached fraction, as the time that is available for degradation depends on the infiltration rate. The seasonal variation in the infiltration rate can influence the amount of leaching (Jury and Gruber, 1989; McGrath et al., 2008b), for instance when contaminants are not transported during a dry summer while degradation continues, or when transport is fast during heavy precipitation. Besides the infiltration rate, the adsorption coefficient of the soil determines the velocity of a contaminant plume.

Similar to PG, pesticides are organic solutes that can be degraded by micro-organisms, but pesticides differ from PG, because they can be adsorbed (Jury et al., 1987). The sorption capacity in soils usually decreases with increasing depth, as the organic matter content decreases with depth (Guo et al., 1997), and organic matter is one of the most important adsorbents for pesticides in soil. Often it is assumed that pesticides can be degraded in the adsorbed and aqueous phase (Jury and Gruber, 1989; Boesten and Van der Linden, 1991). Under this assumption, the contaminant plume propagation can be deduced from the adsorption constant, and the infiltration rate. Then, the heterogeneous adsorption constant can be averaged to obtain a homogeneous soil (Destouni, 1991). Moreover, the transient infiltration rate can be averaged to a stationary infiltration rate. With a homogeneous soil and a stationary infiltration rate, the modelling is simplified and the contaminant plume propagation can be estimated more easily than without these approximations.

However, the assumption that pesticides can be degraded in both the adsorbed and aqueous phase may not be valid. Ogram et al. (1985) states that degradation only occurs in the aqueous phase. When pesticides are only degraded in the aqueous phase, the averaging of both the soil properties and the weather series is different. It is unknown how the

transport of the contaminant plume can be approximated with averaged properties when degradation only occurs in the aqueous phase.

1.5 Degradation of contaminants

Degradation of PG and many pesticides is often approximated as a first order process (French et al., 2001; Jury et al., 1987). However, (French et al., 2001) also mentions that degradation of PG may depend on the biomass, then it is more appropriate to use Monod kinetics for the degradation rate. With Monod kinetics, the degradation rate depends on the concentration of PG, biomass and electron acceptors, which are also needed for biodegradation. With biodegradation electrons are transferred, from which micro-organisms gain energy (Bethke et al., 2011). To maintain electron neutrality, electron acceptors are needed. In soil, different electron acceptors can be used, such as oxygen, nitrate or manganese oxides. Micro-organisms can use multiple electron acceptors, with different preferences. The preferred electron acceptor depends on the availability of the electron acceptor and on the energy that can be gained. The redox regime in the soil is highly influenced by the availability of the electron acceptors (Stumm and Morgan, 1996).

To model degradation of contaminants with different electron acceptors, and the transport of electron acceptors, models can be divided in two categories: the aquifer scale (Hunter et al., 1998; Keating and Bahr, 1998; Brun and Engesgaard, 2002; Mayer et al., 2002) and the aggregate scale (Leffelaar, 1988; Leffelaar and Wessel, 1988; Rappoldt, 1990; Leffelaar, 1993). At the aquifer scale, groundwater gets anaerobic, and then other electron acceptors than oxygen are used (Widdowson et al., 1988; Barry et al., 2002). Also in the unsaturated zone anaerobic degradation can occur (Holden and Fierer, 2005; Blagodatsky and Smith, 2011), for which aggregate scale models are used. At the aquifer scale, oxygen diffusion in the gas phase is not included. At the aggregate scale, oxygen diffusion can be included, but usually diffusion in the soil profile, in which the aggregate is located, is not included.

At the experimental site near Oslo airport, aerobic and anaerobic degradation of PG was observed in the vadose zone (French et al., 2001; Lissner et al., 2011b). For the anaerobic degradation, manganese oxides that are present in this soil are used. Frequent PG application might lower the content of manganese oxides in the soil. As a result, the degradation potential of the soil decreases, and thus the risk of PG leaching increases. To avoid depletion of manganese oxides, and to stimulate biodegradation, electron acceptors such as nitrate might be added (Cunningham et al., 2001). As nitrate can be a contaminant in itself, it is necessary to know the required concentration, which can be estimated with modelling. In the model, we need to include aerobic as well as anaerobic degradation.

As we want to describe transport and degradation in the vadose zone, neither the aquifer scale, nor the aggregate scale is appropriate. Therefore, a new model has to be developed in which transient water flow, degradation and soil chemistry are combined for the vadose zone.

1.6   Research questions and outline

This thesis deals with variability in contaminant leaching, due to spatially variable soil properties and transient infiltration rates.

With transient weather properties, the infiltration rate changes in time. A higher infiltration rate can result in a different spatial variability in the contaminant leaching. As a result, the travel time to the groundwater, which determines the leached fraction of a degradable contaminant, is different. The first research question in this thesis is:

- How consistent are preferential flow paths between two seasons with different infiltration rates?

For this research question, a field experiment with a multi-compartment sampler was performed to investigate the effect of the infiltration rate on the spatial variability in leaching (Chapter 2. This field experiment consisted of two parts, with different infiltration rates. This is the first field experiment in which the consistency of preferential flow paths between two seasons with different infiltration rates was studied. The effect of snowmelt on heterogeneous leaching was investigated. Furthermore, the leaching of degradable PG was compared with the leaching of a non degradable tracer. Chapter 2 presents the results of this field experiment, in which the influence of the infiltration rate on the spatial and temporal variability in contaminant leaching was measured.

This field experiment was also used to answer the following research question:

- How does the infiltration rate determine the spatial distribution and the leached fraction of a degradable contaminant?

Chapter 3 describes how the results from the field experiment from Chapter 2 were used to parameterize a two dimensional field for the hydraulic conductivity and pressure head using a new method. The model is used to study the effect of the infiltration rate on the leaching of degradable contaminants. The spatial distribution and the leached fraction will be discussed in Chapter 3.

Soils can be layered with respect to the adsorption parameters. To simplify transport modelling, heterogeneous soil properties are often averaged to get a homogeneous soil. Furthermore, transient weather properties are often averaged to do steady state simulations. This can be done for nondegrading and nonadsorbing contaminants, as well as for contaminants that are degraded in both the adsorbed and aqueous phase. For adsorbing contaminants that only degrade in the aqueous phase, averaging soil and weather properties to get a homogeneous soil may not be appropriate and calls for a critical evaluation. Therefore, the third research question of this thesis is:

- How can the contaminant plume propagation in a layered soil be approximated with average parameters, temporally as well as spatially?

Chapter 4 discusses the transport of adsorbing contaminants that are only degraded in the aqueous phase in a layered soil. Furthermore, the effect of seasonality in weather series on contaminant leaching is discussed. A one dimensional model with layered soil properties and transient weather series will be used for this.

Concerning the first three research questions, chemical heterogeneity was ignored, or included as an adsorption coefficient that decreased with increasing depth. The effect of chemical heterogeneity on degradation and leaching can be included in a more extended way, by including local differences in the redox regime.

- How does the redox potential in the vadose zone influence contaminant degradation, and how can this be included in a transport model?

In chapter 5, a model is introduced in which contaminant transport, degradation and soil chemistry are combined. Furthermore, applications based on this model are discussed. Transport of oxygen is included in the gas phase, which is driven by diffusion. The diffusion constant depends on the soil moisture content of the soil (Millington and Quirk, 1961). In our model, a mobile and an immobile phase are included. The mobile phase can be seen as the aerobic part of the soil, whereas the immobile phase is the part of the soil that can hardly be reached by oxygen (such as saturated pores). The redox potential is different in both phases, therefore also the electron acceptor that is most favourable for the micro-organisms can be different in both phases. This results in chemical heterogeneity of the soil. In chapter 5 will be discussed how the redox potential influences the degradation and thus the leaching of PG.

Finally in chapter 6 the results and conclusions of the different chapters are summarized and discussed.

2

Quantifying heterogeneous transport of a tracer and a degradable contaminant in the field, with snowmelt and irrigation

Abstract

To examine the persistence of preferential flow paths in a field soil, and to compare the leaching of a degradable contaminant with the leaching of a tracer, two field experiments were performed using a multi-compartment sampler (MCS). The first experiment was carried out during the snowmelt period in early spring, characterized by high infiltration fluxes from snowmelt. The second experiment was carried out in early summer with irrigation to mimic homogeneous rainfall. During the second experiment, the soil was warmer and degradation of the degradable contaminant was observed. For both experiments, the highest tracer concentrations were found in the same area of the sampler, but the leached tracer masses of the individual locations were not highly correlated. Thus, the preferential flow paths were stable between the two experiments. With a lower infiltration rate, in the second experiment, more isolated peaks in the drainage and the leached masses were found than in the first experiment. Therefore, it is concluded that the soil heterogeneity is mainly caused by local differences in the soil hydraulic properties, and not by macropores. With higher infiltration rates, the high and low leaching cells were more clustered. The leached masses of the degradable contaminant were lower than the leached masses of the tracer, but the masses were highly correlated. The first-order degradation rate and the dispersivity were fitted with CXTFIT; the first-order degradation rate was $0.02 \ d^{-1}$, and the dispersivity varied between 1.9 and 7.1 cm. The persistence of the flow paths during the experiments suggests soil heterogeneity as the driver for heterogeneous flow and solute transport in this soil. At the MCS scale, heterogeneous snowmelt did not seem to have much influence on the flow and solute paths.

2.1 Introduction

Preferential flow can lead to rapid transport of nutrients and chemicals through the unsaturated zone, which can result in groundwater contamination. Preferential flow processes are generally studied at either the core, profile or landscape scale (Allaire et al., 2009). Soil heterogeneity hinders the prediction of the movement of mass in field situations, because it often results in faster movement of water and solutes than would be expected from the soil matrix properties. When effective parameters are used for soil and climatic properties, contaminant leaching may be underestimated by a hydrologic model (Allaire et al., 2009). To account for preferential flow in the models, additional parameters are needed to quantify the importance of preferential flow in a field soil (Feyen et al., 1998; Šimunek et al., 2003). It is important to identify the main process that causes preferential flow, when solute transport is modelled. As the soil is a complex system, field experiments can give better insight into which processes are important for the occurrence of preferential flow. Based on this knowledge, a better prediction can be made of the potential risk of groundwater contamination for a particular soil and contaminant.

Preferential flow can be caused by macropore flow (Jarvis, 2007) or spatial variability of the hydraulic properties (Roth, 1995). When the flow rate is high compared to the saturated hydraulic conductivity of the soil, most of the soil is close to saturation. Under these conditions, coarse textured regions are better conductors than fine textured regions (Roth, 1995). Therefore, coarser textured regions are likely to develop flow channels with a vertical orientation under a high infiltration rate. With a water flux that is much lower than the saturated hydraulic conductivity, flow channels will also develop, but then in the fine textured regions instead of the coarse textured.

Preferential flow paths may change in time due to bioactivity, or due to complete saturation or drying of the soil (Öhrström et al., 2004). Williams et al. (2003), Lennartz et al. (2008) and Buchter et al. (1995) found that preferential flow paths are stable. Most studies investigated the leaching of tracers, while the effect of preferential flow on the degradation of degradable contaminants is highly relevant for the potential contamination risk for natural systems (Flury, 1996). The rapid transport in macropores, compared to the matrix, leads to a higher leaching of a degradable contaminant than when only matrix flow occurs (Pot et al., 2005).

When degradation of contaminants is studied, the experimental conditions should resemble the natural field conditions as closely as possible, because the degradation rate depends on temperature and soil moisture content, amongst others (Stotzky, 1997). Furthermore, in a structured soil, degradation may be lower than in a mixed sample, because micro-organisms or the substrate cannot enter all aggregates (Chenu and Stotzky, 2002). Also when soil heterogeneity is quantified, the soil structure should be intact. Most studies have been done in the laboratory, under different conditions than in the field (Quisenberry et al., 1994; Buchter et al., 1995; Pot et al., 2005), and hence may under- or overestimate the soil heterogeneity. Estimations of the effect of soil heterogeneity on contaminant leaching may be more realistic in the field, using wick samplers (Holder et al., 1991; Boll et al., 1997) or suction plates (Kasteel et al., 2007). A disadvantage of wick samplers is that the pressure that is applied to the soil is constant. Using suction plates, the ambient

soil pressure may be applied (Weihermüller et al., 2007). For both wick samplers and suction plates, the patial resolution may be too coarse (around 100 cm^2) to capture all small scale flow processes (Poletika and Jury, 1994; Buchter et al., 1995). To overcome these disadvantages, a multi-compartment sampler (MCS) as introduced by Bloem et al. (2009, 2010) was used in our study, in which the pressure is adjusted according to the pressure in the surrounding soil. Additionally, the spatial resolution of the MCS is high, and therefore, fluxes through individual 3.15×3.15 cm^2 can be measured.

The spatial pattern in leaching of a degrading contaminant might be different than a tracer as a result of differences in travel times. Examples of degradable contaminants for which a travel time distribution in the unsaturated zone may help to estimate the leaching to the groundwater are easily degradable contaminants like pesticides (Flury, 1996). Another easily degradable contaminant is propylene glycol (PG), which is used in de-icing chemicals at airports (Jaesche et al., 2006; French et al., 2001). Propylene glycol is degradable by micro-organisms, and non-adsorbing to soil particles (French et al., 2001). At Oslo airport in Norway de-icing chemicals are used to remove snow and ice from airplanes before departure during winter time. Although this is done on a platform to collect the de-icing chemicals, a fraction of these de-icing chemicals can contaminate the snow surrounding the runway. During snowmelt, the infiltration rates are high, and the de-icing chemicals can be transported rapidly through the coarse textured soil on which the airport is located (French and Van der Zee, 1999). Groundwater contamination with the de-icing chemical should be avoided, as the airport is located on a large unconfined aquifer (French et al., 2001).

Snowmelt may add extra heterogeneity to the water flow, as a snow cover acts as a porous medium, in which meltwater can flow in preferential paths (Waldner et al., 2004; Marsh, 1991). Furthermore, the rate of snowmelt can differ locally which introduces more heterogeneous flow at the plot scale, with horizontal differences in infiltration (French and Van der Zee, 1999).

It has not been investigated often which particular process is responsible for the preferential leaching of a tracer in a field soil. Furthermore, experiments on preferential leaching usually focus on non-degradable tracers, while the preferential leaching of a degradable contaminant might be different. Two field experiments were performed, using the MCS, to quantify the spatial variability in solute leaching, to quantify possible seasonal effects, and to compare the leaching of a tracer with degradable PG. The first experiment was done during the snowmelt period in early spring. This experiment was characterized by high infiltration fluxes from the meltwater and a frozen soil. Furthermore, the heterogeneous flow in the snow cover might result in infiltration at the soil surface that is not uniformly distributed. The second experiment was done in late spring/early summer with irrigation to mimic homogeneous rainfall with known infiltration amounts. In the second experiment, the soil was warmer and degradation of the degradable contaminant was observed.

With the two experiments we answer the following research questions: (1) How persistent is preferential flow in the field for two cases with different boundary conditions? (2) How different is the spatial variability in leaching for a tracer and a degradable solute?

(3) What determines the heterogeneous flow in this soil: soil heterogeneity, the infiltration rate, or snowmelt heterogeneity?

2.2 Materials and methods

2.2.1 Experiment

A multi-compartment sampler (MCS) (Bloem et al., 2010) was installed at the field station Moreppen, near Oslo Airport, Norway, to measure spatial and temporal variability in solute leaching and drainage. Details about the field station can be found in French et al. (1994). The field station is located in a flat area with coarse glaciofluvial sediments (sand and gravel) (French and Van der Zee, 1999). The soil is an Entic Haplorthods (French et al., 2001). The texture distribution is 15 % fine sand, 75 % medium and coarse sand, and 10 % gravel (French et al., 1994). The saturated hydraulic conductivity is 6.65×10^{-4} m s^{-1} (French et al., 2001). The soil surface was covered with short grass. The MCS has a size of 31.5×31.5 cm^2, and consists of 100 separate drainage collectors. The surface of the MCS consists of porous metal plates, to which pressure can be applied. Details about the MCS can be found in Bloem et al. (2010).

From a trench a horizontal tunnel was dug, leaving the soil above this tunnel undisturbed. The tunnel was secured with a wooden frame, to prevent the surrounding soil from collapsing. At 68 cm distance from the trench wall, the MCS was installed at 51 cm below soil surface (Fig. 2.1). A 2 mm thick layer of wetted soil from the tunnel was applied to the surface of the MCS, to ensure a good contact between the MCS and the soil above it. The wooden frame was removed, and the tunnel was backfilled, to avoid boundary effects. Four tensiometers were installed near the trench wall, at 51 cm depth. The average pressure head measured by the four tensiometers was applied to the MCS, plus 15 cm extra pressure head to compensate for a pressure head drop in the porous metal plates (Bloem et al., 2009). The pressure in the MCS was variable in time.

Two experiments were done: one during snowmelt (26 March–23 May 2010) and one with irrigation (23 May–4 July 2010). For the snowmelt experiment 1092 g m^{-2} propylene glycol (PG) and 10 g m^{-2} bromide was diluted in 2 l m^{-2}, and sprayed uniformly on top of an undisturbed snow cover (26 March 2010). De-icing fluid (Kilfrost, 2012) containing PG was diluted to reach this applied mass. The application area was large enough to ensure that boundary effects can be neglected. In the snowmelt experiment the infiltration originated from snowmelt or rainfall. Snowmelt was measured daily by measuring the depth and equivalent water depth of the snow cover at three locations at the field station. At these locations, no de-icing chemical was applied. The snow in the application area melted faster than at these locations, due to the de-icing chemical. On 12 April, the snow was patchy above the MCS, and at 13 April all snow above the MCS was melted. The difference of the equivalent water depth of the snow cover per day, plus the rainfall, was the infiltration per day (Fig. 2.2). The infiltration originating from the snowmelt occurred 1 or 2 days earlier in the area where PG was applied, than in the area were the snowmelt was measured. We will ignore this difference, as it is not important for
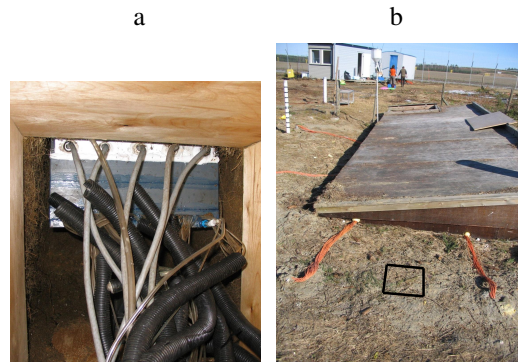
Figure 2.1: Experimental setup. **a**) Installation of the multi-compartment sampler (MCS), shown from the trench. **b**) The location of the MCS shown from above. The marked square indicates the location of the MCS, 51 cm below soil surface. The roof of the trench is visible in the background. The width of the MCS is 31.5 cm.

the current data analysis. No ice layer was found below the snow cover, at the soil surface. This means that the possible heterogeneous infiltration of meltwater was not attributable to ice.

For the irrigation experiment 1103 g m^{-2} PG and 10 g m^{-2} bromide was diluted in 5 l m^{-2}, and sprayed uniformly on the soil surface at 23 May 2010. Also in the irrigation experiment, the application area was large enough to ensure that boundary effects can be neglected. The irrigation scheme and the daily mean air temperature are given in Fig. 2.3. Initially, the irrigation rate was based on the measurements from the snowmelt experiment, such that the irrigation experiment could be finished in the limited time that was available for it. However, during the irrigation experiment, the transport of bromide was found to be too slow. Therefore, the irrigation rate was increased from 2 June onward. In between the irrigations, the soil surface was covered with plastic, to minimize evapotranspiration and to avoid the infiltration of rainwater. Using a nozzle, the soil surface was irrigated with tap water, except on 12 June. This was a rainy day and 7.8 mm of rainwater infiltrated, while the plastic was removed. On 13 June, 7.5 mm water was irrigated. The irrigation rate was approximately 6.6 mm h^{-1}. Neither surface runoff, nor ponding was observed. Between 31 May and 2 June, evaporation was measured in a pan under the plastic. The measured evaporation was 1 mm d^{-1}. These were warm days, the average evapotranspiration rate during the entire irrigation experiment probably was lower.

Drainage was stored in the MCS, samples were taken with a frequency that depended on the amount of drainage. For the snowmelt experiment, samples were taken daily from 1 April until 15 April. Then, samples were taken at 17 and 21 April, and 9 and 23 May. During the irrigation experiment, samples were taken every second day, on the same day as, and prior to, the irrigations. After collecting, the samples were weighted to determine the volume of drainage. If a sample was smaller than 4 ml, it was stored cool. In the
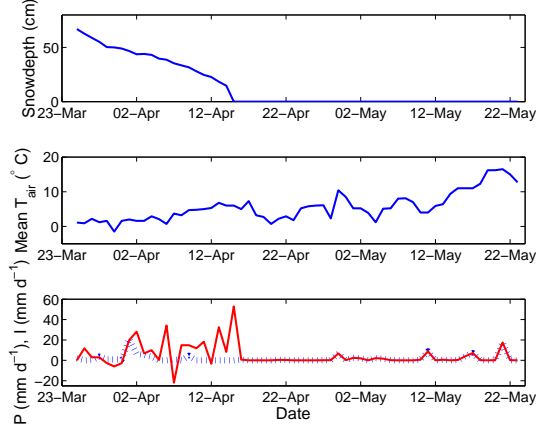
Figure 2.2: Weather series for the snowmelt experiment (in 2010), mean T_{air} is the daily mean temperature (°C), P is the daily precipitation (mm d^{-1}, dotted line), I is the infiltration (mm d^{-1}, solid line). The daily infiltration is calculated from the sum of the change in the equivalent water depth of the snow cover in a day, and the precipitation.

next sampling round, the sample was added to this stored small sample. In samples larger than 4 ml, the bromide concentration was measured with an Orion 9635BNWP Bromide Ion Selective Electrode. Besides, in the irrigation experiment, the PG concentration was measured with a GC analyser. We assumed that degradation of PG during the snowmelt experiment was low, due to the low temperature and high PG concentration in the applied solution (Jaesche et al., 2006). Therefore, the PG concentration was not measured in the snowmelt samples. At the end of the experiment, all samples that still were smaller than 4 ml after the final sampling round were mixed, and Br and PG were measured in this mixed sample.

2.2.2 Data analysis

The experiment lead to a data set with volumes of drainage, and leaching concentrations for each sampling round and each cell. With drainage, we refer to water volumes that were collected, while we use leaching to refer to solute masses. To quantify how the drainage, or the leaching in a particular cell is related to the drainage, or leaching in a neighbouring cell, we calculate the spatial autocorrelation using Moran's I (Strock et al., 2001):

$$I = \frac{n}{S_0} \frac{\sum_i \sum_j W_{ij} \left(X_i - \bar{X} \right) \left(X_j - \bar{X} \right)}{\sum_i \left(X_i - \bar{X} \right)^2}, \quad S_0 = \sum_i \sum_{j \neq i} W_{ij} \qquad (2.1)$$

where n is the number of cells, W_{ij} is a measure of the neighbouring of the cells i and j, and X_i is the measured total drainage, or solute leaching in cell i. Cells are neighbours when they share one side. This means that W_{ij} is 2 for the cells in the corners, 3 for the

15
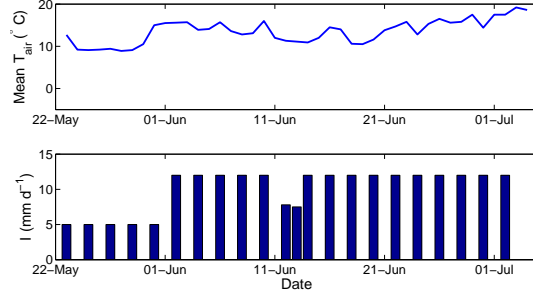
Figure 2.3: Weather series for the irrigation experiment (in 2010), mean T_{air} is the daily mean temperature (°C), I is the infiltration from irrigation (mm d^{-1}).

cells at the borders, and 4 for the other cells. In I both the values of drainage and leaching, and the spatial information, with the weighing W_{ij}, are included. I varies between -1 and 1, where 1 means that the values of neighbouring cells are perfectly positively autocorrelated. When there is no autocorrelation, the expected value of I is $-1/(n-1)$, which is -0.010 with 100 cells.

The velocity, dispersivity, and first order degradation constant were estimated by fitting de convection-dispersion equation to the breakthrough curves with the parameter fitting program CXTFIT (Toride et al., 1995). The dispersivity that was estimated for bromide, was also used for PG. The velocity and first-order degradation constant for PG were fitted.

2.3 Results and discussion

2.3.1 Stability of the spatial patterns of drainage and concentration in time

We will start with describing the spatial patterns of drainage and solute concentrations to determine the stability of these patterns during and between the snowmelt and the irrigation experiment.

Figure 2.4 shows the spatial distribution of the volume of drainage, and of the bromide concentration during the snowmelt experiment at five selected cumulative drainage depths (the amount of total drainage since solute application). The cumulative drainage depth is used as a time axis instead of the day (Wierenga, 1977), to facilitate a comparison with the irrigation experiment, which had a different infiltration rate. The bromide concentration is scaled with the applied mass of bromide per m^2, to facilitate a comparison with propylene glycol (PG) during the irrigation experiment later on. The initial bromide concentration was not used for scaling, because the applied bromide was diluted with meltwater from the snow.

16

Figure 2.4: Spatial distributions of the drainage, and the bromide concentration during the snowmelt experiment over the multi-compartment sampler consisting of 10×10 cells of 3.15×3.15 cm^2 each. The bromide concentration is scaled with the applied mass per m^2. The titles refer to the cumulative drainage since solute application.

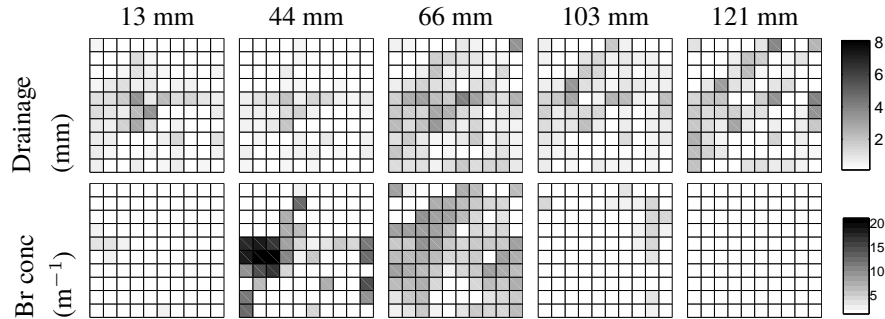At 13 mm after solute application, drainage started in the left middle part of the sampler. At 66 mm, most cells drained water, but the highest water fluxes were still found in the left middle part. Throughout the snowmelt experiment, the highest drainage volumes were found in this area. The bromide concentrations were low in the first drainage at 13 mm. The highest bromide concentrations could be found in the lower left part of the sampler at 44 mm of drainage. At 66 mm, the maximum bromide concentrations were lower than at 44 mm. At 66 mm, bromide leached through a larger part of the sampler and the concentrations were more equally spread in space than at 44 mm. At 103 mm of drainage, the concentrations decreased further, and the highest concentrations were now found on the right side. At 121 mm of drainage, the drainage did not contain bromide anymore.

The drainage patterns showed more isolated peaks than the bromide concentration. The cells with the highest drainage did not necessarily leach the highest concentration of bromide. The spatial pattern of the bromide concentration had a larger variation in time than the pattern of drainage. From Fig. 2.4 it is clear that both water flow and solute transport in this soil are heterogeneous.

Figure 2.5 shows the spatial distributions of the volume of drainage, of the bromide concentration, and of the PG concentration during the irrigation experiment at five selected cumulative drainage depths. During the irrigation experiment, water drained over the whole MCS, with a few isolated peaks that were stable throughout the irrigation experiment. Bromide leaching started at 70 mm, the highest bromide concentrations were found in the lower left area of the sampler. At 101 mm, the bromide concentrations peaked in the lower left, the middle right area, and in the upper left cell. Around those peaks, cells also started leaching bromide, but generally with lower concentrations. At 124 mm, most cells leached bromide and the differences between the concentrations of the cells were small. At 124 mm, the concentrations decreased relatively to the concentrations at 101 mm. In the irrigation experiment, bromide leaching started after a larger amount of

17
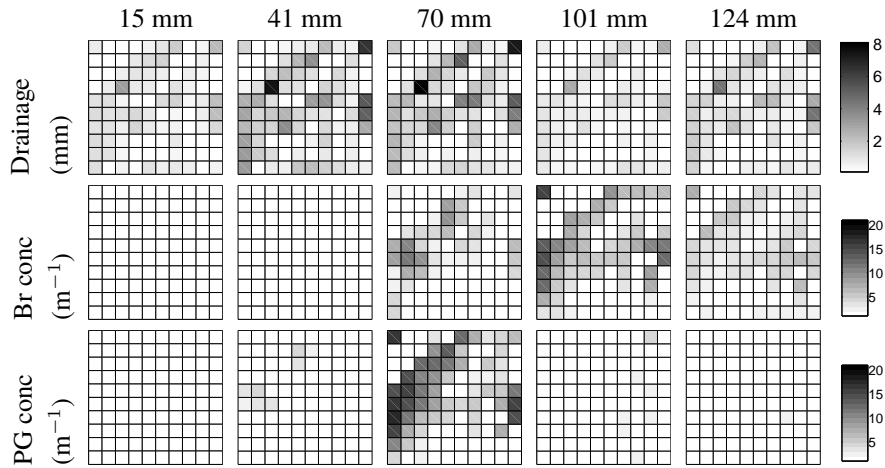
Figure 2.5: Spatial distributions of the drainage, the bromide concentration, and the PG concentration during the irrigation experiment over the multi-compartment sampler consisting of 10×10 cells of 3.15×3.15 cm^2 each. The concentrations of bromide and PG are scaled with the applied mass per m^2. The titles refer to the cumulative drainage since solute application.

drainage than during the snowmelt experiment. Thus, at the start of the irrigation experiment, more water was stored between the soil surface and the MCS than at the start of the snowmelt experiment.

Like the bromide concentration, the PG concentration first increased in the lower left part (at 41 and 70 mm). At 101 mm, the concentrations were lower than at 70 mm, the highest concentrations were found on the right side of the sampler. At 124 mm, the drainage did not contain PG anymore. The leaching of PG started earlier than the leaching of bromide. This was also observed by French et al. (2001), and may be caused by density driven flow. The density of pure de-icing fluid is 1.043 times the density of pure water (Kilfrost, 2012). After dilution the density of the applied solution was approximately 1.005 times the density of water. The PG concentrations decreased both earlier and faster than the bromide concentration. The faster decrease in the concentration can be attributed to degradation of PG by micro-organisms. French et al. (2001) found that the first order degradation constant for PG in a field soil was between 0.015 and 0.04 d^{-1}. Fitted from the breakthrough curves of bromide and PG for the entire MCS, we found a first order degradation constant of 0.02 d^{-1} for PG during the irrigation experiment.

Figure 2.6 shows the mean pressure head at 51 cm depth. The pressure head was generally higher during the snowmelt period than during the irrigation experiment. Peaks in the pressure head during the snowmelt resulted from infiltrating meltwater during warmer days. The maximum pressure heads from the snowmelt and the irrigation experiment
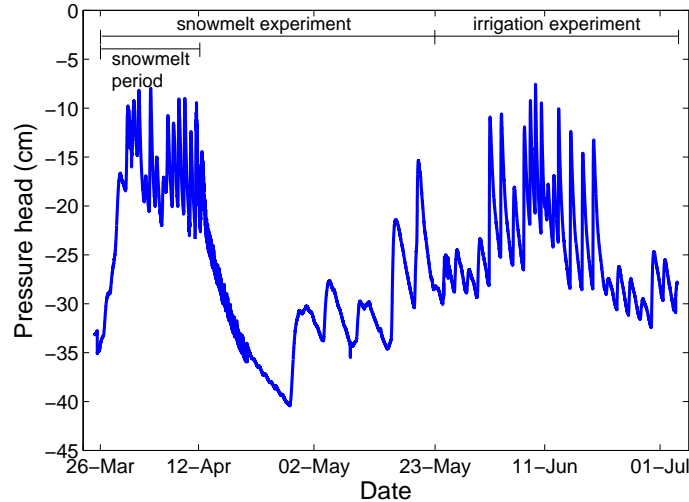
Figure 2.6: Average pressure head (cm) at 51 cm depth during the snowmelt and the irrigation experiment (in 2010).

were similar, but during the snowmelt experiment, the soil drained less than during the irrigation experiment. The average pressure head was -27 cm during the snowmelt experiment (26 March–23 May), -16 cm during the snowmelt period (26 March–12 April), and -25 cm during the irrigation experiment (23 May–4 July). During the snowmelt period, when high infiltration rates occur, the soil is wetter, and therefore a larger part of the coarse textured soil is even higher conductive than under drier conditions as in the irrigation experiment. In the irrigation experiment, the drainage showed more isolated peaks than for the snowmelt experiment. Williams et al. (2003) showed that the degree of preferential flow resulting from macropore flow would increase with increasing flow rate. In the snowmelt experiment with higher infiltration rates, however, the number of isolated peaks in the drainage decreased (comparing the drainage in Figs. 2.4 and 2.5). The heterogeneous flow in the soil, therefore, is probably caused by small changes in the soil hydraulic properties, and not by macropores.

Figure 2.7 shows the areas of the MCS in which the highest concentrations, as plotted in Figs. 2.4 and 2.5, were measured. For both the snowmelt and the irrigation experiment, the areas with the highest concentrations are similar. In the snowmelt experiment, the differences in concentrations between all cells seem to be larger than during the irrigation experiment. The high concentrations in a small area of the sampler can be caused by snowmelt. With a high infiltration rate and a wet soil, a small part of the soil can transport solutes rapidly, while little dilution occurs due to a low exchange with the surrounding soil, as lateral mixing is time dependent. This leads to a larger spatial variability in concentra-

19

tions than for the lower infiltration rates during the irrigation experiment. The differences in the concentrations were not caused by heterogeneous infiltration of the meltwater from the snow. If this was the case, also the drainage should be heterogeneous, with the same spatial patterns as the concentration, which was not observed (Fig. 2.4). Based on this, it is concluded that the infiltration of the meltwater was homogeneous, compared to the soil heterogeneity. Results from a preliminary experiment, which was performed during the spring of 2009, confirm this conclusion. The areas with the highest leaching were similar for 2009 and 2010, which means that the effect the heterogeneous infiltration of meltwater is small compared to the effect of soil heterogeneity.

Based on the snowmelt and irrigation experiment we conclude that generally, the spatial patterns of the concentration are similar with high or low infiltration rates, but the differences between the concentrations are larger with a high infiltration rate.

During the irrigation experiment, the highest PG concentrations, and the highest bromide concentrations can be found in the same areas, but at different times. Thus, the spatial patterns in the concentrations of a tracer and a degradable solute are similar.

2.3.2 Effect of the travel time distribution on BTCs

Figures 2.4 and 2.5 reveal that the soil consisted of fast and slow responding areas. Buchter et al. (1995) made a division of the soil in fast and slow cells, based on the height of the peak concentration of the BTC, and the moment that this peak concentration was reached. For each cell, we determined the number of days from solute application until the peak concentration was reached. The resulting histograms are shown in Fig. 2.8. It must be mentioned that the irrigation experiment was ended before the BTCs were complete for all cells. Cells in which the concentration was still increasing at that time, mostly have their highest concentration at day 40 or 41, which then is called the peak concentration in Fig. 2.8. There were 11 cells that did not leach during the irrigation experiment, these are not included in Fig. 2.8. For the snowmelt experiment, the histogram has a bell-shaped distribution, and shows that most cells reached the peak concentration at 15 days after solute application. For the irrigation experiment, the histogram is not bell-shaped.

Based on the histograms, the cells are divided in three groups: fast, average, and slow cells. Fast cells are the cells that leach before the mode (before day 15 in the snowmelt experiment, and before day 30 in the irrigation experiment). Average cells have their peak concentration when most cells have (at day 15 and 16 in the snowmelt experiment, and at day 30 in the irrigation experiment). Slow cells have their peak concentration later than the average cells (after day 16 in the snowmelt experiment, and after day 30 in the irrigation experiment). Cells can belong to different groups for the snowmelt and the irrigation experiment. The average concentrations of bromide and PG were calculated for the groups of cells. The BTCs of the fast, average, and slow cells for bromide during the snowmelt and the irrigation experiment are given in Fig. 2.9.

During the snowmelt experiment, the bromide concentration increased rapidly in the fast cells, as a result of the high infiltration rate caused by snowmelt. At 66 mm of drainage, only patchy snow was left above the MCS. The bromide concentration decreased rapidly in the fast cells when the snow had melted (79 mm drainage). In the snowmelt
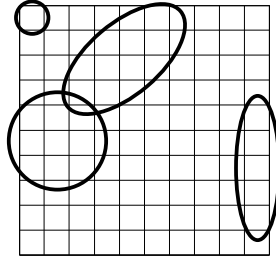
Figure 2.7: The areas from the multi-compartment sampler where the highest leaching of bromide and PG occurred (based on Figs. 2.4 and 2.5).

experiment, the height of the concentration peak was higher than in the irrigation experiment, probably as a result of the higher infiltration rate. The bromide concentration also increased earlier in the snowmelt experiment than in the irrigation experiment. The value of the peak concentration decreased from fast to slow cells in both the snowmelt and the irrigation experiment. This is expected, as the spreading generally increases with time, which will lead to a lower peak concentration for a non-degradable solute.

The solute transport parameters from the convection-dispersion equation were fitted for the BTCs in Fig. 2.9, using CXTFIT (Toride et al., 1995). For the fitting, the cumulative drainage of the entire sampler was used as a time axis, to obtain the required steady state conditions (Wierenga, 1977). This gives the velocity v a unit of cm mm^{-1}, and the dispersion coefficient D a unit of cm^2 mm^{-1}. Using the average drainage per day during either the snowmelt or the irrigation experiment, the parameters were back-transformed to units of cm d^{-1}, and cm^2 d^{-1} (Table 2.1). From the fitted parameters the dispersivity α was calculated ($\alpha = D/v$). Both v and D decrease from fast to slow cells for the snowmelt and the irrigation experiment. As expected, for the fast and average cells, the velocities are higher during the snowmelt than the irrigation experiment. This is caused by the higher infiltration rate, resulting from the snowmelt. Based on the results of Vanderborght and Vereecken (2007) for a database with a large number of laboratory and field experiments, both the flow rate and the flow conditions affect the dispersivity values that are found. As the flow rate increases, they found that dispersivities tend to increase, for relatively small transport distances as in the present study. We find that for the snowmelt experiment, the dispersivity of the fast cells is larger than the dispersivity of the average and slow cells. For the irrigation experiment, the dispersivity increases from slow to average to fast cells. In that respect, our results comply with those of the database. Our dispersivity values are generally of equal value, or perhaps a bit smaller, than those of the database. However, our flow rates on average are smaller than in the shorter travel distance situations (core, column) of the database. Moreover, not only the mean flow rate may affect the dispersivity, but also the flow regime. For conditions sim-
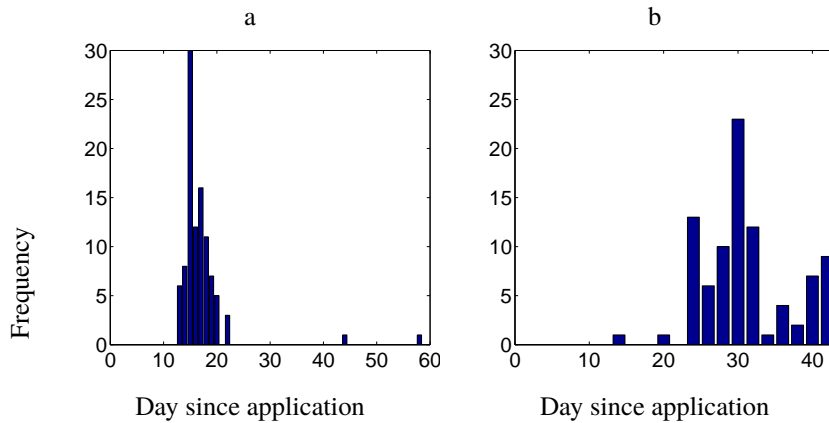
Figure 2.8: Histograms of the day number on which the peak bromide concentration occurred, for the snowmelt experiment **(a)**, and the irrigation experiment **(b)**. Application was on 26 March 2010 **(a)**, and 23 May 2010 **(b)**.

ilar to our experiments, with natural climate and intermittent irrigation upper boundary, Vanderborght and Vereecken (2007) found that smaller dispersivity ranges result in their database. The dispersivities were lower during the irrigation experiment than during the snowmelt experiment, which may have periodically larger flow rates, particularly near the soil surface (Figs. 2.2 and 2.3). This is also in agreement with the database results. Also compared with the review of Beven et al. (1993) our observations agree well.

We hypothesize that in fast cells, the values of the peak concentration (relative to the applied concentrations) of PG and bromide would be similar, because PG degradation can only occur during a short period. In slow cells, the travel time is longer, and therefore, more PG would be degraded than in the fast cells. As a result, in slow cells, the PG concentration would be lower than the bromide concentration, and this difference would increase with increasing travel time.

Figure 2.10 shows the BTCs for PG and bromide in the irrigation experiment, for the fast, average, and slow cells. For the fast cells, the PG concentration increased earlier than the bromide concentration. This was also observed by French et al. (2001), and can be caused by density-driven flow. The values of the peak concentration and the recession thereafter were similar for bromide and PG. The average cells show comparable features, but with lower concentrations than for the fast cells. Also, the PG concentration decreased earlier than the bromide concentration in the average cells, which possibly is attributable to degradation.

Initially, the PG concentrations in the fast and average cells might have been too high for the micro-organisms, and therefore degradation might have been inhibited. PG degradation can be inhibited if the PG concentration is high, and the inhibition limit depends on the type of micro-organisms, and temperature, amongst others (Bausmith and Neufeld,

Table 2.1: Solute transport parameters with pore water velocity v (cm d^{-1}), and dispersivity α (cm) for fast, average, and slow cells, as well as for the entire sampler, for bromide.

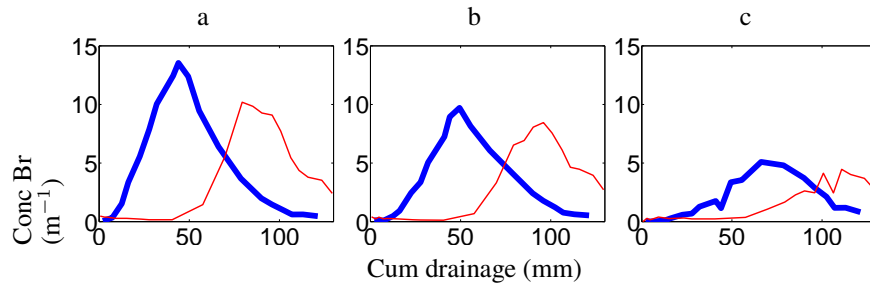| Experiment	Group	v (cm d^{-1})	α (cm)
Snowmelt	Fast	1.8	6.6
	Average	1.5	7.1
	Slow	1.3	2.4
	Total	1.7	5.6
Irrigation	Fast	1.5	4.1
	Average	1.4	3.8
	Slow	1.3	2.0
	Total	1.6	1.9

Figure 2.9: Breakthrough curves of bromide for the snowmelt experiment (thick line) and the irrigation experiment (thin line), for fast cells **(a)**, average cells **(b)**, and slow cells **(c)**.

23

1999; Jaesche et al., 2006). The first order degradation rate of PG increases with a decreasing PG concentration (Bausmith and Neufeld, 1999). Once the concentration was below the inhibition level, as was probably the case in the average cells, the concentration decreased rapidly due to degradation. In the slow cells, PG was degraded before bromide reached the peak concentration. Thus, in the slow cells the PG concentration appears to decrease faster than in the fast cells, the decrease in the bromide concentration appears to be similar in the fast, average, and slow cells. This means that the degree of degradation of PG would increase from fast to slow cells. The degradation constant was only fitted for the entire sampler (k=0.02 d^{-1}), and not for the fast, average, and slow cells separately, because the BTCs of bromide are not complete. The incomplete BTCs hinder the estimation of the degradation constants, mainly in the slow cells.

We conclude that the travel time distribution influences the concentrations of degradable solutes, and the differences between the concentrations of degradable and nondegradable solutes increase from fast to slow transporting areas. Therefore, in parts of the soil that transport water and solutes rapidly, the leaching of degradable contaminants will be higher than in slow transporting areas.

2.3.3 Spatial patterns of total drainage and leaching

The conclusion drawn from Fig. 2.10 was that the degradation of PG appears to increase from fast to slow cells. To further examine this conclusion, we will discuss the spatial pattern of the total leached masses of bromide for both the snowmelt and the irrigation experiment, and PG for the irrigation experiment.

Figure 2.11 shows the total leached mass of bromide for the snowmelt experiment, for the irrigation experiment, and the total leached mass of PG during the irrigation experiment, together with the relative differences between the leached PG and bromide (Fig. 2.11d). The leached masses of PG and bromide should be compared with some caution, because the bromide BTCs were not complete for all cells before the experiment was stopped. Therefore, the total bromide leaching was underestimated, especially for slow cells.

From Fig. 2.11a and b follow that the highest bromide leaching occurred in the same area for the snowmelt and the irrigation experiment. In the snowmelt experiment, most leaching occurred in the middle left part of the sampler, while in the irrigation experiment, most leaching occurred in the areas that are marked in Fig. 2.7. In the low leaching areas, the leaching was higher during the snowmelt experiment than during the irrigation experiment. Apparently, with high infiltration rates, as in the snowmelt experiment, the leaching was more homogeneous. More homogeneous leaching was caused by more homogeneity in drainage, because the spatial variability in the concentration was larger in the snowmelt experiment than in the irrigation experiment (Fig. 2.4). The more homogeneous drainage can be caused by the higher infiltration rate, which results in a wetter soil. In a wetter soil, a larger part of the matrix drains water than in a drier soil, because the hydraulic conductivity is higher. Furthermore, Fig. 2.11a and b show that in the irrigation experiment, with low infiltration rates, there were more isolated peaks in the leached masses than in the snowmelt experiment.

24
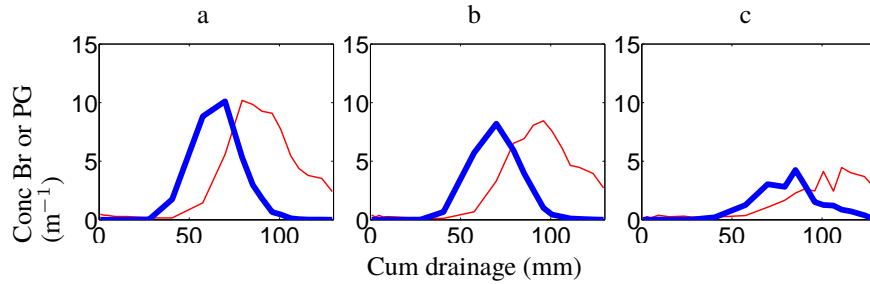
Figure 2.10: Breakthrough curves of bromide (thin line) and PG (thick line) for the irrigation experiment, for fast cells **(a)**, average cells **(b)**, and slow cells **(c)**.
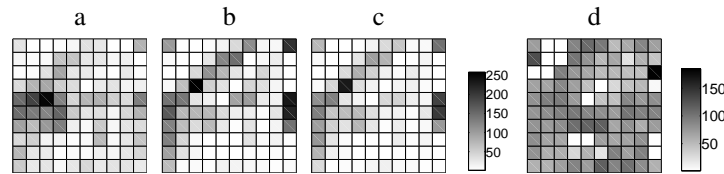
Figure 2.11: Spatial distributions of the total bromide leaching during snowmelt, total bromide leaching during irrigation, and total PG leaching during irrigation over the multi-compartment sampler consisting of 10×10 cells of $3.15 \times 3.15 \text{ cm}^2$ each. Bromide leaching during the snowmelt experiment **(a)**, bromide leaching during the irrigation experiment **(b)**, PG leaching during the irrigation experiment **(c)**, leaching is given in % from what would have leached in each cell with perfect uniform flow. PG leaching divided by bromide leaching during the irrigation experiment **(d)**, both scaled with the applied solute mass per m^2, given in %.

The spatial patterns in the bromide and PG leaching during the irrigation experiment were similar (Fig. 2.11b, c). Figure 2.11d shows that the PG leaching was generally lower than the bromide leaching (i.e. less than 100 %). In the upper right area of the MCS, the leaching of PG was smallest compared to bromide, but also since little bromide was leached that was not well visible in Fig. 2.11b and c. Thus, the spatial distributions of the leached masses are similar, because the leaching of the non-degradable solute in this area was low as well. The highest PG concentrations, and the highest bromide concentrations can be found in the same areas, but at different times (Fig. 2.5), and the cumulative leached masses were similar. This means that the spatial pattern of the drainage was stable in time during the irrigation experiment.

During the snowmelt experiment, the bromide recovery was 43 %. During the irrigation experiment, the bromide recovery was 42 %, and the PG recovery was 32 %. The low bromide recovery suggests flow bypassing the sampler. However, in a closed lysimeter

experiment from the same area, the bromide recovery was 42 % (Lissner et al., 2011a). Thus, the extent of flow bypassing the sampler is probably much lower than would be expected based on the bromide recovery. On average for all cells and for the entire irrigation experiment, the leaching of PG is 75 % from the bromide leaching, which suggests that 25 % of the PG was degraded during this experiment. As mentioned before, the BTCs of bromide were not complete before the irrigation experiment was stopped, and thus the bromide leaching was underestimated. This implies that the PG degradation was also underestimated.

2.3.4 Quantifying preferential flow

Figures 2.4, 2.5, and 2.11 give a visual representation of the results. In the following section we will quantify differences in the spatial distribution of the leaching of bromide and PG, and the drainage.

For this purpose, the cells are sorted with decreasing drained volume or leached mass, and then cumulated as proposed by Quisenberry et al. (1994), Strock et al. (2001), and De Rooij and Stagnitti (2002). The sorting of the cells removed all spatial information. The cumulative drainage and leaching are plotted as a function of the cumulative sampler area in Fig. 2.12. The cumulative sampler area is defined as the surface area of the number of cells that corresponds to the number of the sorted drained volume or leached mass. In Fig. 2.12, the cells are sorted separately for each experiment and solute. Uniform leaching would give a straight line. Figure 2.12 shows that 50 % of the drainage and leaching occurred in 12–20 % of the sampler area.

The curves for the drainage lie below the curves of the solutes for both experiments. This can be caused by the longer time period of sampling for the drainage. The solutes were applied as a pulse, and therefore, the sampling period was generally slightly shorter than for the drainage. When the peak concentration of bromide already passed, drainage water was still sampled. Precipitation events after the snow had melted, or the different irrigation rates may result in a varying water storage in the soil. This water storage affects the spatial distribution of the drainage. Therefore, it is more correct to use the leaching instead of the drainage, as the leaching is labelled using a pulse, and the drainage volume itself is not labelled. However, we did include the drainage in Fig. 2.12, because the sampling period of drainage is not much larger than of bromide, and the drained volumes and leached masses are distributed differently in space (Figs. 2.4 and 2.5).

The drainage during the snowmelt experiment lies below the drainage during the irrigation experiment, which implies a larger homogeneity, and strengthens the conclusion based on Fig. 2.11.

For bromide mass, the curve of the irrigation experiment lies above the curve of the snowmelt experiment. This means that the bromide leaching was more heterogeneous during the irrigation experiment than during the snowmelt experiment. The distances between the curves of the bromide leaching and of the drainage are different for both experiments in Fig. 2.12. Therefore, we conclude that the heterogeneous solute leaching is both caused by differences in the drainage and the spatial distribution of the solute
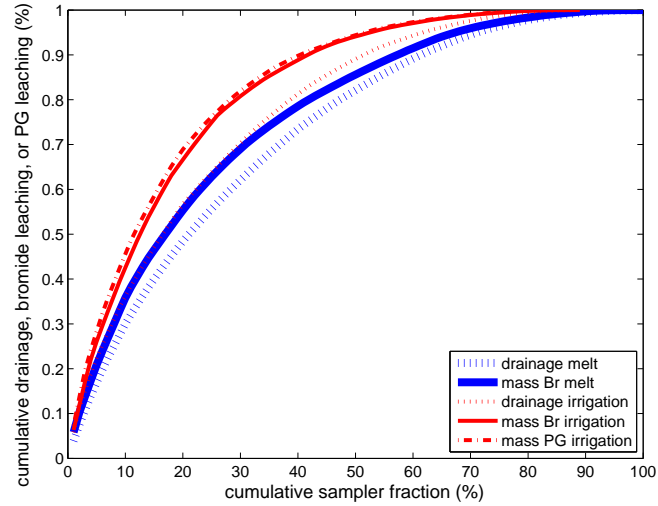
Figure 2.12: Normalised cumulative drainage and leaching of bromide during the snowmelt and irrigation experiments, and PG during the irrigation experiment. The drainage and the leaching per cell were scaled with the total drainage or the total leached mass for the sampler during either the snowmelt experiment or the irrigation experiment. The cells are sorted with decreasing amount of drainage, bromide, or PG leaching.
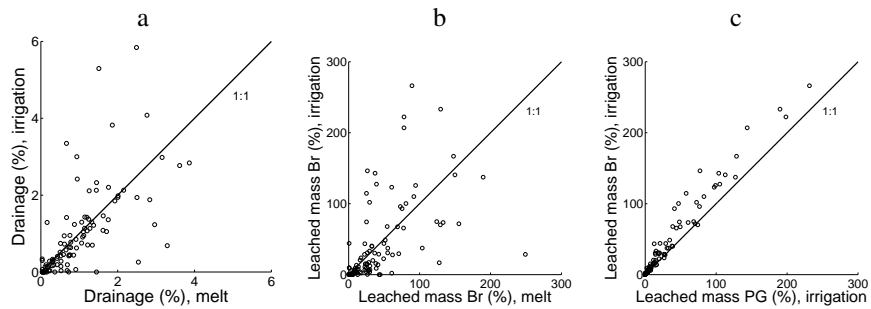
Figure 2.13: Comparison of total leaching per cell. **a**: Drainage of the snowmelt and irrigation experiment. **b**: Bromide leaching of the snowmelt and irrigation experiment. **c**: Bromide leaching and PG leaching of the irrigation experiment. The drainage was scaled with the drainage of the entire sampler of either the snowmelt or irrigation experiment. Solute leaching is given in % from what would have leached in each cell with perfect uniform flow.

27

Table 2.2: Spatial autocorrelation according to Moran's I. A value of 1 indicates perfect spatial autocorrelation, and -0.01 no spatial autocorrelation.

Experiment and drainage/solute	I
Snowmelt drainage (mm)	0.46
Snowmelt bromide (mg)	0.61
Irrigation drainage (mm)	0.14
Irrigation bromide (mg)	0.26
Irrigation PG (mg)	0.30

concentrations. The leaching of bromide and PG during the irrigation experiment was similarly heterogeneous. This was also concluded from Fig. 2.11.

We studied the stability of the preferential flow paths in the field by comparing the drainage and the bromide leaching in each cell in both experiments (Fig. 2.13a, b). The total drainage that occurred during the snowmelt experiment and the irrigation experiment had a low linear correlation coefficient ($R^2 = 0.43$). Also the total bromide leaching that occurred during the snowmelt experiment and the irrigation experiment were not well correlated ($R^2 = 0.56$). We found that the bromide leaching may be different in the exact locations (Fig. 2.13), even though the area of the MCS with the highest bromide leaching is similar for both experiments (Fig. 2.11). Thus, the area with the highest leaching is persistent in time, but the exact locations of the highest leaching might change a bit in time.

Comparing the total bromide leaching with the total PG leaching in each cell in the irrigation experiment (Fig. 2.13c) shows the leached masses per cell were strongly correlated ($R^2 = 0.95$). Thus, with the same infiltration rate, the spatial patterns of the leached masses are similar for a degradable solute and a tracer. In Fig. 2.10, the BTCs for bromide appeared to be different than the BTCs for PG, depending on the division in the fast, average, and slow cells. However, this did not result in a different total PG leaching, relative to the bromide leaching, for the fast, average, and slow cells. Apparently, for solutes with this degradation rate and under this infiltration rate, the travel time distribution does not influence the overall leaching much.

In Figs. 2.12 and 2.13, the cells were approximated as individual stream tubes, while ignoring the possibility of cell clustering. The soil above neighbouring cells could exchange water and solutes, which may have a distinct influence when using a high resolution sampler. We calculated the spatial autocorrelation coefficient of the total drainage and the total leached masses, to determine how the drainage, or the leaching in a particular cell is related to the drainage, or leaching in neighbouring cells. Table 2.2 shows the values for the spatial autocorrelation coefficient I, calculated with Eq. (2.1). With a high spatial autocorrelation coefficient, the cross-sectional area of the preferential flow paths is large, while with a low spatial autocorrelation the preferential flow paths mainly consist of isolated peaks. The spatial autocorrelation was higher for bromide than for the

drainage, for both the snowmelt and the irrigation experiment. As with Fig. 2.12, this may be a result of the slightly shorter sampling time for leaching than for drainage. During the snowmelt experiment, the spatial autocorrelation was higher than during the irrigation experiment. Thus, with high infiltration rates there is more clustering of high leaching cells. This is consistent with Figs. 2.11 and 2.12, which show that with a higher water flux the differences in leaching between the cells are smaller. The reason for this might be that with a higher water flux, a larger part of this coarse textured soil is highly conductive. As expected from Fig. 2.13c, the spatial autocorrelation of PG leaching was similar as that of bromide leaching.

The spatial patterns of the leached masses of bromide and the spatial distribution of the highest bromide concentrations were rather similar for the snowmelt and the irrigation experiment. Therefore, we conclude that soil heterogeneity is the main reason for the heterogeneous water flow and solute transport in this soil. At this scale, the heterogeneous melting of snow does not influence the heterogeneous flow in the soil much. The applied infiltration rate, and the corresponding soil moisture content, influence the differences between the concentrations of the cells. As a result, the areas with the highest leaching were similar for both experiments, but the leached masses in the cells were not highly correlated.

2.4 Conclusions

The leaching of a non-degradable and a degradable solute was measured in two field experiments, with different infiltration rates using a multi-compartment sampler (MCS). The spatial and temporal variability of leaching, and the effect of snowmelt on leaching was quantified, and additionally the leaching of the non-degradable and the degradable solute was compared. One experiment was done during snowmelt, and was characterized by a high infiltration rate from the meltwater. In the other experiment, the soil was irrigated, to mimic homogeneous rainfall with lower infiltration rates.

Regarding the persistence of preferential flow, the highest bromide concentrations were found in the same area for both experiments, and thus were independent of the flow rate. In the snowmelt experiment the spatial differences in the concentrations appeared to be larger than in the irrigation experiment, possibly due to a lower exchange with the surrounding soil (and thus less dilution) caused by the higher infiltration rate.

The highest bromide leaching occurred in the same area for the snowmelt and the irrigation experiments, but not in exactly the same cells. Furthermore, with low infiltration rates, as in the irrigation experiment, there are more isolated peaks in the bromide leaching than in the snowmelt experiment. The heterogeneous flow in the soil, therefore, is probably caused by small changes in the soil hydraulic properties, and not by macropores.

The spatial autocorrelation of the leaching of cells is higher with high infiltration rates. The reason for this might be that with a higher water flux, a larger part of the coarse textured soil is highly conductive.

The highest PG concentrations, and the highest bromide concentrations were found in the same areas in the irrigation experiment. The patterns in the concentrations of a tracer and a degradable solute were similar in space, but not in time, as the leaching of PG started earlier than the leaching of bromide. The leached masses were highly correlated. The leaching of PG was lower than the leaching of bromide, due to degradation.

Soil heterogeneity is the main reason for the heterogeneous water flow and solute transport in this soil. Heterogeneous melting of snow did not influence the heterogeneous flow in the soil much at the scale of the MCS. The applied infiltration rate, and the corresponding soil moisture content, influenced the differences between the concentrations of the cells. As a result the areas with the highest leaching were similar for both experiments, but the leached masses in the cells were not highly correlated.

3

Spatial distribution of solute leaching with snowmelt and irrigation: measurements and simulations

Abstract

Transport of a tracer and a degradable solute in a heterogeneous soil was measured in the field, and simulated with several transient and steady state infiltration rates. Leaching surfaces were used to investigate the solute leaching in space and time simultaneously. In the simulations, a random field for the scaling factor in the retention curve was used for the heterogeneous soil, which was based on the spatial distribution of drainage in an experiment with a multi-compartment sampler. As a criterion to compare the results from simulations and observations, the sorted and cumulative total drainage in a cell was used. The effect of the ratio of the infiltration rate over the degradation rate on leaching of degradable solutes was investigated. Furthermore, the spatial distribution of the leaching of degradable and non-degradable solutes was compared.

The infiltration rate determines the amount of leaching of the degradable solute. This can be partly explained by a decreasing travel time with an increasing infiltration rate. The spatial distribution of the leaching also depends on the infiltration rate. When the infiltration rate is high compared to the degradation rate, the leaching of the degradable solute is similar as for the tracer. The fraction of the pore space of the soil that contributes to solute leaching increases with an increasing infiltration rate. This fraction is similar for a tracer and a degradable solute. With increasing depth, the leaching becomes more homogeneous, as a result of dispersion. The spatial distribution of the solute leaching is different under different transient infiltration rates, therefore also the amount of leaching is different. With independent stream tube approaches, this effect would be ignored.

32

3.1   Introduction

Groundwater contamination by nutrients or chemicals will be enhanced by preferential flow in the unsaturated zone. Preferential flow can be caused by macropore flow (Jarvis, 2007), by small scale differences in hydraulic properties (Roth, 1995), or by water repellency (Van Dam et al., 1990), amongst others. To account for preferential flow in modelling heterogeneous soils, several approaches exist, which were reviewed by Feyen et al. (1998) and Šimunek et al. (2003). Roth (1995) included soil heterogeneity in a numerical model, by the use of a random scaling factor for the retention curve and the saturated hydraulic conductivity, where heterogeneous water flow was studied. Roth and Hammel (1996) extended the study by including solute transport. Roth (1995) showed that the infiltration rate determines which parts of the soil will transport most water and solutes. Another modelling approach is the use of independent stream tubes, which each have a different velocity and dispersion coefficient (Vanderborght et al., 2006; Russo and Fiori, 2009). Solute transport can evolve from a stochastic-convective (independent stream tubes) to a convective-dispersive regime with increasing depth (Seuntjens et al., 2001).

To include soil heterogeneity, a random distribution is needed for the spatial variability of the hydraulic properties like the saturated hydraulic conductivity. This distribution can be based on many samples of a soil profile, on which the hydraulic properties are determined (Rockhold et al., 1996; Hammel et al., 1999). Both used a scaling factor for similar media to define the random distribution of the hydraulic properties (Miller and Miller, 1956; Warrick et al., 1977).

Besides numerous measurements of the soil hydraulic properties, multi-compartment samplers (MCS) can be used to investigate the effect of heterogeneous flow on solute leaching of undisturbed soils in the field (Holder et al., 1991; Quisenberry et al., 1994; Bloem et al., 2009, 2010). The instrument has a porous plate to which suction is applied, and it consists of several cells in which drainage is collected. The volume of the drainage, and the concentration of a tracer or reactive solute are measured in each cell, to quantify the spatial variability in solute leaching. The step from this type of experiments to models that quantify solute leaching under different conditions, has not been made yet.

We use results from experiments with an MCS for transport modelling in a heterogeneous soil, by basing the extent of soil heterogeneity in the model on these experiments. To quantify the spatial variability in solute leaching, and to investigate the effect of infiltration rates on this spatial variability, we performed two field experiments with an MCS in exactly the same location (Schotanus et al., 2012). The first experiment was done during snowmelt, with high infiltration rates. The second experiment was done with irrigation, with lower infiltration rates. In the snowmelt experiment the spatial differences in the solute concentrations were larger than in the irrigation experiment. This is possibly due to lower lateral exchange with a shorter residence time, which results in less dilution, and larger differences in the concentrations. In the irrigation experiment, more isolated peaks in the concentration were found (spatial autocorrelation of 0.26 versus 0.61 during snowmelt), from which can be concluded that heterogeneous flow in the soil was caused by small differences in the soil hydraulic properties. We use these experiments to generate a random field for the scaling factors. This field is then used in a model to further inves-

tigate the effect of the flow rate on the leaching of a tracer and a degradable contaminant. Furthermore, the effect of snowmelt on solute leaching is studied.

A tool to study solute leaching simultaneously in space and time is the leaching surface (De Rooij and Stagnitti, 2002). With a leaching surface, the scaled solute flux density is plotted for each cell of a sampler or model, and the cells are sorted descendingly by total leached mass. Bloem et al. (2008) applied the leaching surface to flow in a heterogeneous aquifer. The leaching surface has not yet been used for degradable solutes. By comparing leaching surfaces of a tracer and of a degradable solute, the effect of a transient flow rate on the heterogeneous leaching of a degradable solute can be investigated.

As experiments with multi-compartment samplers are rarely modelled, and as the leaching surface was not applied yet to degradable solutes, our objectives are to: (1) develop and test a new approach, using multi-compartment sampler data, on which the random field for the scaling factor is based; (2) investigate the effect of the influence of the infiltration rate on the leaching of degradable solutes; (3) apply the leaching surface to degradable solutes.

3.2   Materials and methods

3.2.1   Experiment

A multi-compartment sampler (MCS) (Bloem et al., 2010) was installed at the field station Moreppen, near Oslo Airport, Norway (French et al., 1994). The field station is located in a flat area with coarse glaciofluvial sediments (sand and gravel) (French and Van der Zee, 1999). The soil consists of 15 % fine sand, 75% medium and coarse sand, and 10 % gravel (French et al., 1994). The saturated hydraulic conductivity is 6.65×10^{-4} m s^{-1} (French et al., 2001). The soil surface was covered with short grass. The size of the MCS is 31.5×31.5 cm^2, and consists of 100 separate drainage collectors. The surface of the MCS consists of porous metal plates, to which pressure can be applied. Technical details about the MCS can be found in Bloem et al. (2010).

From a trench a horizontal tunnel was dug, leaving the soil above this tunnel undisturbed. The MCS was installed at 68 cm from the trench wall, and at 51 cm below the soil surface (Fig. 2.1). A 2 mm thick layer of wetted soil from the tunnel was applied to the surface of the MCS, to ensure a good contact between the MCS and the soil above it. After installation, the tunnel was backfilled, to avoid boundary effects. Four tensiometers were installed near the trench wall, at the same depth as the MCS. The average pressure head, which was measured by these tensiometers was applied to the MCS, plus 15 cm extra pressure head to compensate for a pressure head drop in the porous metal plates (Bloem et al., 2009). The pressure in the MCS varied in time.

Two experiments were done, while the MCS remained in the same location: one during snowmelt (26 March–23 May 2010) and one with irrigation (23 May–4 July 2010). For the snowmelt experiment 1092 g m^{-2} propylene glycol (PG) and 10 g m^{-2} bromide was diluted in 2 L m^{-2}, and sprayed homogeneously on top of an undisturbed snow cover (26 March 2010). De-icing fluid (Kilfrost, 2012) containing PG was diluted to reach this

a   b
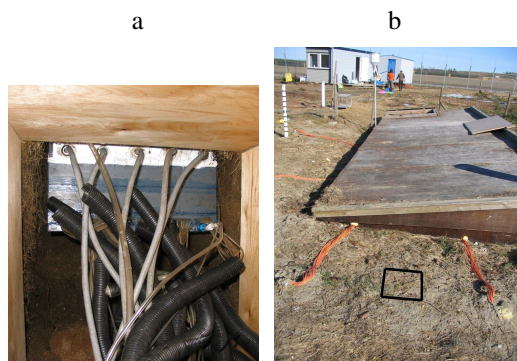
Figure 3.1: Experimental setup. **a**) Installation of the multi-compartment sampler (MCS), shown from the trench. **b**) The location of the MCS shown from above. The marked square indicates the location of the MCS, 51 cm below soil surface. The roof of the trench is visible in the background. The width of the MCS is 31.5 cm.

applied mass. The application area was sufficiently large, such that boundary effects can be ignored. No ice layer was observed under the snowcover, on top of the soil surface. Thus, no ponding could occur on top of the soil surface.

For the irrigation experiment $1103 \, \text{g} \, \text{m}^{-2}$ PG and $10 \, \text{g} \, \text{m}^{-2}$ bromide was diluted in $5 \, \text{L} \, \text{m}^{-2}$, and sprayed homogeneously on the soil surface at 23 May 2010. In between the irrigations, the soil surface was covered with plastic, to prevent evapotranspiration and the infiltration of rainwater. By means of a nozzle, the soil surface was irrigated with tapwater, aside from 12 June. This was a rainy day and 7.8 mm of rainwater infiltrated, while the plastic was removed from the soil surface. On 13 June, 7.5 mm water was irrigated. The irrigation rate was around $6.6 \, \text{mm} \, \text{h}^{-1}$. This was low enough, such that neither surface runoff, nor ponding was observed. Between 31 May and 2 June, evaporation was measured in a pan under the plastic. The measured evaporation was $1 \, \text{mm} \, \text{d}^{-1}$. These were warm days, the average evapotranspiration rate during the entire irrigation experiment probably was lower.

Drainage was stored in the MCS, the sampling scheme depended on the amount of drainage. For the snowmelt experiment, samples were taken every day from 1 April until 15 April. Thereafter, samples were taken at 17 and 21 April, and 9 and 23 May. During the irrigation experiment, samples were taken every second day, on the same day as, and prior to, the irrigations. After collecting, the volumes of the samples were measured by weighing. If a sample was smaller than 4 ml, it was too small to measure the bromide concentration, and it was stored cool. In the next sampling round, the new sample was added to this stored small sample. In samples larger than 4 ml, the bromide concentration was measured with an Orion 9635BNWP Bromide Ion Selective Electrode. Moreover, in the irrigation experiment, the PG concentration was measured with gas-chromatography (Trace GC Ultra, Thermo Scientific). We assumed that degradation of PG during the

35

snowmelt experiment was low, as the soil temperature was low, and the PG concentration in the applied solution was high (Jaesche et al., 2006). Therefore, the PG concentration was not measured in the snowmelt samples.

More details about the experiments can be found in Schotanus et al. (2012).

3.2.2 Models

To simulate the results of the experiment, we used Hydrus-2D, which is a model that can simulate water and solute transport in variably saturated porous media (Šimunek and Sejna, 1999). We did not intend to simulate the results of the experiment such that the simulated and the experimental leaching were similar in exactly the same location in the horizontal plane. Instead, we were looking for a distribution of the soil hydraulic properties in a vertical plane, which will give the same spatial variability of drainage, throughout the entire experiment. The simulated drainage was sorted and cumulated, and then compared to the measured sorted and cumulated drainage. The degree of correspondence was determined with the mean absolute error. We used a model because the breakthrough curves (BTCs) of the experiment were truncated, because the time for the experiment was limited. From the modelling we can use the complete BTCs, and thus study the leaching of a degradable solute and a tracer in more detail.

For the saturated hydraulic conductivity and the pressure head, the standard deviation, and the correlation lengths in depth and width direction were determined with Hydrus-2D, using the spatial distribution of the drainage. The parameter set resulting in the smallest deviation between observed and calculated drainage was selected. As a criterion for the selection of the most appropriate random distribution for this soil, the total drainage per cell was used, sorted in a decreasing order, and then cumulated. Random fields with Miller-similarity were generated in Hydrus-2D. For details on the generation of these fields, we refer to the Hydrus manual (Šimunek and Sejna, 1999). A vertical plane of 2 m width and 1.5 m deep was used. The groundwater level was fixed at 1.5 m depth. The actual groundwater table is situated at 4 m depth. As the soil has a coarse texture, the groundwater did not influence the leaching at 0.5 and 1 m deep, which were the depths of interest in this study. Density driven flow was ignored. The degradation of propylene glycol depends on temperature (Jaesche et al., 2006), but this was ignored. Degradation was modelled as a first-order process, with a half-life time τ of 10 d. In the field, the half-life time of PG can be up to 17 d (French et al., 2001), however, the half-life time can vary in time, for instance as soil temperature or wetness vary. Adsorption was not considered to occur in the model (French et al., 2001).

Output of concentrations and water flow velocities were given four times a day. In the comparison between the leaching surfaces of the snowmelt experiment and the simulation, the simulated values are aggregates to once a day, because the measurements were done daily.

The upper boundary was an atmospheric flux. To investigate the effect of the atmospheric flux on solute leaching, three different atmospheric input fluxes were used, measured at the wheather station at the airport where the field station is situated: the snowmelt of the year 2010, and the year 1997, with and without snowmelt (Fig. 3.2). The
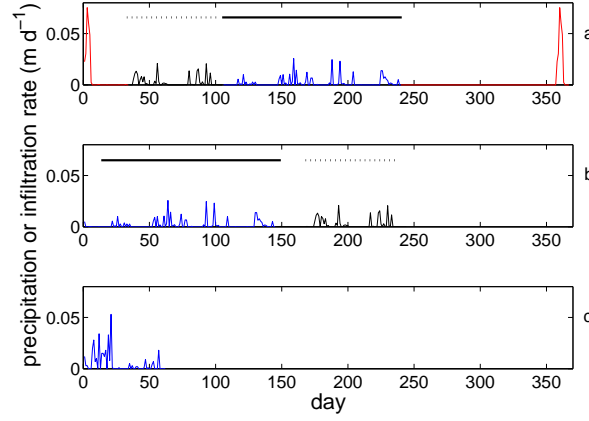
Figure 3.2: Precipitation or infiltration rate. **a)** 1997 with snowmelt, solute application with a pulse of 6 days, snowmelt from day 1 to 6, length of weather series is 367 days. **b)** 1997 without snowmelt, solute application with a pulse of 1 day, length of weather series is 244 days. The lines indicate equal parts of the precipitations series in **(a)** and **(b)**. **c)** Snowmelt experiment 2010, solute application with a pulse of 1 day, length of weather series is 62 days. The day is the number of days since the first solute application.

year 1997 is a generally dry year, but had a thicker snowcover than the year 2010. For the year 2010, the infiltration rate was calculated from the snowmelt and precipitation, which was measured at the field site (Schotanus et al., 2012). For the year 1997, we made an approximation for snow formation and melt in a pre-processing routine:

$$S(t) = bP(t) \qquad\qquad \text{if } T(t) < 0 \qquad\qquad (3.1)$$

$$M(t) = c\left(T(t) - T_{melt}\right) \qquad \text{if } T(t) > T_{melt} \qquad\qquad (3.2)$$

$$B(t) = (1 - 1/b)\, D(t) \qquad\qquad\qquad (3.3)$$

where S is the snowdepth (m), b is a fitting parameter (m snow/m water), P is the precipitation (m), T is the temperature (°C), M is the snowmelt, c is a fitting parameter (m °C^{-1}), T_{melt} is the critical temperature for snowmelt (°C), B is the total storage available for water in the snowcover (i.e. porosity of the snowcover $\times$ depth of the snowcover, m), D is the depth of the snowcover (m). Fresh snow S is added to the snowcover D. When the temperature is higher than 0 °C, P and M are added to the fluid water depth W. When W exceeds B, this is called infiltration. The resulting infiltration rate was used as precipitation in Hydrus-2D. The parameters b and c were fitted with data from other years, and were 8 m snow/m water, and 0.001 m °C^{-1}, respectively. For the year 1997 without snowmelt, the high infiltration rate from the snowmelt, and the low infiltration rate during winter time were removed, and only the precipitation was used. For the year 1997 with snowmelt, solute application started at the beginning of the snowmelt.

Just before snowmelt, the soil is dry, as there is no infiltration during winter, because all precipitation is stored in the snowcover. For the year 1997 without snowmelt, there is infiltration throughout the year, as precipitation is not stored in the snowcover. Therefore, for the year 1997 without snowmelt, the soil moisture content is higher at the moment of solute application than for the year 1997 with snowmelt. In Fig. 3.2b the same infiltration rate is used as in Fig. 3.2a, but the day of solute application differs, and thus the infiltration rate is shifted in the Figure. By using time periods with different colours, the shifting in time is made clear.

3.2.3 Data analysis

Moment's analysis is used to characterize the average transport of the solute plume (Burr et al., 1994). The first temporal moment of the concentration is the mean breakthrough time (Govindaraju and Das, 2007):

$$M_1(z) = \frac{\int_{t=0}^{t=T} C(z,t)t\mathrm{d}t}{\int_{t=0}^{t=T} C(z,t)\mathrm{d}t} \tag{3.4}$$

where $M_1(z)$ is the mean breakthrough time (d), z is depth (L), which is 0 at soil surface, t is the time (d), and C is the solute flux concentration ($\mathrm{M\,m^{-3}}$).

The leached mass is calculated as the sum of the convective and the dispersive flux (Kreft and Zuber, 1978):

$$\mathrm{LM}(z,t) = v(z,t)C(z,t) - D\frac{\partial C(z,t)}{\partial z} \tag{3.5}$$

where LM is the leached mass (M), v is the water flux ($\mathrm{m\,d^{-1}}$), and D is the dispersion coefficient ($\mathrm{m^2\,d^{-1}}$).

From the leached mass, the solute flux density is calculated ($\mathrm{M\,L^{-2}\,T^{-1}}$), which is the leached mass per area at a certain depth per time interval. To visualize the data from the experiments and the simulations, we use leaching surfaces (De Rooij and Stagnitti, 2002). In a leaching surface the leaching in space and time is shown simultaneously. The cells are sorted descendingly by the cumulated leaching per cell. This means that in the leaching surface the high leaching cells can be found at a low cumulative area, whereas the low leaching cells can be found at a high cumulative area. The solute flux density is scaled with the total leaching of all cells ($\mathrm{M\,L^{-2}}$ for the experiment, and $\mathrm{M\,L^{-1}}$ for the simulations). We use the total tracer leaching to scale the solute flux density of the degradable solute. In the snowmelt experiment, the bromide recovery was 43%. In the irrigation experiment, the bromide recovery was 42%, and the PG recovery was 32% (Schotanus et al., 2012). De Rooij and Stagnitti (2002) use a 3-D plot for the leaching surfaces. We use 2-D plots with a colour scale, because 2-D plots are easier to interpret, and to compare with each other.

The leaching surface has two marginals: one in the time axis and one in the spatial axis. The marginal in the time axis is the breakthrough curve of the total area, and the marginal in the spatial axis is the spatial solute distribution. The spatial distributions of
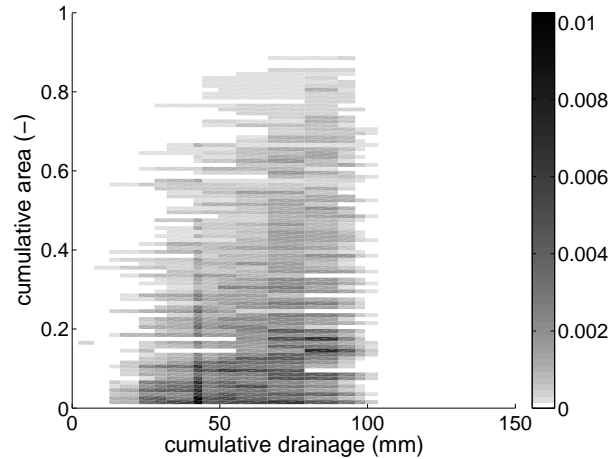
Figure 3.3: Scaled solute flux density (d^{-1}) for bromide for the snowmelt experiment.

the solute leaching under different conditions can be compared by comparing the marginal in the x-axis of the leaching surfaces. The leaching surfaces will be compared with the following characteristics: the instant that the leaching starts (i.e. the amount of cumulative drainage until the first detectable concentration), the magnitude of the solute flux density, the tailing, and the fraction of the soil that contributes to solute leaching. In a cell or node that does not contribute to leaching, no drainage occurs, or the concentration is 0, both throughout the experiment.

3.3 Results and discussion

3.3.1 Leaching surfaces from experiments

Figure 3.3 shows the 2-D leaching surface of bromide during the snowmelt experiment. To facilitate the comparison between the different experiments, the cumulative drainage since solute application is used as a time axis, instead of the number of days, in accordance with Wierenga (1977). In a leaching surface, the highest leaching cells can be found at a low cumulative area. The amount of leaching decreases with an increasing cumulative area. For the snowmelt experiment, the instant that the leaching in a cell starts, is generally later with a decreasing amount of leaching. Generally, the leaching per day decreased with a decreasing leached amount per cell. The experiment was stopped after 111 mm of drainage, which explains the lack of bromide leaching thereafter. About 85% of the cells contribute to the leaching. The CV in the drainage of the cells was 0.9, the CV of the leached bromide was 1.1.

39
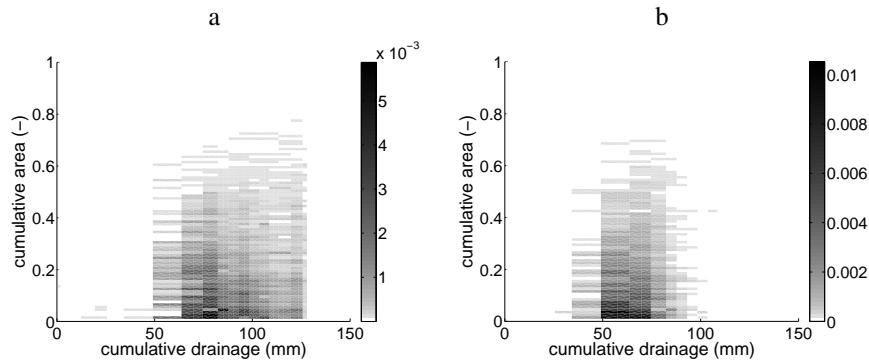
Figure 3.4: Scaled solute flux density (d^{-1}) for the irrigation experiment, bromide **(a)**, propylene glycol **(b)**.

Figure 3.4a shows the leaching surface of bromide during the irrigation experiment. Here, the leaching of the high and mean leaching cells starts at the same time, after 50 mm drainage. The leaching starts after a larger amount of drainage than in the snowmelt experiment (20 mm), because the soil was wetter at the beginning of the irrigation experiment than of the snowmelt experiment (pressure head was -27 cm and -35 cm, respectively). The highest solute flux density observed in any of the cells is lower than in the snowmelt experiment (0.005 against 0.01 d^{-1}), probably caused by the lower water flux in the irrigation experiment (6 mm d^{-1} during irrigation, and 16 mm d^{-1} during snowmelt on average). Fewer cells than in the snowmelt experiment contribute to the leaching, about 70 %. This is supported by the CV in the drainage of the cells, which was 1.1, higher than in the snowmelt experiment. The CV of the leached bromide was 1.3, also higher than in the snowmelt experiment.

Figure 3.4b shows the leaching surface of propylene glycol (PG) during the irrigation experiment. In most cells, the leaching of PG starts earlier than of bromide. After 50 mm of drainage, the solute flux density of PG is higher than of bromide, which is possibly caused by density driven flow. The density of pure de-icing fluid is 1.043 times the density of pure water (Kilfrost, 2012). After dilution the density of the applied solution was approximately 1.005 times the density of water. The tailing is less, probably due to degradation of PG. Slightly fewer cells contribute to the leaching of PG than of bromide, 70 %, which also can be caused by degradation.

The solute leaching becomes more homogeneous with an increasing infiltration rate (comparing Figs. 3.3 and 3.4a). If the heterogeneous leaching would be caused by macropores, the leaching would become more heterogeneous with an increasing infiltration rate (Jarvis, 2007). Therefore, it is concluded that the heterogeneous leaching is caused by small scale differences in the soil hydraulic properties. The soil heterogeneity can thus be described with Miller-similarity.
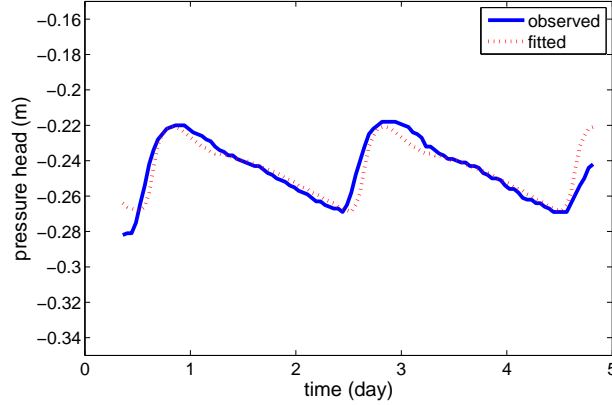
Figure 3.5: Observed and fitted pressure heads at 0.5 m depth for the irrigation experiment.

3.3.2 Model parameterisation

The observations from the irrigation experiment will be used to fit the parameters of the model, because in this experiment the atmospheric boundary condition is well known. Using the inverse mode in Hydrus-2D, the parameters α and n from the van Genuchten equations (Van Genuchten, 1980) were fitted to the measured average pressure heads at 0.51 m depth, where the MCS was located. Figure 3.5 shows the observed and simulated pressure heads at 0.5 m for the irrigation experiment. The optimal value for α was 14.85 m^{-1} (95 % confidence interval: 14.38–15.30) and for n 3.165 (-) (95 % confidence interval: 3.09–3.24). The linear regression coefficient between the observed and fitted values (R^2) was 0.83. The values of the other soil hydraulic parameters were the residual water content $\theta_{\mathrm{r}} = 0.045$ m^3 m^{-3} (from the cathegory "sand", Carsel and Parrish (1988)), the saturated water content $\theta_{\mathrm{sat}} = 0.33$ m^3 m^{-3} (measured), and the saturated hydraulic conductivity $K_{\mathrm{sat}}=6.65 \cdot 10^{-4}$ m s^{-1} (French et al., 2001).

After fitting the soil physical parameters, the standard deviation and the correlation lengths in width x and depth z direction were varied manually for K_{sat} and the pressure head h. The parameter set resulting in the smallest deviation between observed and calculated drainage was selected. As a criterion for the selection of the most appropriate random distribution for this soil, the total drainage per cell was used, sorted in a decreasing order, and then cumulated. Random fields with Miller-similarity were generated in Hydrus-2D. First, the spatial discretization needed to capture all small scale processes was chosen. A random field with standard deviation $\sigma = 0.5$, correlation length in x-direction $\lambda_x = 0.05$ m, and correlation length in z-direction $\lambda_z = 0.6$ m was used to simulate the irrigation experiment, with spatial discretisations of 0.0125 and 0.025 m. The values for σ, λ_x, and λ_z were chosen such that they are extreme values, with a high standard deviation, and correlation lengths that lead to narrow and long flow channels. These values

41
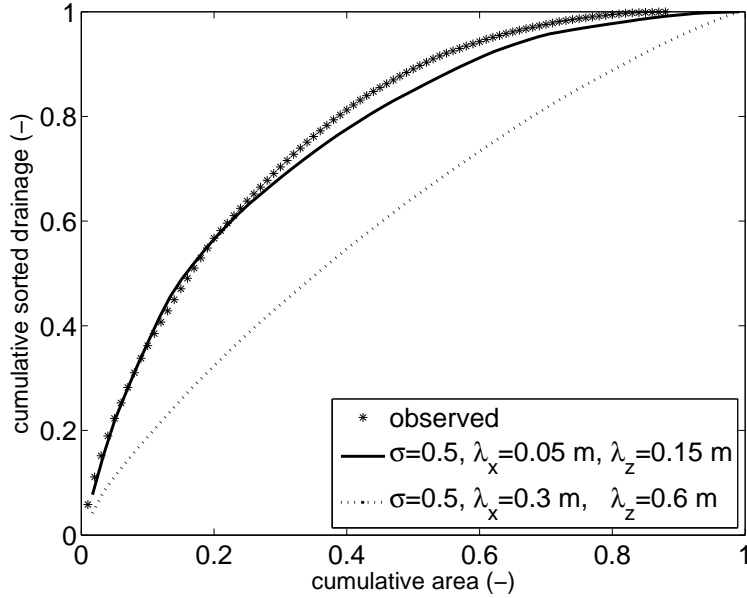
Figure 3.6: Sorted observed drainage, and simulated with two standard deviations and correlation lengths for generated random fields with Miller–similarity.

are only used to test the discretisation, for other simulations other parameter values will be used. The sorted cumulated drainage was similar for the discretisations of 0.0125 and 0.025 m. Therefore, we use a spatial discretisation of 0.025 m, as it captures the small scale processes, and saves computation time. Furthermore, it is concluded that a spatial discretisation of 0.025 m is small enough, when a correlation length of 0.05 m is used. This result is in constrast with Ababou et al. (1989), who found that the spatial discretisation should be at least four times smaller than the correlation length. As the values for σ, λ_x, and λ_z were extreme values, the conclusion that a discretisation of 0.025 m is sufficient, should also hold for smaller σ, larger λ_x, and smaller λ_z. The cell size of the multi-compartment sampler is $0.0315 \times 0.0315 \, m^2$, similar as the discretisation.

In a preliminary investigation of the most suitable parameters for these random fields, σ was 0.1, 0.25, 0.5 or log(0.15), λ_x was 0.05, 0.1, 0.15, 0.2, 0.3 or 0.4 m, and λ_z was 0.1, 0.15, 0.2, 0.3, 0.4 or 0.6 m. With these parameter values, random fields for the scaling factor were generated, which were used to simulate the irrigation experiment. Figure 3.6 illustrates the criterion for the observed sorted drainage and the results from two simulations. In this figure the mean absolute error between the observed and simulated cumulated and sorted drainage is 0.022 and 0.19 (-).

After the preliminary investigation, five parameter sets were selected ($\sigma = 0.5$, $\lambda_x = 0.05$ m, $\lambda_z = 0.6$ m; $\sigma = 0.25$, $\lambda_x = 0.05$ m, $\lambda_z = 0.6$ m; $\sigma = 0.5$, $\lambda_x = 0.3$ m, $\lambda_z = 0.6$ m; $\sigma = 0.5$, $\lambda_x = 0.05$ m, $\lambda_z = 0.15$ m; $\sigma = 0.5$, $\lambda_x = 0.1$ m, $\lambda_z = 0.15$ m).

42

Table 3.1: Mean and standard deviation of the mean absolute error between observed and simulated sorted and cumulated drainage of five realisations, for the irrigation experiment and the snowmelt experiment.

Experiment	Standard deviation	Correlation length in width (m)	Correlation length in depth (m)	Mean mean absolute error	Standard deviation mean absolute error
Irrigation	0.5	0.05	0.6	0.043	0.014
	0.25	0.05	0.6	0.14	0.036
	0.5	0.3	0.6	0.13	0.050
	0.5	0.05	0.15	0.054	0.020
	0.5	0.1	0.15	0.094	0.025
Snowmelt	0.5	0.05	0.6	0.051	0.027
	0.5	0.05	0.15	0.039	0.032
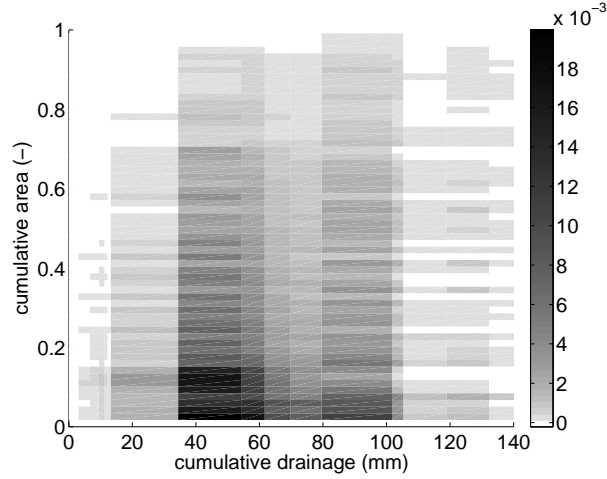
Figure 3.7: Scaled solute flux density (d^{-1}) for tracer, at 0.5 m depth, for the simulated year 2010.

These were used to generate five random fields for each parameter set, to investigate the effect of a particular field, within a parameter set, on the selection criterion. The resulting twenty-five random fields were used to simulate the irrigation experiment. The mean absolute error between the observed and simulated cumulated and sorted drainage was calculated (Table 3.1). The mean absolute error depends on both the particular random field, and on the parameters of the random field. From Table 3.1 is concluded that $\sigma = 0.5$, and $\lambda_x = 0.05$ m give results that correspond best with the observed data. The λ_z does not influence the mean absolute error much. The fields with the two best parameter sets ($\sigma = 0.5$, $\lambda_x = 0.05$ m, $\lambda_z = 0.6$ m; $\sigma = 0.5$, $\lambda_x = 0.05$ m, $\lambda_z = 0.15$ m) were used to simulate the snowmelt experiment. Again, the mean absolute error between the observed and simulated cumulated and sorted drainage was calculated. Table 3.1 shows that $\sigma = 0.5$, $\lambda_x = 0.05$ m, $\lambda_z = 0.15$ m gives the smallest mean absolute error for the snowmelt experiment.

To further examine whether the parameterisation of the model is a good representation of the field site, first we compare the leaching surfaces of the measurements of the snowmelt experiment (Fig. 3.3), and the simulation of the snowmelt experiment (weather series of Fig. 3.2c). Figure 3.7 shows the leaching surface from the simulation of the snowmelt experiment with the realisation with the parameters $\sigma = 0.5$, $\lambda_x = 0.05$ m, $\lambda_z = 0.15$ m that had the smallest mean absolute error. Leaching starts after 15 mm of drainage. After 40 mm of drainage the highest solute flux density occurs in both the experiment and the simulation. To compare the magnitudes of the solute flux densities, the solute flux density of the simulation should be corrected with 59/100, as the simulation consists of 59 cells, and the experiment of 100 cells. The maximum solute flux density is slightly larger for the simulation (0.010 and 0.012 d^{-1}). In the experiment 90 % of the
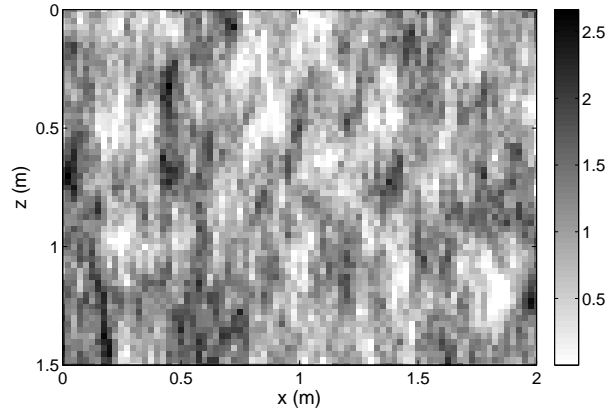
Figure 3.8: Scaling factor of the saturated hydraulic conductivity (-) in depth z and width x, with a standard deviation of 0.5 m and correlation lengths λ_z=0.15 m and λ_x=0.05 m.

soil contributes to solute leaching, against 98 % in the simulation. The mean absolute error between the observed and simulated cumulated and sorted solute leaching was 0.018 (-), which is smaller than the mean absolute error for the drainage for this random field (0.022).

Comparing Figs. 3.3 and 3.7, we conclude that the model captures the magnitude and moment of leaching of the experiment sufficiently well. Comparing the marginal of the spatial axis, which is the spatial distribution of the solute leaching, the model corresponds well with the experiment. Therefore, we conclude that the parameters $\sigma = 0.5$, $\lambda_x = 0.05$ m, $\lambda_z = 0.15$ m can be used to quantify the heterogeneity of this soil. The realisation with these parameters that had the smallest mean absolute error was selected for further simulations, to study the effect of different infiltration rates on the heterogeneous solute leaching in more detail. Figure 3.8 shows the random field for the scaling factor of the saturated hydraulic conductivity with $\sigma = 0.5$, $\lambda_x = 0.05$ m, $\lambda_z = 0.15$ m which is used in the simulations.

When the total leached amount of the cells in Fig. 3.7 is related to the scaling factor in the particular cells at 0.5 m depth (Fig. 3.8), the leached amount generally decreases with an increasing scaling factor. The saturated hydraulic conductivity (French et al., 2001) is high compared to the water flux (respectively 57 m d^{-1} versus 0.016 m d^{-1}). As a result, the parts of the soil where the scaling factor is lowest, transport most water and solutes, as was shown by Roth (1995). Where the scaling factor is small, the saturated hydraulic conductivity is still high, because of the high mean saturated hydraulic conductivity, therefore, transport is fast in this soil.
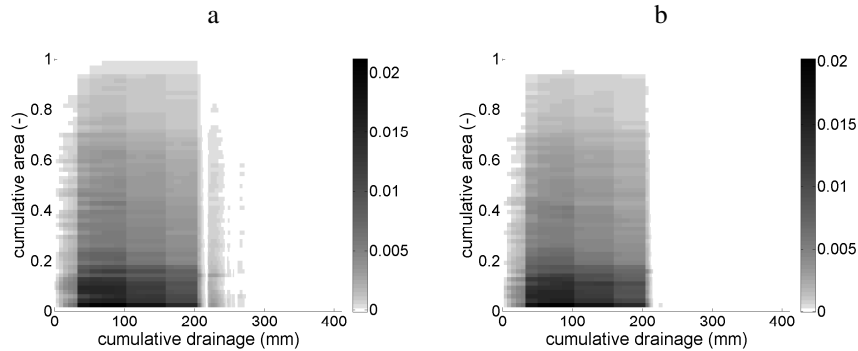
Figure 3.9: Scaled solute flux density (d^{-1}) from simulations, at 0.5 m depth, for the year 1997. **(a)**. Tracer, **(b)**. Degradable solute (half-life time τ=10 d).

3.3.3 Leaching surfaces from model

Transient simulations

To investigate the effect of snowmelt on the leaching of a tracer and a degradable solute, a simulation with the weather series of the year 1997 with snowmelt (Fig. 3.2a) was done. Figure 3.9a shows the simulated leaching surface for a tracer at 0.5 m depth with the random field of Fig. 3.8. The depth of the snowcover was 240 mm. In the highest leaching cells, the leaching starts immediately with the drainage. The magnitude of the solute flux density is higher as for the experiment and Fig. 3.7. The highest solute flux density occurs after 40 mm of drainage, similar as in the experiment and in Fig. 3.7. The highest solute flux density continues longer, because the snowcover is thicker, and the solute was applied during the snowmelt period, which was 6 days. The entire soil contributes to solute leaching during the snowmelt. After 210 mm, when all snow had infiltrated, there is some drainage with little solute. The solute still leaches, but due to the low drainage, the solute flux density is very small. Then, after a precipitation event, the water and solute fluxes increase again. In the first precipitation events since snowmelt (after 220 mm of drainage), the leaching occurs in 80 % of the cells. The percentage of the soil that contributes to solute leaching decreases with increasing time since snowmelt.

In Fig. 3.9a the solute flux density is relatively high in the entire area, which larger than in Figs. 3.3, and 3.7. This can be caused by the higher infiltration rate in the year 1997, as the snowcover was thicker in 1997 than in 2010, this results in a higher water content of the soil. As a result, a larger fraction of the soil is highly conductive than in 2010.

Figure 3.9b shows the simulated leaching surface for a degradable solute with half-life time τ=10 d. Until 210 mm (during snowmelt), the leaching of the degradable solute is similar as of the tracer, both in space and time. Also the magnitude of the solute flux density is similar. This means that the infiltration rate is high compared to the degradation
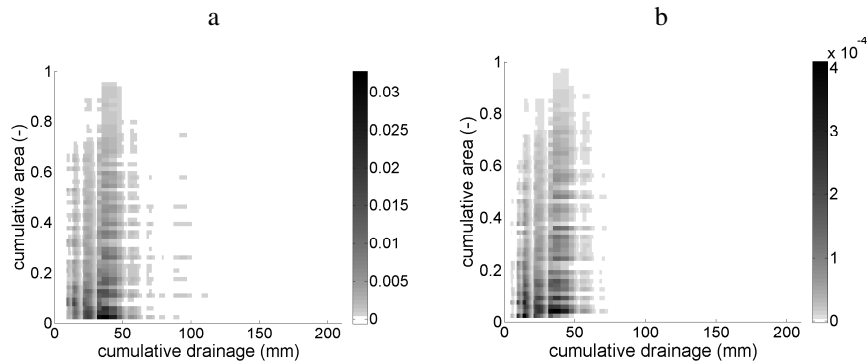
Figure 3.10: Scaled solute flux density (d^{-1}) from simulations, at 0.5 m depth, for the year 1997 without snowmelt. **(a)**. Tracer, **(b)**. Degradable solute (half-life time τ=10 d).

rate of the solute. After 210 mm, the leaching of the degradable solute differs from the leaching of the tracer. After a precipitation event, at 220 mm drainage, the tracer leaches in approximately 80 % of the cells, while the degradable solute leaches in only 1 % of the cells. The reason for this is that the degradable solute is mostly degraded in the period between the snowmelt and the precipitation event, which is 32 days long. As a result, then the solute flux density of the degradable solute is smaller than for the tracer.

From Figs. 3.3, 3.7, and 3.9 can be concluded that the leaching surface is highly influenced by the snowmelt. This is caused by the high water flux, which results in a high solute flux. To study the effect of the snowmelt on the leaching surface, we also performed a simulation without snowmelt, but with only the precipitation from the year 1997. The weather series is given in Fig. 3.2b. The high infiltration rate during snowmelt, and the low infiltration rate during winter were removed from the weather series. The day of the solute application is different in Fig. 3.2a and b, therefore the infiltration rate is shifted in time. Figure 3.10a shows the leaching surface of a tracer with a pulse and with the weather series 1997 without snowmelt. Leaching starts after 10 mm of drainage, in the highest leaching cells. This is later than in Fig. 3.9a, because the soil moisture content is higher without the low infiltration rates during winter time with snowmelt. With decreasing leached solute mass (i.e. increasing cumulative area), the cumulative drainage at which solute leaching starts in a cell increases, as was also the case in Figs. 3.3 and 3.4. Without snowmelt, the highest solute flux density in a cell is higher than with snowmelt. The solute flux density highly depends on the precipitation rate, leaching only occurs after a precipitation event. In between precipitation events, water may drain, but the solute flux density is much lower than after a precipitation event, as the amount of drainage per day is much lower.

Figure 3.10b shows the leaching surface of a degradable solute with a pulse, and with the weather series of Fig. 3.2b. The magnitude of the maximum solute flux density is about 80 times lower as for the tracer (Fig. 3.10a). This ratio is lower than in the simu-

Figure 3.11: Scaled solute flux density (d^{-1}) from simulations, at 0.5 m depth, for a steady state atmospheric flux of 2.5 mm d^{-1}. **(a)**. Tracer, **(b)**. Degradable solute (half-life time τ=10 d).

lations with snowmelt, where the maximum solute flux density of the degradable solute is similar as of the tracer. The lower solute flux density is caused by the longer residence time in Fig. 3.10 than in Fig. 3.9, which leads to more degradation. In contrast to Fig. 3.9, in Fig. 3.10, the infiltration rate is low compared to the degradation rate of the solute. Tailing is less for the degradable solute than for the tracer. The tracer still leaches after a precipitation event around 100 mm of drainage, while the degradable solute hardly leaches anymore at that time. The fraction of the soil that contributes to solute leaching is similar for the degradable solute and the tracer, which is about 95 %.

Steady state simulations

As solute leaching is shown to depend on the distribution of the infiltration rate, also a steady state simulation is done with the same random field for the saturated hydraulic conductivity (Fig. 3.8). Figure 3.11a shows the leaching surface for a steady state simulation for a tracer. The infiltration rate was 2.5 mm d^{-1}, which is the average infiltration rate in the snowmelt simulations (averaged over 365 days). In the steady state simulation, the moment of leaching generally increases with decreasing total leaching in a cell, like in the transient simulations. The highest solute flux density is lower than for the transient simulations (0.007 m^{-2} d^{-1}). Approximately 90 % of the cells contribute to the solute leaching, which is less than in the transient simulation during snowmelt (100 %). This is probably caused by the higher soil moisture content during snowmelt in the transient simulations, due to the high infiltration rate. As a result, a larger fraction of the soil is highly conductive. Thus, the leaching is different in a transient simulation than in a steady state simulation. Meyer-Windel et al. (1999) experimentally found that solute breakthrough was similar for transient and steady state conditions in a sandy soil. Kuntz and Grathwohl (2009) found that steady state flow can be used instead of transient flow, except when

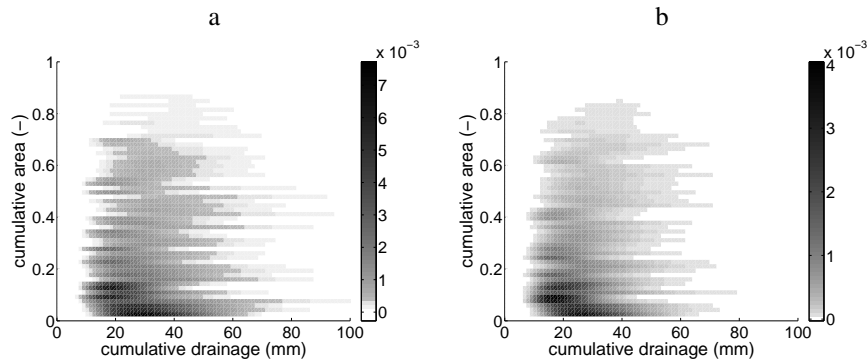a   b
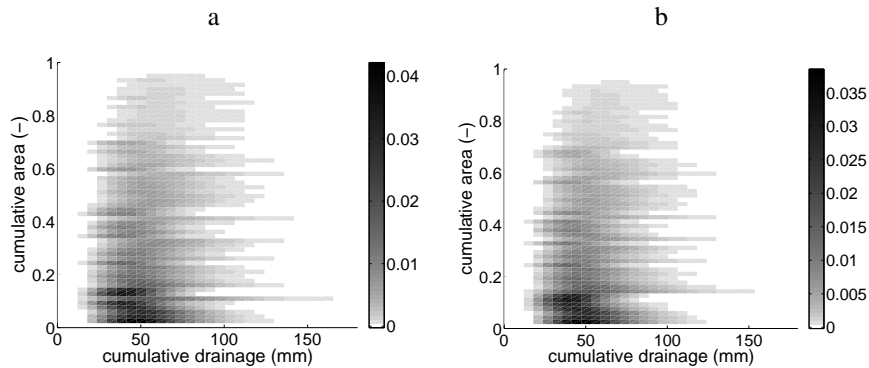
Figure 3.12: Scaled solute flux density (d^{-1}) from simulations, at 0.5 m depth, for a steady state atmospheric flux of 25 mm d^{-1}. **(a)**. Tracer, **(b)**. Degradable solute (half-life time τ=10 d).

extreme infiltration events occur. Then, solute leaching was higher in transient simulations than in steady state. On the contrary, in a numerical study Russo et al. (1998) found that transient flow enhances lateral dispersion, mostly at shallow depths. We found that a larger area contributes to solute leaching in the transient simulation, but this is attributed to the higher soil moisture content, not to lateral dispersion.

Figure 3.11b shows the leaching surface for a steady state simulation for a degradable solute, with an infiltration rate of 2.5 mm d^{-1}. For the degradable solute, the solute flux density is lower, and the tailing is shorter, due to degradation. The fraction of the soil that contributes to solute leaching is similar for the tracer (88 %) and the degradable solute (86 %) in the steady state simulation. When the marginals of the leaching surfaces in the x-axis are compared, the leaching of the degradable solute is more heterogeneous than of the tracer. This suggests that the heterogeneous soil influences the leaching of the degradable solute more, due to the differences in the travel time, which result in different leached fractions.

To study the influence of the flow rate on the leaching surface, also a steady state simulation with an infiltration rate of 25 mm d^{-1} was done (Fig. 3.12a). The solute flux density is higher with an infiltration rate of 25 mm d^{-1} than of 2.5 mm d^{-1}, because the water flux is higher. The fraction of the soil that contributes to solute leaching increases with an increasing infiltration rate (96 %). Figure 3.12b shows the leaching surface of a degradable solute with an infiltration rate of 25 mm d^{-1}. With a high infiltration rate, the tailing of the degradable solute is more similar to the tailing of the tracer than with a low infiltration rate. When the marginals of the leaching surfaces of the tracer and the degradable solutes in the x-axis are compared, the leaching of the degradable solute is similar as of the tracer, with an infiltration rate of 25 mm d^{-1}, while they differed when the infiltration rate was 2.5 mm d^{-1}. With an infiltration rate of 25 mm d^{-1}, the infiltration

49
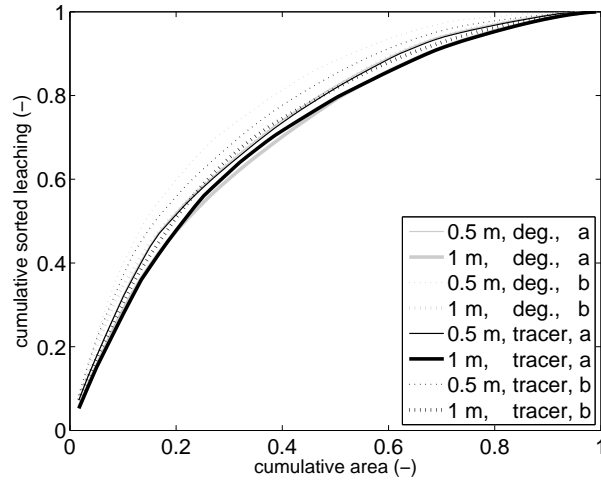
Figure 3.13: Sorted and cumulated leached solute masses at 0.5 and 1 m depth, for a tracer and degradable solute (half-life time τ=10 d), in the legend a is used for 1997 with snowmelt, and b is used for 1997 without snowmelt.

rate is high compared to the degradation rate, therefore there is little time for degradation and thus the spatial distribution of the degradable solute and the tracer are more similar.

In an artificial medium consisting of three different types of sand, Rossi et al. (2008) found that solute mixing between the different types of sand increased with an increasing flow rate. Our results confirm this conclusion. Opposed to a spatially correlated approach, when independent stream tubes are used, the effect of the infiltration rate on the spatial distribution of the solute leaching is ignored, as solutes cannot move laterally.

Effect of depth

In the experiments, the MCS was located at 0.51 m depth. At the field site, the groundwater table is located at 4 m depth. The random field for the scaling factor (Fig. 3.8) is based on the measurements until 0.51 m. We want to investigate whether, and how, the solute flux density would change with increasing depth. Figure 3.13 shows the marginal distribution of the x-axis of the leaching surfaces at 0.5 m and 1 m depth, both for a tracer and a degradable solute, for the year 1997 with and without snowmelt. Leaching at 1 m depth is more homogeneous than at 0.5 m depth, for cases with and without snowmelt alike, and both for the degradable solute and the tracer. This is in agreement with Persson and Berndtsson (1999), who found that the effect of soil heterogeneity on solute leaching is larger at shallow depth. For snowmelt, the difference between the curves at 0.5 m and 1 m depth is smaller than without snowmelt. Thus, with a high infiltration rate, and a high soil moisture content, the depth has little influence on the spatial distribution. With snowmelt, the leaching is more homogeneous than without snowmelt. With the higher

infiltration rate, a larger part of the soil is highly conductive. As a result, the leaching is more homogeneous. The same result was found by Persson et al. (2005): in a homogenised soil column the homogeneity in flow increased with an increasing water flux. They stated that a critical soil moisture content might exist. Below this critical content, independent stream tubes might develop, and above it, solute mixing might increase leaching to a more convective-dispersive transport regime.

The spatial distribution for the leaching of the tracer is similar as for the degradable solute, in all cases, except at 0.5 m depth for the simulation without snowmelt. Thus, at smaller depth, the soil heterogeneity is more important for the leaching of degradable solutes. The solute flux density is lower at 1 m depth than at 0.5 m. For the tracer this is caused by dilution and dispersion over a longer distance and time. Besides these effects, degradation lowers the solute flux density for the degradable solute at a larger time.

In the simulations, the properties of the random field for the saturated hydraulic conductivity and the retention curve were uniform. This field was based on the measurements, which were done at 0.51 m depth. Below this depth, the soil heterogeneity might be different than above this depth, attributable to root growth, bioactivity or geology (Pierret et al., 2007; Oades, 1993; French et al., 1994), amongst others. As we have observations until 0.51 m depth, we will assume that the same random field can be used below this depth.

Mean breakthrough and leached mass

From Figs. 3.9–3.12 was concluded that the fraction of the soil that contributes to solute leaching increased with an increasing infiltration rate. Here, we will investigate how this conclusion affects the mean breakthrough of a tracer, and the leached mass of a degradable solute.

Figure 3.14 shows the mean breakthrough time for the model with snowmelt, and without snowmelt, calculated with Eq. (3.4). The points do not follow a 1:1 line. The mean breakthrough time with snowmelt is lower than without snowmelt, because the infiltration rate during the snowmelt is higher. With snowmelt, the mean breakthrough time increases slower than without snowmelt. This means that with snowmelt a larger fraction of the soil is high conductive than without snowmelt. In the simulation with snowmelt, the solutes were applied with a pulse of six days, while in the simulation without snowmelt the pulse was only one day. When a pulse of one day would be used in the simulation with snowmelt, the effect shown in Fig. 3.14 is enlarged.

The mean breakthrough time, and its distribution influence the leaching of a degradable solute. Figure 3.15 shows the fraction of the leached mass of a degradable solute divided by the leached mass of a tracer, for each cell. These fractions are compared for the simulation with and without snowmelt. With snowmelt, the fractions are higher, because of the lower mean breakthrough time, as expected. With snowmelt, the fraction decreases slower than without snowmelt. This is caused by the difference in the distribution of the mean breakthrough time, with and without snowmelt. With a stream tube approach this effect would be neglected. As stream tubes are independent and one di-
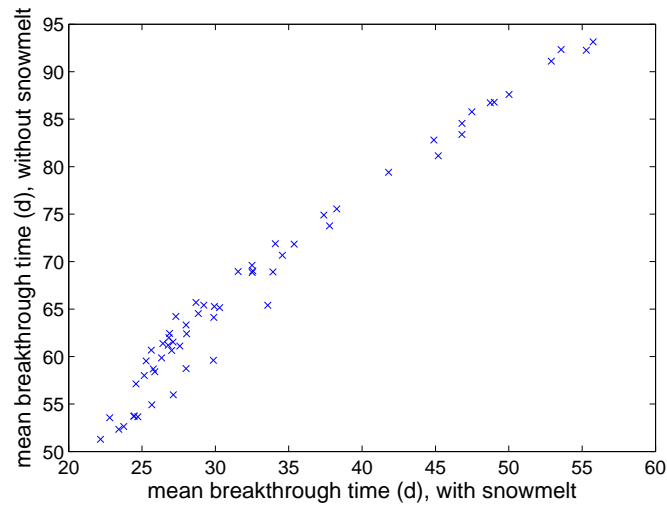
Figure 3.14: Mean breakthrough time calculated with moment analysis, for the year 1997 with and without snowmelt, at 0.5 m depth.
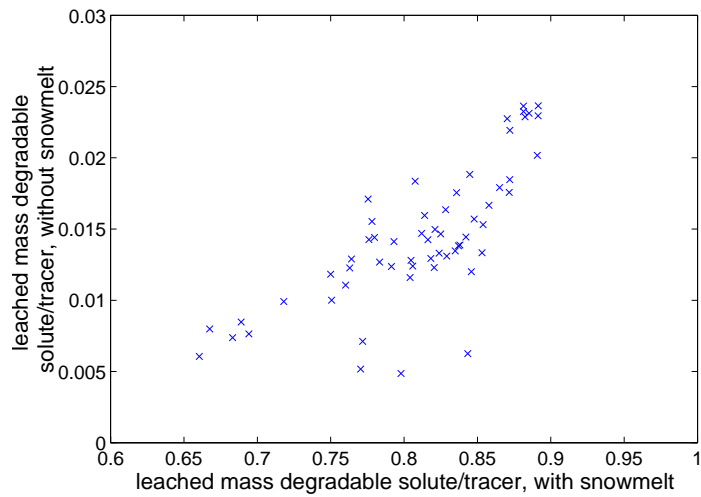
Figure 3.15: Leached mass of degradable solute (half-life time τ=10 d) divided by the leached mass of the tracer per cell, for the year 1997 with and without snowmelt, at 0.5 m depth.

mensional, the effect of the infiltration rate on the spatial distribution of the drainage is ignored. This can lead to underestimation of the leaching of degradable solutes.

3.4 Conclusions

Two experiments with a multi-compartment sampler (MCS) were done, to investigate the effect of different infiltration rates on the spatial distribution of solute leaching. From the experiment, a random field for a scaling factor for the retention curve was deduced. This random field was used in a model, with different transient and steady state infiltration rates.

The standard deviation and the correlation lengths of the random field for the scaling factor can be based on the observations of the experiment. Comparing the spatial distribution of leaching, the model corresponds well with the experiment. The agreement between the observations and the simulations depends both on the standard deviation and the correlation lengths, and on the particular random field. A discretisation of half the correlation length was sufficient to capture all small scale processes. The correlation length in depth did not influence the spatial distribution of the solute leaching much.

The spatial distribution of solute leaching, and which fraction of the soil contributes to solute leaching, is determined by the flow rate. When a stream tube approach would be used, this effect of the infiltration rate would be ignored, as stream tubes are independent.

The infiltration rate largely influences the leaching of the degradable solute. One reason for this is obviously the residence time, which is determined by the infiltration rate. The infiltration rate also determines the fraction of the soil that contributes to solute leaching. Therefore, the infiltration rate also influences the spatial distribution of the solute leaching. For a degradable solute this means that the leaching will be higher than would be estimated with independent stream tubes.

The distribution of the infiltration in time determines the residence time until a control plane at a particular depth. For the case of snowmelt, a steady state simulation with an average infiltration rate would underestimate the leaching of a degradable solute. Without snowmelt, a steady state simulation could overestimate the leaching of a degradable solute. The ratio of the degradation rate over the infiltration rate determines the amount of leaching.

3.4. Conclusions
_____

4

Transient transport of degradable and adsorbing contaminants in layered soils: Effective behavior

Abstract

We considered transient flow and solute transport for a soil where sorption and degradation varied as a function of depth, with the aim of assessing effective average properties. Assuming that only dissolved solute is degradable, and adsorbed solute is not, our primary interest was the average transport velocity of the solute plume, its effective retardation factor, and the leached fraction past a control plane. Furthermore, the effect of transient weather conditions on the solute leaching was investigated. If the soil layers differ with respect to adsorption, the velocity of a solute plume depends not only on the adsorption constant, but also on the degradation rate and dispersion. Effective retardation factors based on temporal moments or spatial moments give different values. Seasonal fluctuations in transient weather series lead to large differences in travel times in a dry climate, and thus large differences in the leached fraction of a solute. This is especially the case for solutes with little adsorption. For a wet climate with seasonal fluctuation in the weather series, the coefficient of variation in the leached fraction is lower with adsorption than without adsorption, thus a high precipitation surplus diminishes the effect of seasonality.

4.1 Introduction

Organic solutes may present a hazard to the environment, both in surface and subsurface water systems. When entering the soil, organic contaminants enter the unsaturated zone, and may leach to the groundwater, where high concentrations could be harmful. Whether an organic solute is harmful in the groundwater not only depends on the substance itself, but also on what happens with the solute when it is transported through the unsaturated zone. In this context, pesticides are of special interest as these are frequently used in agriculture, and are more likely to appear in groundwater than any other organic contaminant. Under EU law, groundwater used for drinking water may contain a maximum pesticide concentration of 0.1 μg l^{-1} (Council of the European Communities, 1980).

To quantify the effect of soil and pesticide properties on the amount of pesticide leaching to groundwater, several experimental and modeling studies on the fate of pesticides in the vadose zone have been conducted. These studies focused on the impact of physical (McGrath et al. (2008b); Lewan et al. (2009)), chemical (Boesten and Van der Linden (1991); Don Wauchope et al. (2002)), and biological (Ogram et al. (1985)) processes on pesticide leaching.

It is often assumed that contaminants can be similarly degraded in solution and when they are adsorbed to soil particles (Jury and Gruber (1989); Boesten and Van der Linden (1991)). However, this assumption might be invalid, as the degradation rate of a solute in the soil can be different if it is adsorbed or in solution (Das and Kluitenberg, 1996) as solutes might not be accessible for micro-organisms if they are adsorbed (Ogram et al., 1985). There are three special cases in considering degradation: (1) degradation does not occur at all (tracer studies); (2) degradation occurs in both the adsorbed phase and the aqueous phase, and the degradation rates are identical (most discussed in literature, e.g. Jury and Gruber (1989); Boesten and Van der Linden (1991)); (3) the degradation rate in the adsorbed phase is zero and only degradation in the aqueous phase occurs (less discussed in literature, e.g. McGrath et al. (2008b); Kuntz and Grathwohl (2009)). Although it has not been emphasized in the transport literature, the concepts where adsorbed solute can or can not be degraded are very different. If both fractions can be degraded, solute leaching past a control plane depends strongly on soil chemical behavior, and this concept has been investigated mostly. However, if degradation occurs only in solution, the leached fraction depends neither on the extent of sorption, nor on the type of sorption (linear, non-linear, equilibrium or kinetic). This concept has received much less attention, and therefore will be discussed in this paper.

Solute transport in soils is generally modeled with the convection-dispersion equation (Bear (1972); Kreft and Zuber (1978)). To account for soil heterogeneity transversal to the mean flow direction, the assumption of non-interacting parallel stream tube approaches have been used, following Dagan and Bresler (1979). For such stream tubes, originally pore scale dispersion has been ignored to enable simple analytical solutions. However, pore scale dispersion and preferential flow effects within the stream tubes can also be taken into consideration (Destouni and Cvetkovic, 1991). Mostly, though, as the focus is towards larger scale heterogeneity, variability within stream tubes is ignored. This implies

that the local transport behavior in stream tubes can be adequately averaged. For this reason, rigorous averaging has received considerable attention in contaminant hydrology.

The sorption capacity of a soil often decreases with increasing depth, as the organic matter content decreases with increasing depth (Guo et al., 1997). To account for randomly chemical heterogeneous soils (Attinger et al. (1999); Chrysikopoulos et al. (1990), and Dentz and Castro (2009)) or layered aquifers (Valocchi (1989) and Leij et al. (1991)), heterogeneous media were approximated by equivalent homogeneous media using effective soil properties. It is still unclear how the chemical heterogeneity of a layered unsaturated zone can be approximated as an equivalent medium, as the flow usually is perpendicular to the layers in unsaturated soils, and not parallel as in aquifers. Moreover, the length scales of the saturated and unsaturated zone differ in orders of magnitude.

For an adsorbing and degrading solute and with transient weather series, the effective transport properties, like the average velocity and retardation factor, are not defined clearly. When effective properties are used, only the breakthrough at the outlet can be determined, while for degrading solutes the soil moisture distribution needs to be known (Durner et al., 2008). In stream tube models the soil moisture distribution is ignored, and may therefore be inappropriate to estimate effective properties. Furthermore, the effective properties may depend on whether degradation occurs in the aqueous phase only, or in both the aqueous and adsorbed phases. This effect has not been investigated.

Besides effective properties for spatial variability, temporal variability in the weather series affects the amount of leaching of an adsorbing and degrading solute (Jury and Gruber, 1989; McGrath et al., 2008a). Also for the temporal variability, effective weather series may depend on the type of degradation.

Transient weather has received modest attention at best, in solute leaching modeling. However, adopting the concept that only dissolved solute may degrade, the impact of soil chemistry becomes smaller (Beltman et al., 2008), and it is plausible that weather forcing has larger impact. Therefore, our scope is to assess whether for transient weather, effective properties for the travel time (velocity and retardation) for a stream tube between soil surface and groundwater can be determined. In addition, we aim to assess the impact of weather forcing on the leached fraction of applied solute. The methodology and results are applicable to contaminants that can be adsorbed and degraded in soils, such as pesticides.

4.2 Theory

4.2.1 Model

The convection-dispersion equation for a solute with adsorption and degradation is:

$$\rho\frac{\partial q}{\partial t} + \frac{\partial \theta c}{\partial t} = \frac{\partial}{\partial z}\left(\theta D\frac{\partial c}{\partial z}\right) - \frac{\partial \theta v c}{\partial z} - Q \tag{4.1}$$

where ρ is the dry bulk density (M L^{-3}), q is the mass sorbed per mass of dry soil (M M^{-1}), t is time (T), θ is the volumetric soil moisture content of the soil (L^3 L^{-3}), c is the concentration in solution (M L^{-3}), D is the hydrodynamic dispersion coefficient (L^2

T^{-1}), z is the distance (L), v is the filtration velocity (L T^{-1}), and Q is a degradation term (M L^{-3} T^{-1}). v and θ follow from the Richards equation with appropriate consecutive relations for capillary pressure and relative permeability (Van Genuchten equations).

Equilibrium sorption to organic matter was assumed linear and pH independent (Leistra et al., 2001):

$$q = K_{om} f_{om} c \tag{4.2}$$

where K_{om} is the coefficient of adsorption to organic matter (L^3 M^{-1}), and f_{om} is the organic matter content of the soil (M^1 M^{-1}). The degradation rate in the adsorbed phase can be different from the degradation rate in the aqueous phase. We assume that the degradation rate in the adsorbed phase is either equal to the degradation rate in the aqueous phase, or zero. Therefore, the last term in equation 4.1 can be written as:

$$-Q = -k(\theta + f_d \rho K_{om} f_{om})c \tag{4.3}$$

where k is the effective degradation rate constant (T^{-1}), and f_d is a parameter with the value 1 if the degradation rate in the adsorbed phase and the aqueous phase is equal, and with the value 0 if degradation occurs only in the aqueous phase.

The retardation factor R can be defined as:

$$R = 1 + \frac{\rho K_{om} f_{om}}{\theta} \tag{4.4}$$

In Appendix A, a semi-analytical derivation of the convection-dispersion equation for a two layered soil is given, where the solute is adsorbed in the upper layer, and only degraded in the aqueous phase.

Degradation was assumed to be first order with the degradation rate constant dependent on soil temperature and soil moisture content. For each depth and time, the effective degradation rate constant was calculated as:

$$k = f_T f_\theta \frac{ln(2)}{\tau} \tag{4.5}$$

where τ is the half-life time of the solute (T) and

$$f_T = e^{-\frac{E_a}{R_c}\left(\frac{1}{T} - \frac{1}{T_{ref}}\right)} \tag{4.6}$$

and

$$f_\theta = min\left(1, \left(\frac{\theta}{\theta_{fc}}\right)^{0.7}\right) \tag{4.7}$$

where f_T is a factor that corrects degradation for temperature (-), f_θ is a factor that corrects degradation for soil moisture content (-), E_a is the molar activation energy, R_c is the gas constant, T is the soil temperature at a certain depth (K), T_{ref} is the reference soil temperature (K), and θ_{fc} is the volumetric soil moisture content when the soil is at field capacity (L^3 L^{-3}). The factors f_T and f_θ varied in time and depth. The temperature

in the soil was dependent on the heat transport in the soil, which was modeled with a conductive heat-flow model (Leistra et al., 2001). The upper boundary condition of this heat-flow model was the average air temperature, which was included as a daily input value.

PEARL is a model that can be used to simulate pesticide transport and degradation with transient flow (Leistra et al., 2001). In this paper, it was used to simulate contaminant transport, and to estimate the leached fraction below a designated depth. In the standard model setup degradation occurs in both aqueous and adsorbed phase. The model PEARL was adjusted to also be able to consider the case that degradation occurs in the aqueous phase only (Beltman et al., 2008), because degradation rates can be different in the adsorbed phase and in the aqueous phase (Ogram et al. (1985) and Eq. 4.3).

By Jury et al. (1987) pesticides have been described as being different with regard to the sorption constant and the half-life time only. To consider transport and degradation of a range of contaminants, we varied the coefficient for sorption by organic matter K_{om} and the half-life time τ. K_{om} was 0, 20, 40, 60, 80, or $100\,\mathrm{l\,kg^{-1}}$, τ was 10, 20, 50, 100, 150, or 10^6 days. These two solute properties combined, gave a set of 36 different solutes. Unless stated otherwise, degradation occurred only in the aqueous phase.

To standardize pesticide registration, the database FOCUS has been developed with various soils, climates, and crops that are representative for different areas in Europe (FOCUS, 2006). A combination of soil and climate gives a FOCUS scenario, which can be used as input in a model like PEARL. From the FOCUS database, we chose one soil and three climates to study the effect of different climates on contaminant leaching. The Hamburg soil from the FOCUS scenarios was chosen, which is a sandy loamy soil (Table 4.1). The soil consisted of 6 layers, each with different organic matter content. The upper 3 layers (0-0.75 m) contained organic matter, thus only in these layers, solute could be adsorbed. The hydraulic parameters are similar for all layers. Thus, the Hamburg soil is relatively homogeneous for water flow, but layered in adsorption parameters. We only consider matrix flow, macropore flow is neglected.

In PEARL, water uptake by roots is non–uniform with depth. When root growth is modeled, as would be needed for a crop, it is not traceable from which depth solute is taken up by the roots. Therefore, root water uptake is ignored in this study, simulations were done for bare soil. At the lower boundary the flux depended on the groundwater level (Leistra et al., 2001). PEARL calculated the groundwater level, which fluctuated with a mean of 1.6 meter below soil surface and a standard deviation of 0.29 meter.

For simulating climate, weather series of the FOCUS scenarios of Hamburg, Porto, and Thiva were used in combination with the same Hamburg soil. The Hamburg meteorological time series had precipitation, reference evaporation, mean wind speed, maximum temperature, minimum temperature, humidity, and solar radiation as input (daily values). In these simulations, actual evaporation was calculated by SWAP (Van Dam et al., 1997). To study the effect of precipitation and evaporation, only precipitation and reference evaporation series of Porto and Thiva were used. All other weather variables were used from the Hamburg weather series, to exclude the effect of for instance air temperature on degradation. Porto and Thiva were selected from FOCUS, because the climate of Porto has a much higher precipitation but equal evaporation as Hamburg, and the climate of Thiva

Table 4.1: Soil physical parameters of the Hamburg soil from the FOCUS scenarios. Bulk density ρ, saturated soil moisture content θ_{sat}, residual soil moisture content θ_{res}, drying and wetting parameters a_{dry} and a_{wet}, parameters n and λ for the Mualem-van Genuchten soil hydraulic functions, and saturated conductivity K_{sat}.

layer	depth (m)	ρ (kg l^{-1})	f_{om} (kg kg^{-1})	θ_{sat} (m^3 m^{-3})	θ_{res} (m^3 m^{-3})	a_{dry} (m^{-1})	a_{wet} (m^{-1})	n (-)	λ (-)	K_{sat} (m d^{-1})
1	0-0.30	1.50	0.0260	0.391	0.036	0.0149	0.0298	1.468	0.5	2.016
2	0.30-0.60	1.60	0.0170	0.370	0.030	0.0126	0.0252	1.565	0.5	2.736
3	0.60-0.75	1.56	0.0034	0.351	0.029	0.0181	0.0362	1.598	0.5	2.448
4	0.75-0.90	1.62	0	0.310	0.015	0.0281	0.0562	1.606	0.5	2.448
5	0.90-4.5	1.60	0	0.310	0.015	0.0281	0.0562	1.606	0.5	2.448

61

Table 4.2: Properties of used climates. The precipitation series and potential evaporation series of the FOCUS Hamburg, Porto, and Thiva scenarios were used.

Location	mean annual precipitation (m)	mean annual potential evaporation (m)	mean temperature (°C)
Hamburg	0.795	0.374	9.0
Porto	1.116	0.375	9.0 [1]
Thiva	0.473	0.272	9.0 [1]

[1] We used temperature series of the FOCUS Hamburg scenario for Porto and Thiva in order to cancel out temperature dependent degradation.

has less precipitation and less evaporation than Hamburg (Table 4.2). Figure 4.1 shows the distribution of precipitation and evaporation per month of an average year for the three climates.

The climate series of FOCUS consist of a repetition of 20 years of measurements. The data of the 20 years are repeated to construct a weather time series of 66 years (FOCUS, 2006). In our simulations, the solute was applied once, at March 31. The year of solute application was shifted by one year, such that each of the 20 years was used as a starting year. This was done in 20 separate realizations, and for each solute. All simulations were long enough to ensure that all solute was either degraded or leached from the upper meter.

4.2.2 Data analysis

Our main interests were the moment of arrival of the solute plume at the groundwater, and the fraction of the contaminant that leached. For each realization and for all solutes, the moment of arrival and the leached fraction were calculated. The dispersive flux is small compared to the convective flux, therefore the leached fraction of applied contaminant was calculated as the convective flux:

$$LF = \frac{\int_{t=0}^{t=T_e} c(L,t)v(L,t)\theta(L,t)dt}{M_0} \qquad (4.8)$$

where LF is the leached fraction, T_e is the end of the simulation, and M_0 is the applied mass ($M\,L^{-2}$).

We used statistical moments to follow the mass in the aqueous phase and the mean and spread of the solute plume in time or depth (Bresler and Dagan (1981); Leij and Dane (1991); Burr et al. (1994); Attinger et al. (1999)). The n–th spatial moment of the concentration is (Govindaraju and Das, 2007):

$$m_{s,naq}(t) = \int_{z=0}^{z=Z} c(z,t)\theta(z,t)z^n dz \qquad (4.9)$$

where $m_{s,naq}(t)$ is the n–th spatial moment, and z is depth (L), which is 0 at soil surface, and Z at the lower end of the domain. The zeroth spatial moment is the mass in solution
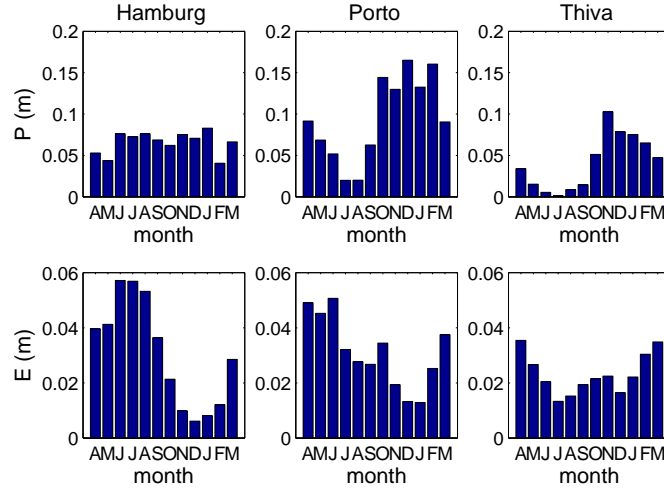
Figure 4.1: The distribution of the precipitation P and evaporation E over the year, for the FOCUS Hamburg, Porto, and Thiva scenarios. The upper row shows the mean P per month of the 20 realizations, the lower row shows the mean E per month.

($M_{s,0aq}$). The zeroth spatial moment was calculated from the concentration and the soil moisture content, both given as output by PEARL. The first central normalized spatial moment is the depth of the center of mass in solution (Govindaraju and Das, 2007):

$$M_{s,1aq}(t) = \frac{m_1}{m_0} \qquad (4.10)$$

where $M_{s,1aq}$ is the depth of the center of mass (L).

Besides the amount of contaminant that would leach, we were interested to know the moment of arrival at a certain depth. This can be described with temporal moments. Biodegradation decreases with increasing depth (Veeh et al., 1996), therefore, we assume that no solutes are degraded below 1 m depth. Thus, the fraction of applied solutes that reaches 1 m depth, will also leach to the groundwater. The first temporal moment is the mean travel time in the soil. We defined the travel time as the number of days it took from application until half of the fraction that is going to leach, was leached (at 1 m depth). In this way, however, the travel time could only be calculated afterwards, when it was known how much contaminant leached. Das and Kluitenberg (1996) give a relation between the theoretical travel time and the flow velocity:

$$M_{t,1}(z) = \frac{Rz}{\sqrt{v^2 + 4kD}} \qquad (4.11)$$

where $M_{t,1}$ is the theoretical first temporal moment (T). Equation 4.11 is only valid under steady state conditions, and with uniform water content. We only use Eq. 4.11 to qualitatively explain the effect of the dispersivity on the travel time.

63
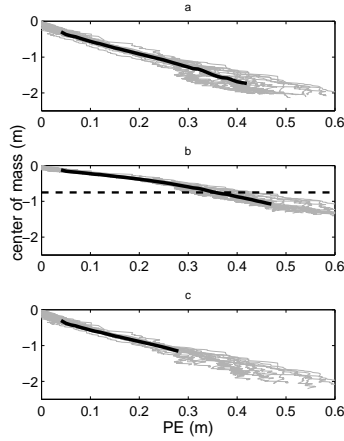
Figure 4.2: Depth of the center of mass versus precipitation surplus PE. a: a non-adsorbing and non-degrading solute; b: an adsorbing and non-degrading solute. Adsorption is in the upper 0-0.75 m with adsorption constant K_{om} = 20 1 kg^{-1}; c: a non-adsorbing and degrading solute, half-life time τ = 10 d. 20 realizations of the FOCUS Hamburg scenario are shown. The thick line is the average of the 20 realizations.

To facilitate the comparison between different years and different climates, the precipitation surplus will be used as a time axis. The precipitation surplus PE is the cumulative precipitation P minus the cumulative evaporation E. PE during the travel time (defined as when half of leaching occurred) was used to compare the leaching behavior (precipitation surplus during travel time and leached fraction) between the different climates of Hamburg, Porto, and Thiva.

4.3 Results and discussion

We are interested in effective properties, both for spatial and temporal variability, for solutes in layered soil and with transient weather series. It is assumed that the solute is only degraded in the aqueous phase. For the effective spatial properties, the average plume velocity, average soil hydraulic parameters and the effective retardation factor will be discussed.

4.3.1 Spatial variability

Average plume velocity

As the effective velocity is derived from moments analysis, we first discuss the first spatial moment of the solute plume, which is the center of mass. The average velocity of the

plume is the slope between the precipitation surplus and depth of the center of mass. To illustrate the effects of adsorption and degradation on the statistical moments, we start with simple cases: neither adsorption nor degradation; adsorption without degradation; and degradation without adsorption.

Figure 4.2a shows the relation between depth of the center of mass of a non-degrading and non-adsorbing solute and the precipitation surplus for the FOCUS Hamburg scenario. The precipitation surplus PE is the cumulative precipitation P minus the cumulative evaporation E, $PE = P - E$ (m). The depth of the center of mass for all 20 realizations shows the variation in the depth of the center of mass between different years, for the Hamburg climate. In Fig. 4.2a, the depth of the center of mass increases approximately linear with increasing precipitation surplus. Transient flow in a layered soil can thus be approximated as stationary flow, replacing time by the cumulative net infiltration, PE. This is similar to Wierenga (1977), who showed cumulative drainage can be used as time axis for unlayered soils without adsorption and degradation.

Figure 4.2b shows the depth of the center of mass versus the precipitation surplus for an adsorbing and non-degrading solute (K_{om} is $20 \, \mathrm{l \, kg^{-1}}$). The center of mass does not reach the same depth as in Fig. 4.2a with a designated precipitation surplus, because transport is retarded due to adsorption. To compare the results of Fig. 4.2a and b, the precipitation surplus of the adsorbing solute should be divided by a retardation factor R. This, however, is not possible, as R is unknown. To facilitate comparison, an effective retardation factor is needed, for which the considerations of estimating will be given in section 4.3.1.

Figure 4.2c shows the relation between the depth of the center of mass and the precipitation surplus for a degrading and non-adsorbing solute (half-life time $\tau = 10 \, \mathrm{d}$). Without adsorption, degradation of the solute does not influence the relation between the precipitation surplus and depth of the center of mass, when degradation is constant with depth. Thus, if a solute does not adsorb, but can be degraded, the depth of the center of mass is similar to the depth of the center of mass of a non-adsorbing and non-degrading solute, which is shown in Fig. 4.2a.

When a solute both degrades and adsorbs, the relation between the depth of the center of mass and the precipitation surplus is different. Figure 4.3a and b show the relation between depth of the center of mass and the precipitation surplus for a degrading and adsorbing solute. In Fig. 4.3a the depth of the center of mass is shown for 2 different solutes. One solute is non-degradable and the other is degradable with $\tau = 10 \, \mathrm{d}$, both solutes adsorb in the upper layers with $K_{om} = 20 \, \mathrm{l \, kg^{-1}}$. The depth of the center of mass of a non-degradable solute increases with PE (the solute as in Fig. 4.2b). For a degradable solute, the depth of the center of mass increases slower with increasing PE at a depth between 0.5 and 1 m than at shallower depth, which is in the vicinity of the transition between layers with adsorption and layers without adsorption. Thus, the depth of the center of mass, and thus the velocity, is affected both by the adsorption and the degradation in a layered soil. When degradation is neglected in transport modeling (Rajaram (1997), Burr et al. (1994)), only the adsorption constant influences the velocity of a solute plume. We assumed linear adsorption, which means that in the upper layer a constant fraction of the mass in solution is adsorbed. As mentioned before, in our model,
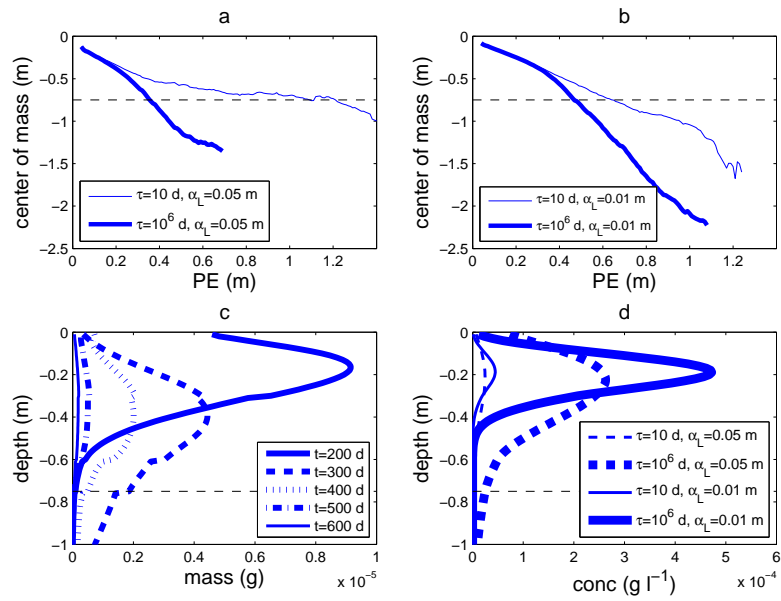
Figure 4.3: a: Depth of the center of mass versus precipitation surplus PE, adsorption is in the upper 0-0.75 m with adsorption constant $K_{om} = 20 \, \text{l} \, \text{kg}^{-1}$, two solutes: half-life time $\tau = 10^6$ d (thick line) or $\tau = 10$ d (thin line). Dispersivity $\alpha_L = 0.05$ m; b: same remarks as a, but $\alpha_L = 0.01$ m.; c: Mass distribution as a function of depth at various time steps t after application for year 1925 of the FOCUS Hamburg scenario. Adsorption constant $K_{om} = 20 \, \text{l} \, \text{kg}^{-1}$, half-life time $\tau = 10$ d; d; Concentration as a function of depth for adsorption constant $K_{om} = 20 \, \text{l} \, \text{kg}^{-1}$, dispersivity $\alpha_L = 0.01$ m (continuous lines) or $\alpha_L = 0.05$ m (dotted lines), two solutes: half-life time $\tau = 10^6$ d (thick lines) or $\tau = 10$ d (thin lines.)

the fraction of a solute that is adsorbed, cannot be degraded. In the lower layers (>0.75 m), no solute is adsorbed and all solute in this layer can be degraded. This means that the degradation rate of the total mass in the upper layers is smaller than in the lower layers, therefore the depth of the center of mass increases slower with increasing precipitation.

To explain Fig. 4.3a, Fig. 4.3c shows profiles of mass at various times after application (in the year 1907 from the FOCUS Hamburg scenario) for the same solute as in Fig. 4.3a (K_{om} = 20 l kg^{-1} and τ = 10 d). The depth of the peak concentration increases with increasing time, but not as fast as would be expected for the precipitation surplus that occurs. The reason for this is that most mass is located in the upper layers, because of the lower degradation rate in the upper layers than in the lower layers. Since the center of mass is based on the distribution of mass as a function of depth, the depth of the center of mass increases slower with increasing PE for a degrading solute than for a non-degrading solute in a layered soil. The difference in the location of the center of mass between the two solutes increases with increasing sorption and degradation rates.

Figure 4.3b shows the relation between the depth of the center of mass and the precipitation surplus for two adsorbing solutes: one non-degradable solute and one degradable solute, like in Fig. 4.3a. The difference with Fig. 4.3a is the dispersivity that is used (dispersivity $\alpha = D/v$). For Fig. 4.3a, a dispersivity of 0.05 m is used, while for Fig. 4.3b a dispersivity of 0.01 m is used. With a smaller dispersivity, the depth of the center of mass of a degradable solute differs less from the depth of the center of mass of a non-degradable solute (Fig. 4.3b) than with a larger dispersivity (Fig. 4.3a).

Thus, the velocities of the center of mass of solutes with different degradation rates are more similar if dispersion decreases. This can be explained as follows. Fig. 4.3d shows the concentration as a function of depth for the solutes with the properties of the solutes used for Fig. 4.3a and b at 250 days after application of one of the realizations. The spread of the plume around the center of mass is larger with larger dispersivities . The period in which the plume is divided over both upper and lower layers is longer with larger dispersivities, resulting in larger differences between the velocity of the center of mass of a non-degradable solute and a degradable solute for larger dispersivities. Without dispersion, the relation between the precipitation surplus and the depth of the center of mass, would be the same for different degradation rates.

Figure 4.3 shows that the dispersivity is needed to estimate the velocity in a layered soil. The velocity of the solute plume thus depends on the adsorption coefficient, the dispersivity and the degradation rate, which also follows from Eq. 4.11. This dependency is of particular interest in view of the commonly made assumption in parallel stream tube modeling that D = 0 m^2 d^{-1}, for simplicity (Bresler and Dagan (1981); Destouni and Cvetkovic (1991)). In the stream tube approach, dispersion has often been ignored, based on the assumption that at the field scale, the differences in flow velocity between the independent stream tubes dominate, over dispersion within a stream tube, on spreading of solute arrival time (Destouni and Graham (1995); Destouni and Cvetkovic (1991)). But, due to dispersion, part of the solute plume is transported faster through the microbially active layer to a lower layer with slower degradation (Das and Kluitenberg, 1996). For a soil with the conditions used here, this assumption would introduce a systematic bias, if degradation occurs.
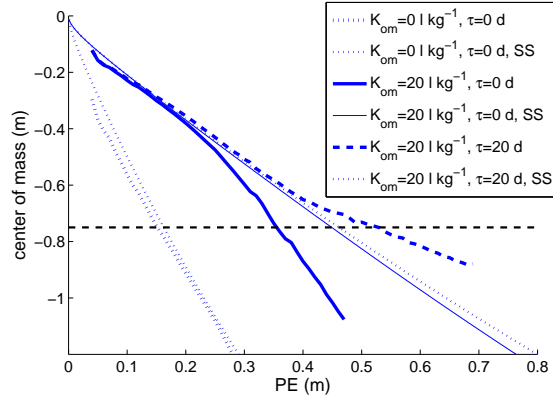
Figure 4.4: Depth of the center of mass versus precipitation surplus PE. The thick lines are the average of 20 similations with layered soil and transient weather. The thin lines are simulations with a homogeneous soil and stationary PE. The soil properties of Table 4.1 are harmonically averaged. The average precipitation and evaporation of the FOCUS Hamburg scenario are used. The adsorption constant K_{om}=20 l kg^{-1} and half-life time τ =20 d.

Average soil hydraulic and chemical properties

Solute transport modeling in heterogeneous soils is often simplified by using effective properties for the hydraulic and chemical properties for an equivalent medium. An equivalent medium can easily be found for a layered soil with steady state flow and with solutes that neither degrade nor adsorb (Barry and Parker, 1987). Destouni (1991) showed that heterogeneous soil hydraulic properties in a layered soil can be approximated by homogeneous soil hydraulic properties by taking the harmonic average. Furthermore, Destouni (1991) showed that a transient water flux can be approximated with a stationary water flux, by taking the average of the precipitation surplus. This was done for nonadsorbing and nondegrading solutes.

To check whether averaging is also possible for adsorbing and degrading solutes, we averaged the soil properties of the layered FOCUS Hamburg soil to create a homogeneous soil. The properties were harmonically averaged. Because f_{om} has values of zero, f_{om} cannot be harmonically averaged and the arithmetic average was taken. We wanted to compare the moment of leaching past 1 m depth in a layered and a homogeneous soil, and therefore only the values of 0–1 m of the layered soil were averaged. The averaged values of 0–1 m were used for the entire profile. We arithmetically averaged the FOCUS Hamburg scenario weather properties, to obtain a constant temperature and precipitation surplus.

Figure 4.4 shows the relation between the precipitation surplus and the depth of the center of mass for a homogeneous soil and with constant precipitation for solutes with

adsorption constant K_{om}=0 or 20 l kg^{-1} and half-life time τ=10^6 or 20 d. The precipitation surplus that is needed to transport the center of mass of a non-adsorbing solute to 1 m depth is similar for a layered soil with transient precipitation and evaporation as for a homogeneous soil with stationary precipitation and evaporation. This result is consistent with Delay et al. (1997), who experimentally showed that the tracer outflow of a medium that consists of several homogeneous layers can be modeled as the convolution of the individual layers with stationary water flow. In the experiment, Delay et al. (1997) mixed the layers to get a homogeneous medium. The effective properties of this medium could be based on the fractions of the original layers, but the relations between the layer fractions and the parameter values were different for each parameter. Delay et al. (1997) also mention this is only valid for nondegrading solutes.

For an adsorbing and nondegrading solute, the precipitation surplus that is needed to transport the center of mass to 1 m depth is larger in the homogeneous soil than in the layered soil, whereas is it smaller for an adsorbing and degrading solute. Thus, the layered soil cannot be approximated with a homogeneous soil with arithmetically or harmonically averaged soil properties when the solute adsorbs and degrades, and the weather is variable. Destouni (1991) used a stream tube approach, which means soil heterogeneity is parallel to the water flow. Furthermore, only hydraulic parameters were averaged. Chemical heterogeneity caused by a depth-dependent organic matter content was not considered by Destouni (1991).

Besides soil properties, we averaged the transient weather series to get steady state precipitation and evaporation. When transient weather series are used, layer ordering is important, because the upper layers will affect the evaporation more than the lower layers (Durner et al., 2008). With large differences in hydraulic properties for the two layers used by Durner et al. (2008), they showed that soil moisture content could not be approximated with effective hydraulic parameters, using a natural transient weather series. The distribution of the soil moisture content with depth influences the effective degradation rates, and the adsorbed fraction of the solute, when transport of adsorbing and degrading solutes is modeled. No equivalent medium of a layered soil can be found for a degrading and adsorbing solute, and with transient weather.

Effective retardation factor

To compare the velocity of the center of mass of the solute plume with water flow, and with other solute plumes, we were interested in the effective retardation factor. Two definitions of the effective retardation factor have been commonly used, that are either based on temporal moments or on spatial moments (Rajaram, 1997). Using temporal moments the effective retardation factor R_t may be defined as the ratio of breakthrough time at a certain control plane of an adsorbing solute to that of a non-adsorbing solute. Based on spatial moments, the effective retardation factor R_s may be defined as the ratio of the velocity of center of mass of a non-adsorbing solute to that of an adsorbing solute at any time (Rajaram, 1997). In a heterogeneous aquifer, R_t is not equal to R_s, and both vary when the plume propagates. The reason for this difference is that the retardation factors along the path of migration are cumulated in R_t, while R_s reflects a retardation factor at a
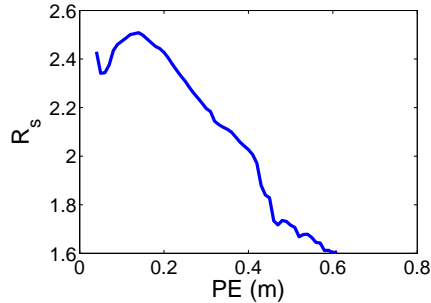
Figure 4.5: Retardation factor based on the velocity of the center of mass R_s, adsorption constant $K_{om} = 20\,l\,kg^{-1}$ and half-life time $\tau = 150\,d$. The average of 20 realizations of the FOCUS Hamburg scenario is shown.

designated time (Burr et al., 1994). According to Rajaram (1997), R_s gives the harmonic average of the retardation factor and R_t the arithmetic average.

Although it is known that the effective retardation factors R_s and R_t change in time, it is unclear how they evolve. Rajaram (1997), Burr et al. (1994), and Fernàndez-Garcia et al. (2005) discussed the determination of effective retardation factors in heterogeneous aquifers with random distributions of hydraulic conductivity and adsorption constants. In horizontally layered aquifers with water flowing parallel to the layers, the effective retardation factor may be taken as the average of the retardation factors of the separate layers (Valocchi, 1989). For a soil with horizontal layers and the water flow perpendicular to these layers, we determined the effective retardation factors with temporal and spatial moments.

Figure 4.5 shows the relation between R_s and time, with the precipitation surplus on the time axis. Figure 4.5 shows that initially, R_s increases, which is caused by the upper boundary condition. A solute pulse is applied at the upper boundary, and initially the solute concentration is larger than 0 at the upper boundary (Kasteel et al., 2009), as is shown in Fig. 4.3d. This influences the mass distribution in the soil and thus the depth of the center of mass. For an adsorbing solute, more time is needed before the effect of the boundary condition has vanished than for a non-adsorbing solute, which leads to an increasing retardation factor R_s shortly after application. After a precipitation surplus of 0.2 m, the effective retardation factor decreases, because part of the plume of the adsorbing solute is in the deeper layers without adsorption. This leads to a larger slope of the depth of the center of mass as a function of the precipitation surplus. Thus, the effective retardation factor based on spatial moments is time dependent.

Figure 4.6 shows the relation between R_t and depth. R_t decreases with increasing depth, because the effect of the layers with adsorption (0–0.75 m) on the effective retardation factor decreases. Thus, the effective retardation factor based on temporal moments depends on the travelled distance in a soil. Chrysikopoulos et al. (1990) found that with a spatially variable retardation factor, the movement of the center of mass is delayed, com-
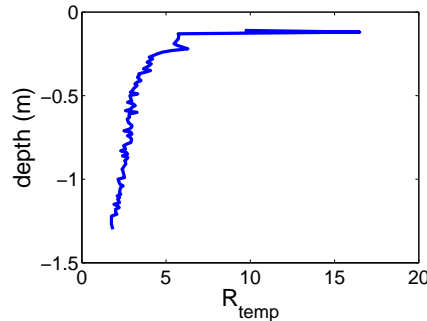
Figure 4.6: Retardation factor based on first temporal moment R_t, adsorption constant K_{om} = 20 l kg^{-1} and half-life time τ = 150 d. The average of 20 realizations of the FOCUS Hamburg scenario is shown.

pared to a uniform retardation factor. This analysis was based on nondegrading solutes, where the retardation factor was randomly heterogeneous. At long times after solute application, an effective retardation factor may be used. According to Burr et al. (1994) R_s fluctuates more than R_t, whereas we conclude that R_t decreases much more in the beginning, and also fluctuates more as a function of depth than R_s. Burr et al. (1994) discussed steady state flow in an randomly heterogeneous aquifer, while we study transient flow in a layered soil.

4.3.2 Temporal variability

For the temporal variability, first we discuss how the solute leaching depends on the adsorption constant and the degradation rate, with transient weather series. Then, these results will be compared with results from two other transient weather series.

Time and fraction of leaching

To investigate the effect of temporal variability in the precipitation surplus on the leaching of an adsorbing and degrading solute, the leaching moment and the leached fraction will be discussed. The leaching moment was defined as the moment when half of the total leachable solute mass had leached. This definition was used, because the center of mass of several degrading and adsorbing solutes did not reach 1 m depth (Fig. 4.3). The moment of leaching is used to determine the travel time, which is the time between application of the solute and the moment of leaching. Figure 4.7a shows the mean precipitation surplus PE during the travel time of the 20 realizations for the FOCUS Hamburg scenario. With a decreasing adsorption constant and a decreasing half-life time, the travel time decreases (Eq. 4.11), which causes an decrease in the mean precipitation surplus during the travel time. The differences between soil moisture content θ (averaged over 0-1 m) for these

Figure 4.7: FOCUS Hamburg scenario, precipitation surplus PE during travel time and leached fraction: mean and coefficient of variation. a: mean PE (m); b: CV PE; c: $\log_{10}$ of mean leached fraction (-); d: CV leached fraction. The figure is based on 6 values for the half-life time (10, 20, 50, 100, 150, and 10^6 d) and 6 values for the adsorption constant (0, 20, 40, 60, 80 and $100\,\mathrm{l\,kg^{-1}}$).

adsorption constants and degradation rates are small compared to the differences in PE during the travel time.

Figure 4.7b shows the coefficient of variation (CV) in the precipitation surplus during the travel time for the 20 realizations. The CV in the precipitation surplus increases with a decreasing adsorption constant and with a decreasing half-life time. Solutes without adsorption and with low half-life times have travel times of less than one year, whereas solutes with high adsorption and high half-life times have travel times up to 6 years. If it takes several years before the solute leaches, the effect of one particularly wet or dry year on the precipitation surplus during the travel time is smaller than when the solute leaches within one year.

Figure 4.7c shows the $\log_{10}$ of the mean leached fraction of an applied solute of the 20 realizations. The leached fraction increases with an increasing half-life time, as ex-

pected. The leached fraction of the applied solute is lower without adsorption than with adsorption, which is caused by the temperature dependency of the degradation rate. The degradation rate decreases with decreasing temperature (Eqs. 4.5 and 4.6), leading to larger degradation rates in summer than during winter for the Hamburg climate. As contaminant application is in spring, and the travel time of a non-adsorbing solute is less than one year, the average degradation rate for the non-adsorbing solute is larger than for adsorbing solutes. If the solute adsorbs, the leached fraction is independent of the adsorption constant. This is only valid for a solute that cannot be degraded in the adsorbed phase. When a pesticide can be degraded in both phases, the leached fraction of such a pesticide would be smaller with a larger adsorption constant (Boesten and Van der Linden, 1991).

Figure 4.7d shows the CV of the leached fraction of an applied solute of the 20 realizations. The CV in the leached fraction increases with a decreasing adsorption constant and with a decreasing half-life time, for the same reasons as the CV in the precipitation surplus during the travel time, namely the shorter travel time. For long travel times, short term fluctuations, including dry or wet years, are balanced out, leading to less variation in the leached fraction. Thus with more adsorption, the average precipitation surplus of a particular area would give a better prediction of the leached fraction of a contaminant than without adsorption.

From the results in Fig. 4.7, we conclude that when there is no degradation in the adsorbed phase, the leached fraction of an applied adsorbing solute is independent of the adsorption constant. Furthermore, the coefficient of variation in the leached fraction decreases with increasing travel times, i.e. for increasing adsorption constants and increasing half-life times. For large travel times, the seasonal and yearly fluctuation in the precipitation and evaporation rates is averaged, leading to a smaller variation in the leached fraction.

Effect of seasonality in the precipitation surplus on the time and fraction of leaching

To generalize the results of section 4.3.2, and to study the impacts of drier or wetter climate on the moment and the amount of leaching with degradation in the aqueous phase, both precipitation and evaporation of the Hamburg climate were substituted by those of a wetter climate (Porto) and of a drier climate (Thiva) (Fig. 4.1 and Table 4.2). The soil properties and the solutes remained the same as for the climate of Hamburg. Air temperature series of Hamburg were used for all three locations, as this influences the degradation (Eq. 4.6), and we wanted to emphasize differences in PE only. Differences in soil moisture content, however, have a small effect on soil temperatures, therefore f_T is slightly different for the three locations. This has a small effect on degradation rates. For Porto, f_T deviates at most 3% from Hamburg, for Thiva f_T, deviates at most 5% from Hamburg, and is therefore ignored.

Figure 4.8 shows the mean and CV of both the precipitation surplus during the travel time, and the leached fraction for the wetter climate of Porto. The relations between τ, K_{om} for the mean and CV in precipitation surplus, and for the mean and CV in the leached fraction are comparable to the results of the moderate climate of Hamburg. Due to the larger annual precipitation at Porto, the travel times are shorter than for Hamburg.
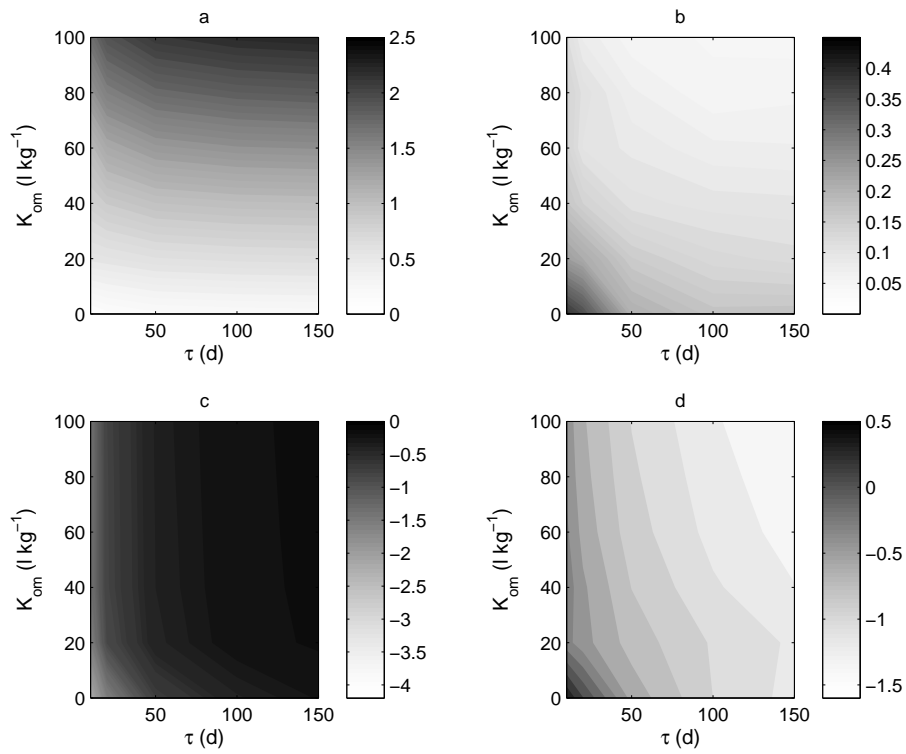
Figure 4.8: FOCUS Porto scenario, precipitation surplus PE during travel time and leached fraction: mean and coefficient of variation. Same remarks as Figure 4.7.
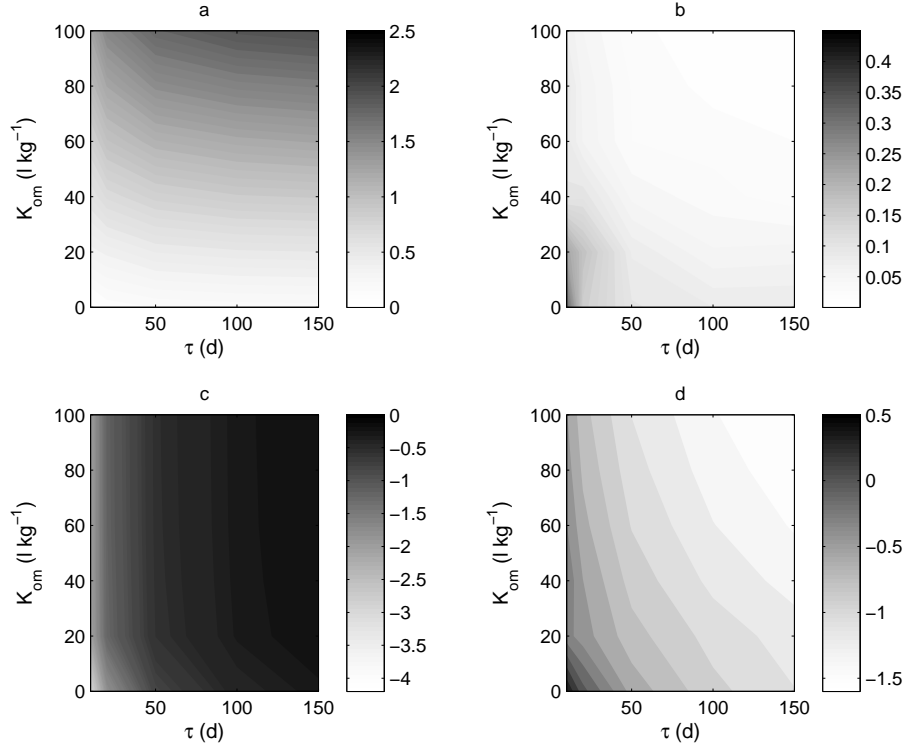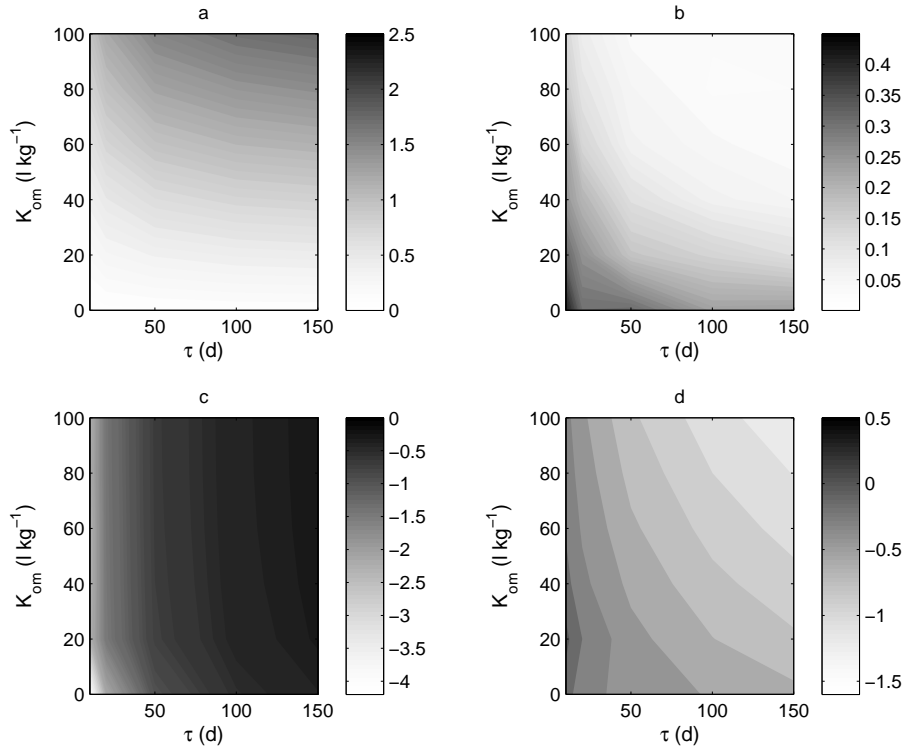
Figure 4.9: FOCUS Thiva scenario, precipitation surplus PE during travel time and leached fraction: mean and coefficient of variation. Same remarks as Figure 4.7.

During this shorter travel time, less solute can be degraded and thus the mean leached fraction is higher for Porto than for Hamburg. With a larger precipitation surplus, the leached fraction of contaminants would be higher in the same soil type (Beulke et al., 2002). The CV in the precipitation surplus is higher for Porto than for Hamburg, because of shorter travel times, resulting in less averaging of extremes in precipitation. The CV of the leached fraction is similar for both climates.

Figure 4.9 shows the mean and CV of the precipitation surplus during the travel time, and of the leached fraction for the drier climate of Thiva. The annual precipitation surplus is lower for Thiva, therefore the travel times are longer, which in turn results in a lower mean leached fraction. Similar to Porto, the relations between τ, K_{om} and mean precipitation surplus, CV in the precipitation surplus, and mean leached fraction are comparable to the results of the moderate climate of Hamburg. The CV in the leached fraction for Thiva shows a different pattern than for Hamburg. The CV in leached fraction is highest for a solute with $K_{om} = 20\,\mathrm{l\,kg}^{-1}$ and low τ. This can be explained with Fig. 4.10 that shows the monthly distribution of the precipitation surplus and leaching of a solute with
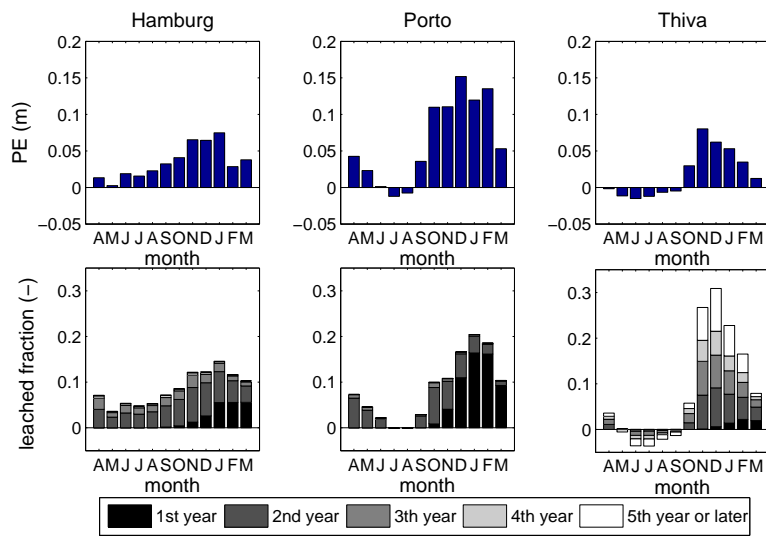
Figure 4.10: The distribution of the precipitation surplus PE and the leached fraction over the year, for the FOCUS Hamburg, Porto, and Thiva scenarios. The upper row shows the mean PE per month of the 20 realizations. The lower row shows the mean leached fractions per month (summed over the years following the application) of the 20 realizations for a solute with adsorption constant $K_{om} = 20\,\mathrm{l\,kg^{-1}}$ and half-life time $\tau = 10^6$ d. The legend item "1st year" means that this part leached in the first year after application.

$K_{om} = 20 \, \mathrm{l\,kg^{-1}}$ and $\tau = 10^6$ d for Hamburg, Porto, and Thiva. For Hamburg, the precipitation surplus is distributed most evenly over the months. For Porto, seasonal fluctuation is more distinct for a total annual precipitation surplus that is higher than for Hamburg. For Thiva, the seasonal fluctuation is more distinct than for Porto, and the total annual precipitation surplus is lower than for Hamburg. The monthly pattern in the leached fraction follows the monthly pattern in the precipitation surplus for the three climates. The leached fraction can be negative, if solutes are transported from depths larger than 1 m to depths smaller than 1 m with upward water flow. For a solute with $K_{om} = 20 \, \mathrm{l\,kg^{-1}}$ in the climate of Thiva, with seasonal fluctuation and low annual precipitation surplus, this results in leaching events that are separated by at least one year. The difference of at least one year between leaching events gives large differences in travel times, and therefore in the leached fraction.

For $K_{om} = 100 \, \mathrm{l\,kg^{-1}}$ the differences in travel time are smaller than for $K_{om} = 20 \, \mathrm{l\,kg^{-1}}$, as all travel times are larger than a year. The chance that a year with high precipitation is compensated with years with moderate and low precipitation is higher with a higher adsorption constant. The travel times for a solute with $K_{om} = 0 \, \mathrm{l\,kg^{-1}}$ are shorter than one year, therefore the CV in the leached fraction is smaller than for solutes with $K_{om} = 20 \, \mathrm{l\,kg^{-1}}$. Our results show a dependence of the leached fraction on the temporal distribution of precipitation and evaporation. Stochastic analyses that do not include this seasonality, can therefore over- or underestimate the leached fraction.

Our results correspond with McGrath et al. (2008a) who found that the travel time was smaller for a humid climate than for a semiarid climate. But they also found that the CV in the travel time was larger for a humid climate. The latter does not correspond with our results, we found the highest CV in the travel time (not shown) in the driest climate of Thiva. This difference is probably caused by that McGrath et al. (2008a) did not include seasonality in the rainfall properties.

4.4 Conclusions

Solute transport in a chemically heterogeneous, layered, soil was studied. The solute was only degradable in the aqueous phase, not in the adsorbed phase. Effective transport properties like the average plume velocity and the effective retardation factor were studied. Furthermore, we investigated the effect of transient weather conditions on the solute leaching.

The average velocity and the retardation factor were based on moments analysis. In particular, the adsorption constants and degradation rate were varied. Both for homogeneous soils with adsorption and for layered soils without adsorption, the depth of the solute plume increases linearly with increasing precipitation surplus, if the water storages at application and the moment of leaching are similar. However, if the adsorption constant varies as a function of depth, the depth of the center of mass of the solute plume does not increase linearly anymore with increasing precipitation surplus. Instead, in this paper, the velocity of the center of mass of a solute plume in a layered soil is found to depend on the adsorption constant, degradation rate, and dispersivity, if degradation occurs only in the

aqueous phase. This highlights that degradation and dispersion cannot be ignored when the travel time in a layered soil is estimated.

The effective retardation factor is usually determined by comparing either the velocities of the center of mass, or the travel times, of non-adsorbing and adsorbing solutes with each other. The effective retardation factor is shown to depend, besides adsorption, on dispersion and degradation. The effective retardation factor based on spatial moments is time dependent, and the effective retardation factor based on temporal moments depends on the distance travelled in a soil. As a result, it is not possible to derive one effective retardation factor for layered soils.

The leached fraction of an adsorbing solute, averaged over longer time series, is independent of the adsorption constant, if degradation occurs in the aqueous phase only. However, in this study, the leached fraction was lower for nonadsorbing solutes than for adsorbing solutes, but this is caused by the temperature dependency of the degradation rate and moment of application. The degradation rate decreases with decreasing temperature, causing higher degradation rates in summer than during winter. With pesticide application in spring, and a travel time of a non-adsorbing solute less than one year, the average degradation rate for the non-adsorbing solute is, therefore, larger than for adsorbing solutes. When the solute could be adsorbed, the leached fraction was independent on the adsorption constant. In this case, leaching is different from the case where a solute that degrades in both the adsorbed and aqueous phase, as then, the leached fraction is strongly affected by adsorption.

The precipitation and evaporation rates of a climate affect the travel time of a solute in the soil. With an increasing precipitation surplus, thus a decreasing travel time, there is less time for degradation, and obviously the leached fraction will be higher. Besides with the amount of precipitation and evaporation, the climate can influence the leached fraction by seasonality. Seasonal fluctuations in precipitation lead to large differences in travel times in a dry climate, and thus large differences in the leached fraction. This is especially the case for solutes with little adsorption. For a wet climate with seasonal fluctuation in the precipitation surplus, the CV in leached fraction is lower with adsorption than without adsorption, thus a high precipitation surplus diminishes the effect of seasonality.

5

Transport and degradation of propylene glycol in the vadose zone: model development and sensitivity analysis

Abstract

Transport and degradation of de-icing chemical (containing propylene glycol, PG) in the vadose zone was studied with a lysimeter experiment and a model, in which transient water flow, kinetic degradation of PG, and soil chemistry were combined. The lysimeter experiment indicated that aerobic as well as anaerobic degradation occurs in the vadose zone. Therefore, the model included both types of degradation, which was made possible by assuming an advection controlled (mobile) and a diffusion controlled (immobile) zone. In the mobile zone, oxygen can be transported by diffusion in the gas phase. The immobile zone is always water saturated, and oxygen only diffuses slowly in the water phase. Therefore, the model is designed in a way that the redox potential can decrease when PG is degraded, and thus anaerobic degradation can occur. In our model, MnO_2 (which is present in the soil) and NO_3^- (applied to enhance biodegradation) can be used as electron acceptors for anaerobic degradation. The application of NO_3^- does not result in a lower leaching of PG, nor in a slower depletion of MnO_2. The thickness of the snow-cover influences the leached fraction of PG, as with a high infiltration rate, transport is fast, there is less time for degradation, and thus more PG will leach. The model showed that, in this soil, the effect of the water flow dominates over the effect of the degradation parameters on the leaching at 1 meter depth.

5.1 Introduction

At Oslo airport in Norway de-icing chemicals are used to remove snow and ice from airplanes before departure during winter time. This is done on a platform, such that about 80% of the de-icing chemicals are collected, but the remaining is spread along the runways or carried further by the aircraft (OSL Airport, 2013). This results in an annual contaminant load of 100-200 tons to the airfield soil along the runways (Øvstedal and Wejden, 2007). During snowmelt, the infiltration rates are high, and the de-icing chemicals can be transported rapidly through the coarse textured soil on which the airport is located (French et al., 2001). The airport is located on a large unconfined aquifer, and groundwater contamination with the de-icing chemical should be avoided.

In the soil, de-icing chemicals consisting of the organic compound propylene glycol (PG) may be degraded by micro-organisms (Klecka et al., 1993; Veltman et al., 1998; Jaesche et al., 2006). Micro-organisms need electron acceptors for degradation of PG. This can be oxygen or in absence of oxygen other electron acceptors that are present in the soil, like manganese- or iron-oxides. Continuous application of PG may lead to a depletion of manganese and iron, and therefore lower the degradation potential of the soil. To avoid depletion of manganese and iron and to enhance biodegradation, remediation techniques can be used, for instance by applying nitrate, which can also be used as an electron acceptor (Cunningham et al., 2001). To study the degradation pathways of PG, we performed a lysimeter experiment. Both aerobic and anaerobic degradation products were observed in the experiment, in the form of metabolites, and leaching of manganese and iron.

To study the leaching of PG to groundwater, the long term effects of continuous PG application on manganese concentrations in the soil, and potential remediation strategies, modelling is needed. Commonly, models describing anaerobic degradation can be divided in two scales: either the aquifer scale (Hunter et al., 1998; Brun and Engesgaard, 2002; Mayer et al., 2002), or the aggregate scale with the order of centimeters (Leffelaar, 1988; Leffelaar and Wessel, 1988; Rappoldt, 1990; Leffelaar, 1993). At the aquifer scale, often steady state flow is assumed. In the vadose zone, this assumption is not valid with snowmelt when water flow is very dynamic, and a transient water flow approach is needed. Furthermore, as aquifers are saturated, they become anaerobic when oxygen is depleted. As was observed in the lysimeter experiment, in the vadose zone anaerobic zones may develop in aggregates. A model to describe transport and degradation of a contaminant, which can be used at the plot scale, and which includes anaerobic degradation, is rarely found according to Dassonville and Renault (2002). Therefore, we constructed a model for this purpose, by combining a hydrological model with a soil chemical model.

As both aerobic and anaerobic degradation were observed in the experiment, we want to combine transport in the vadose zone with the redox regime in an aggregate. We use a mobile-immobile concept for the soil, which conceptualizes an aerobic mobile zone, and an anaerobic immobile zone. In the model, the anaerobic immobile zone reflects water-saturated aggregates, or hardly accessible pores. In the aerobic mobile zone, solutes are transported by advection. Exchange of solutes between the aerobic and the anaerobic zones occurs by diffusion.

Different electron acceptors can be used for degradation, in both the aerobic and the anaerobic zones. One approach to model the transition between different electron acceptors is the use of a critical concentration for the most favourable (in gained energy) electron acceptor, below this concentration the less favourable electron acceptor will be used (Barry et al., 2002). Another approach was used by Kindred and Celia (1989) and Brauner and Widdowson (1997), who modelled simultaneous use of two electron acceptors by two different microbial communities for the degradation of a substrate. Some bacteria are known to be able to respire nitrate in the presence of O_2, although the physiological advantage is not clear (Carter et al., 1995). As the redox chemistry of the soil is included in our transport model, multiple electron acceptors can be used.

The objectives of this study are to (1) develop a conceptual model in which water flow, degradation, and soil chemistry in the vadose zone are combined, to study transport and degradation of a contaminant. The model contains an aerobic mobile zone and an anaerobic immobile zone. This model will be used to investigate (2) the long term effects of frequent PG application on the availability of electron acceptors, (3) the effect of nitrate application on PG leaching and availability of electron acceptors, and (4) the effect of the snowmelt (intensity and duration) on PG leaching.

5.2 Materials and methods

5.2.1 Biodegradation of propylene glycol

PG degradation by micro-organisms was modelled in this study by using O_2, NO_3^-, and MnO_2 (in order of preference) as electron acceptors. The redox equations are (Stumm and Morgan, 1996):

$$\frac{1}{4}O_2(g) + H^+ + e^- \rightleftharpoons \frac{1}{2}H_2O \qquad pe(W) = 13.75 \quad (5.1)$$

$$\frac{1}{5}NO_3^- + \frac{6}{5}H^+ + e^- \rightleftharpoons \frac{1}{10}N_2(g) + \frac{3}{5}H_2O \qquad pe(W) = 12.65 \quad (5.2)$$

$$\frac{1}{2}MnO_2(s) + 2H^+ + e^- \rightleftharpoons \frac{1}{2}Mn^{2+} + H_2O \qquad pe(W) = 9.8 \quad (5.3)$$
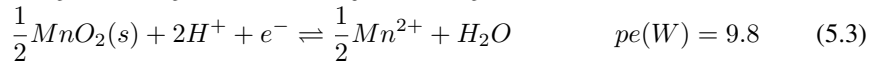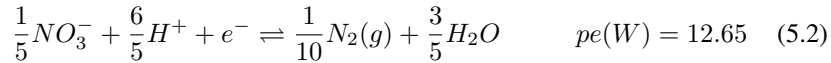
where pe is the redox potential. At lower redox potential, Fe-oxides can be used as electron-acceptor. Theoretically MnO_2 is a stronger oxidizer, so with equilibrium, reduction of Fe-oxides would only start after all MnO_2 is reduced. So, in the modelling adding Fe-oxides would not change the results.

The biodegradation rate is modelled with Monod kinetics (Barry et al., 2002):

$$\frac{d[O_2]}{dt} = \mu \frac{[O_2]}{K_{O_2} + [O_2]} \frac{[PG]}{K_{O_2,PG} + [PG]} B \tag{5.4}$$

$$\frac{d[NO_3^-]}{dt} = \mu \frac{[NO_3^-]}{K_{NO_3^-} + [NO_3^-]} \frac{[PG]}{K_{NO_3^-,PG} + [PG]} B \frac{K_{I,O_2}}{K_{I,O_2} + [O_2]} \tag{5.5}$$

$$\frac{d[MnO_2]}{dt} = \mu \frac{[MnO_2]}{K_{MnO_2} + [MnO_2]} \frac{[PG]}{K_{MnO_2,PG} + [PG]} B \frac{K_{I,O_2}}{K_{I,O_2} + [O_2]} \frac{K_{I,NO_3^-}}{K_{I,NO_3^-} + [NO_3^-]} \tag{5.6}$$

where $[O_2]$, $[NO_3^-]$, and $[MnO_2]$ are the concentrations of the electron-acceptors (mol m^{-3} water), t is time (s), μ is the maximum growth rate (s^{-1}), K_Y is the half saturation constant of substance Y (mol m^{-3} water), $[PG]$ is the concentration of propylene glycol (mol m^{-3} water), B is the biomass (mol m^{-3} soil), and $K_{I,Y}$ is an inhibition parameter (mol m^{-3} water). In Equations 5.5 and 5.6, the terms $\frac{K_{I,O_2}}{K_{I,O_2}+[O_2]}$ and $\frac{K_{I,NO_3^-}}{K_{I,NO_3^-}+[NO_3^-]}$ are introduced to ensure the order of preference for the electron-acceptors (Gallo, 2003). With a high O$_2$ concentration, the term $\frac{K_{I,O_2}}{K_{I,O_2}+[O_2]}$ is small, meaning that almost no NO$_3^-$ or MnO$_2$ will be used for biodegradation. The terms increase from 0 to 1, while the O$_2$ or NO$_3^-$ concentrations decrease.

The redox equations of NO$_3^-$ and MnO$_2$ (Eqs. 5.2 and 5.3) are rewritten to equivalent O$_2$ degradation rates. The sum of the three (rewritten) degradation rates is used to calculate PG degradation. The O$_2$ concentration is adjusted with the three (rewritten) degradation rates. In this way, the redox potential is correct. The reduction of NO$_3^-$ and MnO$_2$ is calculated automatically using the redox potential and chemical equilibria. Moreover, re-oxidation of reduced forms of nitrogen and manganese is included.

The biomass grows when PG is degraded:

$$\frac{dPG}{dt} = -\left(\frac{d[O_2]}{dt} + \frac{d[NO_3^-]}{dt} + \frac{d[MnO_2]}{dt} \right) \tag{5.7}$$

$$\frac{dB}{dt} = G \left(\frac{d[O_2]}{dt} + \frac{d[NO_3^-]}{dt} + \frac{d[MnO_2]}{dt} \right) \tag{5.8}$$

where G is a yield parameter (mol biomass mol^{-1} PG).

5.2.2 Sources and transport of electron-acceptors

For each electron-acceptor a different process is important for the transport or source of this electron-acceptor.

O$_2$ is transported by advection in water, and by diffusion in air. The diffusion constant of oxygen in air is higher than in water. As soil consists of water, air, and solids, the O$_2$ diffusion in soil depends on the fraction of air-filled pores. Furthermore, diffusion depends on the connectivity of the air-filled pores (Jin and Jury, 1996; Kawamoto et al., 2006). Soil respiration, which consumes oxygen, is caused by respiring micro-organisms and roots, where root respiration may be as large as microbial respiration (Kelting et al., 1998; Hanson et al., 2000). However, root respiration is ignored in the model, as it probably will be low during snowmelt when the temperature is low.

The model of Millington and Quirk (1961) calculates the diffusion constant of O$_2$ in soil:

$$D_s = D_a \frac{(n - \theta)^{\frac{10}{3}}}{n^2} \tag{5.9}$$

where D_s is the oxygen diffusion constant in soil (m^3 air m^{-1} soil s^{-1}), D_a is the oxygen diffusion constant in air (2×10^{-5} m^2 air s^{-1} (Denny, 1995)), θ is the soil moisture content
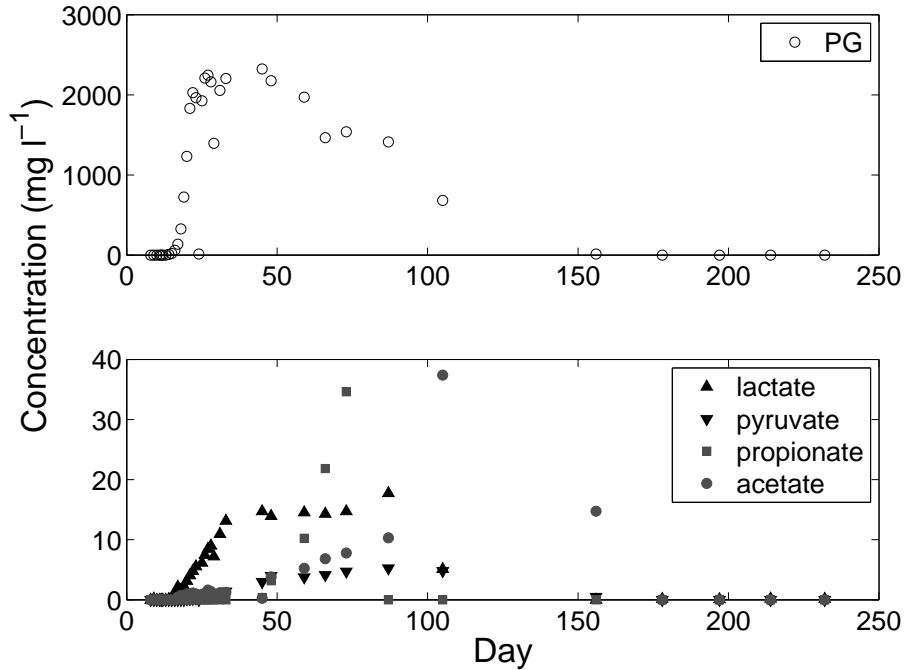
Figure 5.1: Measured concentration of propylene glycol and its degradation products. Lactate and pyruvate are formed with aerobic degradation of PG, propionate and acetate are formed with anaerobic degradation.

(m^3 m^{-3}), and n is the total porosity (m^3 m^{-3}). As the soil moisture content varies in time and in depth, also the diffusion constant varies in time and in depth. When D_s/D_a is smaller than 0.02, it is likely that anaerobic degradation occurs (Kristensen et al., 2010). O_2 in the gas phase is in equilibrium with O_2 in the water phase.

NO_3^- is applied to the soil surface, at the same time as PG. NO_3^- is only transported by advection in the water phase. With a decreasing redox potential, NO_3^- is transformed into N_2, via NO_2^- (Groffman et al., 2009; Laudone et al., 2011).

The most abundant form of manganese in soil is MnO_2. This manganese oxide can be used as electron acceptor, which gives Mn^{2+}. Re-oxidation and precipitation of other manganese(hydr)oxides are taken into account ($MnHCO_3^+$, MnO_4^-, MnO_4^{2-}, $MnOH^+$, and $Mn[OH]_3^-$). The chemical equilibria, and the present forms of nitrogen and manganese are calculated in ORCHESTRA (Objects Representing CHEmical Speciation and TRAnsport models, Meeussen (2003)).

84

5.2.3 Rationale for model structure and sensitivity analysis

To monitor the transport and degradation of the de-icing chemicals PG and potassium formate under close-to natural conditions, eight undisturbed soil cores (with diameter 0.3 m, and length 1 m, 0.071 m^3) were retrieved at the Oslo airport, Norway, and installed as non-weighable small scale lysimeters at the nearby research station, Moreppen, Gardermoen (Lissner et al., 2013). A description of the research station can be found in French et al. (1994). A vacuum control station (VS, UMS GmbH, Germany) that was connected to a sample bottle at the lysimeter outlet at 1 m depth regulated the applied suction of 60 hPa. Before snowmelt in March 2010, a mix of snow containing 350 g m^{-2} PG (Type I, Kilfrost), 71 g m^{-2} formate (Aviform L50, Addcon), and 17 g m^{-2} of bromide as conservative tracer were applied uniformly to the snow on top of each lysimeter on March 23. Following this, the lysimeters were exposed to natural weather conditions for one year. Due to high infiltration rates sampling was conducted intensively during snowmelt. The remaining year, the drainage was collected according to meteorological conditions as it became available.

Figure 5.1 shows the concentrations of propylene glycol (PG) and its degradation products measured in one of the lysimeters. Lactate and pyruvate are products that are formed with aerobic degradation of propylene glycol (PG), and propionate and acetate are formed with anaerobic degradation. From the observations is concluded that aerobic as well as anaerobic degradation occurs in the vadose zone in the lysimeter. Therefore, the model that will be used to study transport and degradation in this soil should include both degradation pathways, especially when the long term effects of degradation on the availability of electron acceptors are studied. The metabolites only serve as an indicator for the pathways, and are not included in the model, as eventually PG is degraded to CO_2.

5.2.4 Model structure

The snow, contaminated with PG, melts during spring and can infiltrate rapidly in the coarse textured soil (see Lissner et al. (2013) for a description of the texture). During snowmelt, PG is transported to about 2 m depth (French et al., 2001). Then, during summer, evaporation balances precipitation and PG transport is limited. The PG transport is transient and thus the flow model should include transient weather series as atmospheric boundary conditions. The degradation of PG depends on the availability of electron acceptors, like oxygen, nitrate and manganese oxide (in this study). The oxygen concentration in an unsaturated soil depends on the soil moisture content, which can be high during snowmelt. Concentrations of nitrate and manganese oxide, and the form in which these occur, depend on the redox conditions. Therefore, the redox chemistry in the soil should be included in the model.

To model transport and degradation of PG in the vadose zone, a hydrological and a chemical model need to be combined, which was done with the hydrological model SWAP (Soil, Water, Atmosphere and Plant, Van Dam et al. (1997)) and the code ORCHESTRA . Both models have been tested previously (Van Dam, 2000; Kroes et al., 2000; Van Beinum et al., 2000). SWAP can be used to model transient unsaturated water flow. Transient
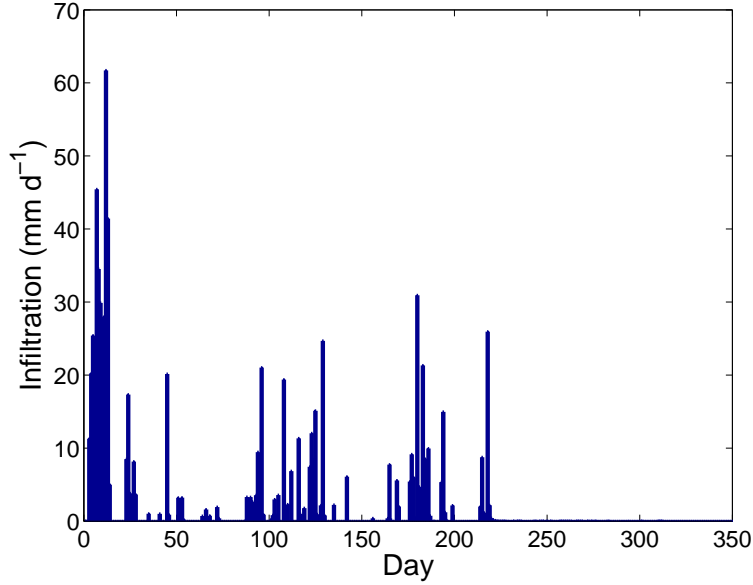
Figure 5.2: Infiltration rate.

precipitation and evaporation series from the year 1993 are used from the Gardermoen site, which is a year with an average amount of snow and precipitation. Before simulating with SWAP, snow formation and melt is simulated in a separate routine:

$$S(t) = bP(t) \qquad\qquad \text{if } T(t) < 0 \qquad\qquad (5.10)$$
$$M(t) = c\,(T(t) - T_{melt}) \qquad \text{if } T(t) > T_{melt} \qquad (5.11)$$
$$B(t) = (1 - 1/b)\,D(t) \qquad\qquad\qquad\qquad (5.12)$$

where S is the depth of fresh snow (m), b is a fitting parameter (m snow/m water), P is the precipitation (m), T is the temperature (°C), M is the snowmelt, c is a fitting parameter (m/°C), T_{melt} is the critical temperature for snowmelt (°C), B is the total storage available for water in the snowcover (i.e. porosity of the snowcover $\times$ depth of the snowcover, m), D is the thickness of the snowcover (m). Fresh snow S is added to the snowcover D. When the temperature is higher than 0 °C, P and M are added to the liquid water depth W. When W exceeds B, this is called infiltration. The resulting infiltration rate was used as precipitation in SWAP. The parameters b and c were fitted with data from other years, and were 8 m snow/m water, and 0.001 m/°C, respectively. The resulting infiltration rate is given in Fig. 5.2.

First, the water fluxes are generated as output by SWAP, then these are used as input for ORCHESTRA. Advection, kinetic degradation of PG, and chemical redox equilibria in the soil are modelled with ORCHESTRA. The solutes were transported by advection and numerical dispersion with the water fluxes. With snowmelt, the effect of advection is
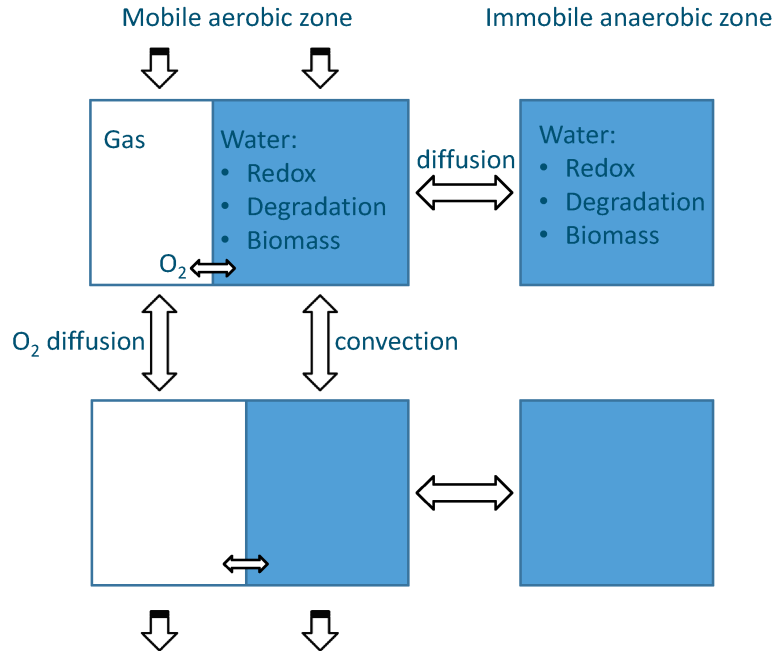
Figure 5.3: Schematic overview of the mobile-immobile model with redox chemistry.

probably larger than dispersion. Moreover, by including a mobile and immobile zone, and detailed chemistry, the calculation time is quite long. For these two reasons, we decided to not include dispersion explicitly. ORCHESTRA has a modular and object oriented architecture, which implies that new biogeochemical functionalities can be relatively easily implemented. The chemical reactions have been modelled assuming equilibrium.

From the lysimeter study was concluded that the soil should contain anaerobic zones (Lissner et al., 2013). Therefore, in the model, the soil was divided in aerobic and anaerobic zones. Figure 5.3 shows a schematic overview of the conceptual model with a mobile and immobile zone. The size of the zones is constant in time. The immobile zone is always saturated with water, and therefore can be anaerobic. In the mobile zone, water flows and solutes are advected, and oxygen is transported by diffusion in the gas phase. The water content in the mobile zone varies in time and depth, therefore, the diffusion constant for oxygen also varies (Eq. 5.9). The total water content of both zones is the same as the water content in a soil with only one zone. Therefore, the water content in the mobile zone is lower than the water content would be with one zone. Solutes are exchanged between the two zones, driven by the gradient in concentration. One diffusion constant was taken for all solutes: $1 \times 10^{-9} \, \text{m}^2 \, \text{s}^{-1}$, which is the diffusion constant of oxygen in water at $0\,^\circ$ C (Denny, 1995). The radius of the aggregates was 0.015 m. In both zones, PG is degraded (Eq. 5.7), and the biomass grows (Eq. 5.8). The chemical equi-

libria are calculated in both zones. As the redox potential can be different in both zones, the preferred electron acceptor can be different. From soil water retention characteristics was concluded that the saturated soil water content was 0.39 m^3 m^{-3}, and the immobile water content was 0.13 m^3 m^{-3}. In the model the immobile part covers 12.5% of the soil. Within the aggregates, a homogeneous solute and O$_2$ concentration is assumed.

5.2.5 Model parameterisation

The soil hydraulic parameters used in SWAP are given in Table 5.1. The infiltration rate is given in Fig. 5.2. The degradation parameters μ and K_Y in Eqs. 5.1-5.3 were fitted to obtain kinetic degradation rates that are similar to a total first order degradation rate of approximately 0.02 d^{-1} (derived by French et al. (2001) and Schotanus et al. (2012), see Table 5.1). These parameters are difficult to experimentally determine independently. The critical environmental factors controlling in situ biodegradation are soil water, oxygen, pH, nutrient status and temperature (Leahy and Colwell, 1990). The relationship between these factors, and μ and K_Y, is not only quite complex and nonlinear, but affected by these different factors differently. Experimental assessment of dependencies is difficult and costly, as the laboratory conditions are not representative for the field scale (Holden and Firestone, 1997). Therefore, we based the kinetic degradation parameters on the first order degradation rate that was determined for field conditions, and investigate the complexity by parameter variation.

5.2.6 Sensitivity analysis

Two case studies with the model will be discussed. First, the effect of nitrate application on the PG degradation and manganese oxide (MnO$_2$) will be shown. Second, the effect of the intensity and duration of the snowmelt on the leached fraction of PG is discussed. We have opted for these case studies to investigate the leaching risk of PG and use of nitrate as remediation measure at Oslo Airport. In Table 5.1, an overview of the used parameter values is given.

Nitrate application

Nitrate can be used as electron acceptor by micro-organisms, and therefore could lead to a lower PG leaching than without nitrate application. A sensitivity analysis of the degradation parameters and the inhibition parameter will be done. These parameter values were chosen, to be close to an apparent total first order degradation rate of approximately 0.02 d^{-1}, which was measured in the field (French et al., 2001). Furthermore, the PG leaching with nitrate application will be compared with PG leaching without nitrate application.

The first sensitivity analysis was done as follows:

1. Degradation parameters for PG:

    - μ: $3\times10^{-6}, 6\times10^{-6}, 9\times10^{-6}$ s^{-1}

Table 5.1: Overview of parameters.

	name	symbol	[]	standard value	sensitivity analysis
Applied or initial concentration	propylene glycol	[PG]	mol m^{-3}	5×10^{-3}	
	oxygen air	O$_2$ (g)	atm	0.2	
	nitrate	[NO$_3^-$]	mol m^{-3}	2×10^{-4}	
	manganese oxide	[MnO$_2$]	mol m^{-3}	3×10^{-4}	
Degradation	maximum growth rate	μ	s^{-1}	6×10^{-6}	6×10^{-7}, (1;3;9)$\times10^{-6}$, 6×10^{-5}
	half saturation constant PG	K$_{PG}$	mol m^{-3} water	1.25×10^{-3}	0, (1.25;6.25)$\times10^{-4}$, (1.25;1.88)$\times10^{-3}$, 1.25×10^{-2}
	half saturation constant O$_2$	K$_{O_2}$	mol m^{-3} water	5×10^{-5}	0, 5×10^{-6}, 5×10^{-4}
	half saturation constant NO$_3^-$	K$_{NO_3^-}$	mol m^{-3} water	5×10^{-5}	0, 5×10^{-6}, 5×10^{-4}
	half saturation constant MnO$_2$	K$_{MnO_2}$	mol m^{-3} water	1×10^{-4}	0, 1×10^{-5}, 1×10^{-4}, 1×10^{-3}
	inhibition O$_2$	K$_{I,O_2}$	mol m^{-3} water	2×10^{-4}	5×10^{-5}, 8×10^{-4}
	inhibition NO$_3^-$	K$_{I,NO_3^-}$	mol m^{-3} water	8×10^{-5}	
	initial biomass	B	mol m^{-3} soil	8.75×10^{-4}	8.75×10^{-5}, 8.75×10^{-3}
	yield parameter	G	mol biomass mol^{-1} PG	0.5	
Snowcover	infiltration rate		mm d^{-1}		20, 30, 40, 60
	duration		d		5, 10, 15
Soil hydraulic parameters	residual water content	θ_{res}	m^3 m^{-3}	0.0298	
	saturated water content	θ_{sat}	m^3 m^{-3}	0.3852	
		α	m^{-1}	2.61	
		n		1.4517	
	saturated conductivity	K$_{sat}$	m d^{-1}	1.13	
		l		0.5	
Miscellaneous	diffusion constant air	D$_a$	m^2 s^{-1}	2×10^{-5}	
	apparent diffusion constant	D$_w$	m^2 s^{-1}	1×10^{-9}	1×10^{-5}, 1×10^{-8}
	fraction immobile zone		%	12.5	5

- K_{PG}: 6.25×10^{-4}, 1.25×10^{-3}, 1.88×10^{-3} mol m^{-3} water

2. Inhibition parameter:

  - K_{I,O_2}: 5×10^{-5}, 2×10^{-4}, 8×10^{-4} mol m^{-3} water

3. Degradation parameters, with or without nitrate application:

  - μ: 6×10^{-7}, 6×10^{-5}
  - K_{PG}: 1.25×10^{-4}, 1.25×10^{-3}, 1.25×10^{-2} mol m^{-3} water
  - K_{O_2}: 5×10^{-6}, 5×10^{-5}, 5×10^{-4} mol m^{-3} water;
  - $K_{NO_3^-}$: 5×10^{-6}, 5×10^{-5}, 5×10^{-4} mol m^{-3} water
  - K_{MnO_2}: 1×10^{-5}, 1×10^{-4}, 1×10^{-3} mol m^{-3} water
  - B: 8.75×10^{-4}, 8.75×10^{-3} mol m^{-3} soil
  - the highest and lowest leaching resulting from 1

4. Inhibition parameter, with or without nitrate application:

  - K_{I,O_2}: 5×10^{-5}, 8×10^{-4} mol m^{-3} water

5. Apparent diffusion constant:

  - D$_w$: 1×10^{-8}, 1×10^{-5} m^2 s^{-1}

Intensity and duration of snowmelt

To investigate the effect of the thickness of the snowcover on the leached fraction of PG; the length of the snowmelt period, and the infiltration rate were varied. The length of the snowmelt was 5, 10, or 15 days, and the infiltration rate was 20, 30 40, or 60 mm d^{-1}. PG was applied with a constant concentration during the snowmelt period. Thus, the applied PG mass varied between 0.5 and 3 mol m^{-2}. The degradation rate was either kinetic with Monod (Eqs. 5.4-5.6), or zeroth order (by taking $K_Y \ll [Y]$ in Eqs. 5.4-5.6, and adjusting μ to reach a similar rate as with Monod). With zeroth order degradation, the degradation rate only depends on the biomass, not on the concentration of PG.

Furthermore, with the same initial mass of snow, the degradation parameters, the infiltration rate and the duration were varied:

- μ: 6×10^{-7}, 6×10^{-5} s^{-1}

- K$_{PG}$: 1.25×10^{-4}, 1.25×10^{-2} mol m^{-3} water

- K$_{O_2}$: 5×10^{-6}, 5×10^{-4} mol m^{-3} water

- K$_{NO_3^-}$: 5×10^{-6}, 5×10^{-4} mol m^{-3} water

- K$_{MnO_2}$: 1×10^{-5}, 1×10^{-3} mol m^{-3} water

- B: 8.75×10^{-5}, 8.75×10^{-4}, 8.75×10^{-3} mol m^{-3} soil

- infiltration rate: 20, 40 mm d^{-1}

- duration: 5, 10 d.

5.3 Results and discussion

5.3.1 Concentrations of PG, tracer and electron acceptors

Figure 5.4a shows the concentrations of PG and a tracer, scaled with the applied concentrations, in both the mobile and the immobile zone. In the mobile zone, the concentrations of PG and the tracer increase rapidly. The peak concentration is reached later in the immobile zone, and is lower than in the mobile zone. This is caused by diffusion between the two zones.

Figure 5.4b shows the concentrations of different nitrogen species. In the immobile zone, the NO_3^- is rapidly transformed to NO_2^- and then to N_2 (Groffman et al., 2009; Laudone et al., 2011). This is caused by the decreasing redox potential in the immobile zone, due to the consumption of oxygen by the micro-organisms. When the PG concentration is low, and thus the degradation rates are low, N_2 is transformed into NO_2^-, and then in NO_3^- as can be seen in Fig. 5.4b from day 320 onwards. As N_2 is a gas, in reality it probably would be transported by diffusion to the soil surface, and the nitrogen would leave the soil system. In the model however this is ignored. Also transformation of NO_3^- in NH_4^+ was included in the model, but this did not occur in the simulations.

Figure 5.4c shows the redox potential (expressed as pe) in the mobile and immobile zone. In the mobile zone, the pe is almost constant in time. This means that oxygen transport is always larger than oxygen consumption. In the immobile zone, the pe decreases when degradation of PG starts in the immobile zone. The pe increases again when PG degradation is small, and oxygen diffuses into the immobile zone. The pe increases quite suddenly, at the same time, N_2 is transformed in NO_2^-, because of the increase in the pe. Then, the PG concentration is low, and oxygen consumption does not exceed the diffusion anymore. The maximum value of the pe is higher, and the minimum value is lower than can be expected in a soil solution. In the model not all processes that occur in soil water can be included, these processes can buffer the pe. Therefore, in the model, the values of the pe are more extreme than would be expected in the field.

Figure 5.4d shows the degradation rates caused by O_2, NO_3^- and MnO_2 reduction (Eqs. 5.1 - 5.3). The rates increase because of an increasing PG or electron acceptor concentration, or because of an increasing biomass. In the mobile zone, O_2 results in the highest degradation rate, followed by NO_3^- and then MnO_2. This is caused by the definition of the rates, including the inhibition term(s) in the rates for NO_3^- and MnO_2. In the immobile zone, MnO_2 is the most important electron acceptor, as the concentrations of O_2 and NO_3^- are low in the immobile zone. The degradation rate by MnO_2 decreases from day 90 on, because the MnO_2 concentration decreases. Thus, different electron acceptors are used in the mobile and the immobile zone.
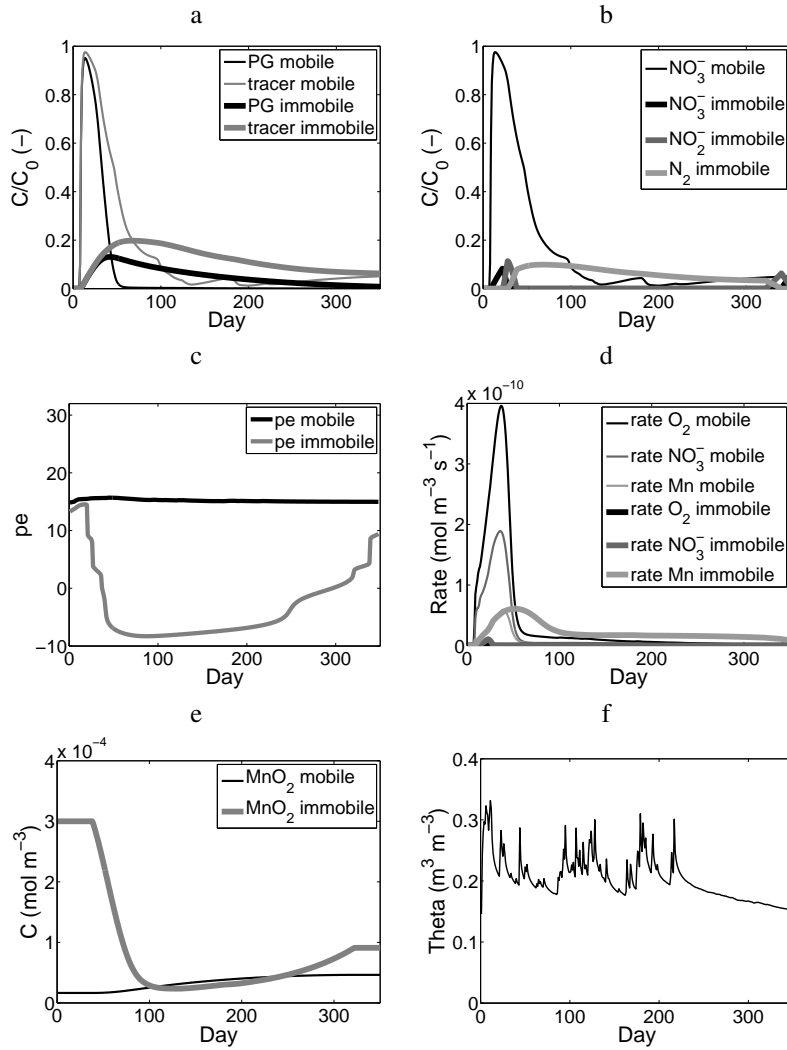
Figure 5.4: Concentrations of propylene glycol and a non-degradable tracer, in the mobile and immobile zone of the soil, at 1 m depth (**a**). Concentrations of NO_3^-, NO_2^- and N_2 (**b**). Redox potential (**c**). Degradation rates of O_2, NO_3^-, and MnO_2 (**d**). Concentration of manganese oxide (MnO_2) (**e**). Soil moisture content (**f**).

Figure 5.4e shows the manganese oxide (which is MnO_2) in both zones. The mineral is not transported by advection or by diffusion. In the immobile zone, the MnO_2 concentration decreases, while in the mobile zone the MnO_2 concentration increases. This is caused by diffusion of dissolved and reduced manganese from the immobile to the mobile zone. As O_2 and NO_3^- are consumed by the micro-organisms, the pe lowers and MnO_2 can be used as electron acceptor. This results in dissolved Mn^{2+} (and other dissolved forms of manganese). The dissolved forms can be transported by diffusion from the immobile to the mobile zone. In the mobile zone, the dissolved Mn^{2+} re-oxidizes and forms precipitates again to manganese oxide (MnO_2), as the pe is higher, and MnO_2 is the most common form at a higher pe. In the lysimeter experiment, dissolved manganese was observed in the drainage. This indicates that re-oxidation of dissolved manganese might be a rate limited process. However, for the chemical reactions, equilibrium was assumed in the model. Figure 5.4e shows that the manganese oxide concentration decreases in the immobile zone over the course of one year. With frequent PG application, manganese oxide might be further depleted in the immobile zone. As a result, the degradation in the immobile zone will become lower, and thus more PG may leach.

5.3.2 Sensitivity analysis

Nitrate application

In Fig. 5.4, nitrate was applied to enhance biodegradation. Nitrate can be used as electron acceptor by micro-organisms, and therefore could lead to a lower PG leaching than without nitrate application. As nitrate could be a contaminant in itself, the required application concentration should be known, to prevent nitrate leaching. In this section the effect of nitrate application on PG leaching will be investigated. As PG leaching depends on the degradation rate, first a sensitivity analysis of the degradation parameters and the inhibition parameter will be done. Then, for different parameter combinations, the PG leaching with nitrate application will be compared with PG leaching without nitrate application.

Figure 5.5a shows the leaching of a tracer and PG at 1 m depth. For PG, the maximum growth rate μ and the half saturation constant K_{PG} in Eqs. 5.4-5.6 were varied to study how sensitive PG leaching is to these parameters. For all parameter combinations, most leaching occurs in the first 50 days, during or just after snowmelt. With the high infiltration rate, solutes are transported rapidly in the coarse-textured soil (details on the texture distribution can be found in Lissner et al. (2013)). This was also found in the field experiment (Fig. 5.1). The highest leaching was found with a low μ and high K_{PG}, and the lowest leaching was found with a high μ and low K_{PG}, as was expected. In this coarsely textured soil, the effect of the water flow dominates the effect of the degradation parameters on the leaching at 1 meter depth. With increasing depth, the effect of the degradation parameters increases.

Figure 5.5b shows the effect of the inhibition parameter K_{I,O_2} in Eqs. 5.5-5.6 on the leached fraction of PG. When the inhibition parameter is lower, the leaching of PG is higher, because the oxygen concentration has to be lower before NO_3^- will be used for degradation. Figure 5.5c shows the leached fraction of PG with and without nitrate
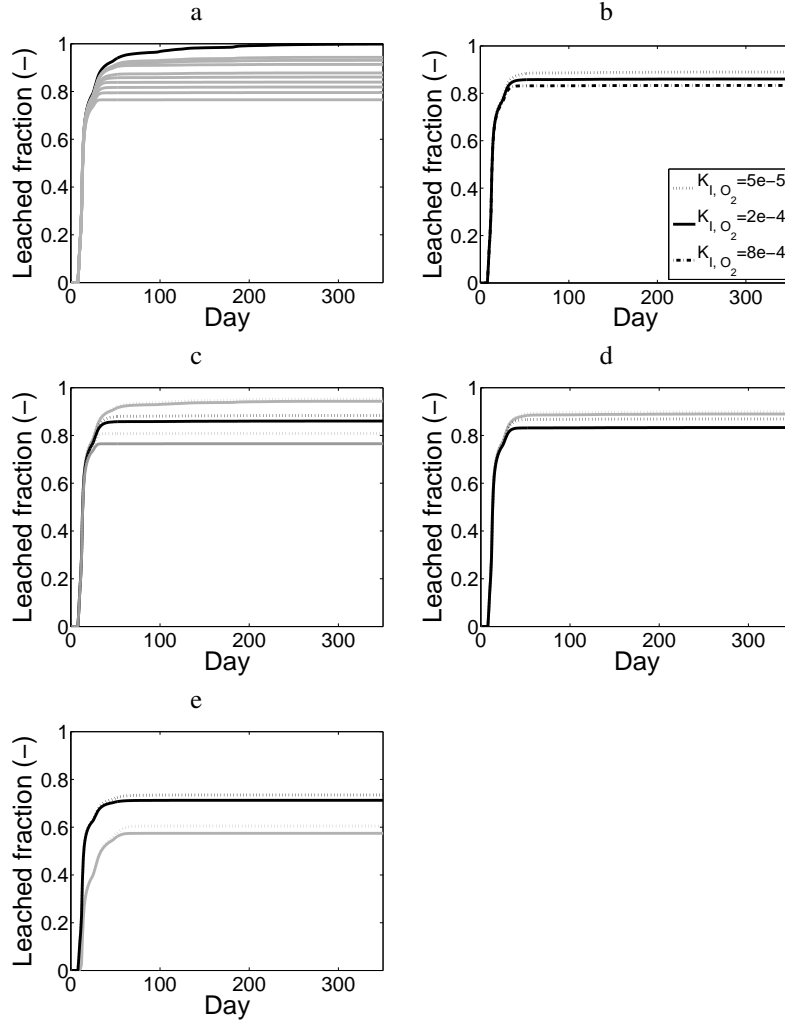
Figure 5.5: **a)** Sensitivity of leached PG fraction to parameters μ (values of 3×10^{-6}, 6×10^{-6}, and 9×10^{-6} s^{-1}), K_{PG} (values of 6.25×10^{-4}, 1.25×10^{-3}, and 1.88×10^{-3} mol m^{-3} water) in grey. The black line is a tracer. **b)** Sensitivity of leached PG fraction to inhibition parameter K_{I,O_2}. **c)** Sensitivity of leached PG fraction, with (solid lines) and without (dotted lines) nitrate application. The black line has the parameters μ=6×10^{-6} s^{-1}, K_{PG}=1.25×10^{-3} mol m^{-3} water, and K_{I,O_2}=2×10^{-4} mol m^{-3} water. The grey solid lines are the lines with the maximum and minimum PG leaching in **(a)**. **d)** Sensitivity of leached PG fraction to inhibition parameter K_{I,O_2}, with (solid lines) and without (dotted lines) nitrate application, with K_{I,O_2}=5×10^{-5}, and 8×10^{-4} mol m^{-3} water . **e)** Sensitivity of leached PG fraction to apparent diffusion constant D_w, with (solid lines) and without (dotted lines) nitrate application, with D_w=1×10^{-8} (black), and 1×10^{-5} (grey) m^2 s^{-1}.

application. Three combinations of μ and K_{PG} are shown: with the highest and lowest leaching in Fig. 5.5a, and with the median values. The leaching of PG is slightly lower when NO_3^- is applied, than without NO_3^- application. The immobile zone, in which anaerobic degradation occurs, is small (12.5%) compared to the mobile zone, in which aerobic degradation occurs. To study the effect of NO_3^- application on PG in more detail, the maximum growth rate, the half saturation constants and the initial biomass were varied over at least one order of magnitude. Also for these values, the difference between PG leaching with and without nitrate application was small. For the highest degradation rate resulting from these parameters, the difference was largest (9%), but this degradation rate was actually higher than the total first order degradation rate of approximately $0.02\ \mathrm{d}^{-1}$. Figure 5.5d shows the combined effect of the inhibition parameter and nitrate application. Also here, the effect of nitrate application on PG leaching is small ($<4\%$). The difference with and without nitrate application in PG leaching is largest for the lowest PG leaching. Finally, Fig. 5.5e shows the effect of the exchange between the mobile and immobile zones, which was approximated by changing the apparent diffusion constant. The leached fraction of PG decreases with an increasing D_w, because more PG can be degraded in the immobile zone. However, the effect of nitrate application on PG leaching is still small ($<3\%$).

For the different sets of parameters, the effect of the application of NO_3^- is small. This can be explained as follows (Figs. 5.6-5.7). Figure 5.6 shows the degradation rates of PG that are caused by O_2, NO_3^- and MnO_2, in both the mobile and the immobile zone, and with and without nitrate application. The degradation rates of O_2 are similar with and without nitrate application, in the mobile zone, and initially in the immobile zone. The reason for this is that O_2 is more preferred as an electron acceptor than NO_3^-, therefore, NO_3^- application does not influence the degradation rate for O_2 much. Obviously, due to the absence of NO_3^-, the degradation rate of NO_3^- is zero without nitrate application. In the mobile zone, the degradation rate for MnO_2 is lower with nitrate application than without. This is caused by the inhibition term in Eq. 5.6, which results in a lower degradation rate for MnO_2 in the presence of NO_3^-. On the other hand, in the immobile zone, the degradation rate for MnO_2 is higher with nitrate application than without. To explain this, the concentrations of PG, O_2, NO_3^- and MnO_2 in the mobile and the immobile zone, and with and without nitrate application will be discussed (Fig. 5.7). With nitrate application, the PG concentration is slightly lower than without. The O_2 concentrations are equal with and without nitrate application, for the same reason as explained in the previous paragraph. With nitrate application, the NO_3^- concentration decreases rapidly in the immobile zone. The redox potential decreases in the immobile zone, and thus NO_3^- is transformed into reduced forms of nitrogen. As a result, the NO_3^- concentration becomes zero, and NO_3^- cannot be used as electron acceptor anymore. The MnO_2 concentration in the immobile zone is slightly higher with nitrate application than without, because also NO_3^- was used as an electron acceptor. This means that less MnO_2 is reduced and thus mobilised. Thus, less manganese can diffuse to the mobile zone, and as a result the concentration MnO_2 in the mobile zone is slightly lower with nitrate application than without. As the MnO_2 concentration is higher with nitrate application, than without, and as a result, the degradation rate for MnO_2 is higher (Eq. 5.6).

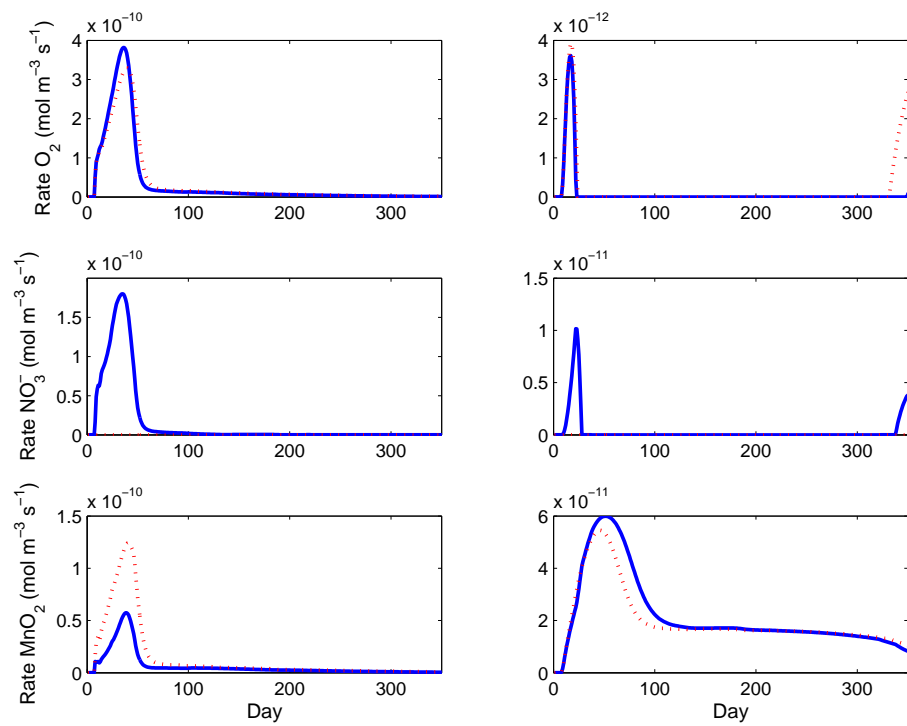Figure 5.6: Degradation rates of O_2, NO_3^-, and MnO_2 in the mobile (left) and immobile (right) zone of the soil, at 1 m depth, with (solid lines) and without (dotted lines) nitrate application.

Figure 5.7: Concentrations of PG, O_2, NO_3^-, and MnO_2 in the mobile (left) and immobile (right) zone of the soil, at 1 m depth, with (solid lines) and without (dotted lines) nitrate application.
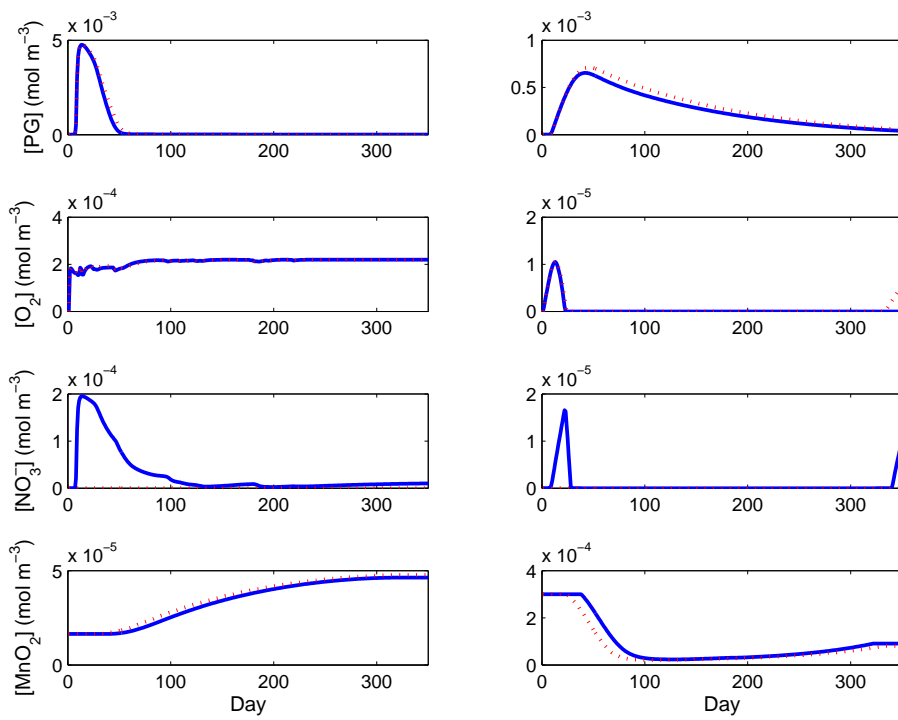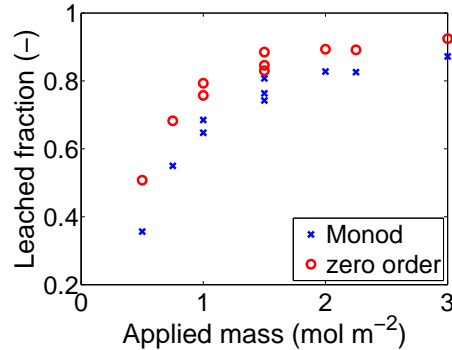
Figure 5.8: Leached fraction of PG, at 1 m depth, with Monod kinetics degradation or zero order degradation.

From Figs. 5.5 – 5.7 is concluded that with the chosen parameter values the application of nitrate does not result in a much lower PG leaching, nor a much slower depletion of MnO_2. Under low redox conditions, NO_3^- is transformed into reduced forms of nitrogen, and therefore the effect of NO_3^- as electron acceptor is small. In the mobile zone, sufficient O_2 is available, which is preferred as an electron-acceptor above NO_3^-. Thus, both in the mobile and immobile zone, the effect of NO_3^- application is small.

The parameter K_{I,O_2} in the inhibition term in Eq. 5.5 should be chosen such, that NO_3^- is used as an electron acceptor before it is chemically transformed in NO_2^-. In the simulations, the PG leaching may become lower, due to NO_3^- application, when the parameter K_{I,O_2} in the inhibition term in Eq. 5.5 is increased. Then, the inhibition term is closer to 1 at the same O_2 concentration, and thus the degradation rate by NO_3^- is higher. However, in Fig. 5.5b was shown that increasing K_{I,O_2} only results in a slightly lower PG leaching. This observation supports the conclusion that application of nitrate does not result in a lower PG leaching.

At larger depth, the effect of nitrate application may be larger, as oxygen diffusion to larger depths may be lower. Also in the groundwater, nitrate application may enhance biodegradation. Cunningham et al. (2001) added nitrate and sulphate to an aquifer contaminated with BTEX. They found that both nitrate and sulphate were used as electron acceptor, and that biodegradation could be enhanced. In the saturated aquifer, addition of electron acceptors may enhance biodegradation, while in the vadose zone addition would not lead to enhanced biodegradation.

Intensity and duration of snowmelt

The thickness of the snowcover might influence the redox potential in the soil during snowmelt. With a thicker snowcover, a higher infiltration rate, and thus a higher soil moisture content, might occur, leading to a lower oxygen diffusion in to the soil (Eq. 5.9).

Furthermore, with a thicker snowcover, the solute can be transported more rapidly in to the soil, which can lead to a higher solute leaching.

Figure 5.8 shows the simulated leached fractions of PG at 1 meter depth. The leached fractions differ from the leached fractions in Fig. 5.5 because the atmospheric boundary condition was changed. For both types of degradation, the leached fraction increases with increasing initial mass. The leached fraction only depends on the initial mass of snow, as different thicknesses of the snowcover and different meltrates, result in the same leached fraction. Furthermore, with the same initial mass of snow, the degradation parameters, the infiltration rate and the duration were varied. The leached fraction was found to depend on the degradation parameters, not on the infiltration rate or the duration, similar as in Fig. 5.8.

The high infiltration rate during snowmelt, and the subsequent high soil moisture content do not lower the degradation rate with the chosen parameter values. Moreover, as the biomass is low during snowmelt, and the degradation rate increases with increasing biomass, the degradation rate is low during snowmelt. The O_2 concentration in the mobile zone is always high enough, such that aerobic degradation is not limited. The effect of the low biomass on the degradation rate is larger than the effect of the high soil moisture content. However, the amount of snow influences the leached fraction of PG, as with a large amount of snow, transport is fast, there is less time for degradation, and thus more PG will leach.

5.4 Conclusions

Transport and degradation of de-icing chemical (containing propylene glycol, PG) in the vadose zone were studied with a lysimeter experiment and with a model. The lysimeter experiment indicated that aerobic as well as anaerobic degradation occurs in the vadose zone. One way to simulate this in a model was to assume the existence of both diffusion and advection controlled zones.

To model transport and degradation of PG in the vadose zone, a hydrological and a chemical model were combined. The combined model can simulate transient water flow, soil chemistry and PG degradation. The model includes an aerobic mobile zone and an anaerobic immobile zone. This was necessary, as with only a mobile zone, the anaerobic degradation which was measured, could not be explained. We first compared the combined model with a mobile zone only model: the diffusion of O_2 in the soil was high enough to maintain a high O_2 concentration in the coarse soil, while O_2 was used for degradation. The high soil moisture content caused by the snowmelt did not result in anaerobic soil parts. Including the immobile zone in the model, the redox potential decreased, and thus anaerobic degradation could occur.

In the immobile zone, the MnO_2 concentration decreased, while in the mobile zone the MnO_2 concentration increased. This was caused by diffusion of dissolved manganese from the immobile to the mobile zone. The application of NO_3^- to enhance biodegradation did not result in a lower leaching of PG, nor in a slower depletion of MnO_2. In the mobile

zone, O_2 was preferred over NO_3^-, and in the immobile zone, NO_3^- was transformed in reduced nitrogen forms.

The length of the snowmelt and the infiltration rate were varied, to study the effect on the PG leaching. The mobile zone was always aerobic, such that degradation was not limited. The amount of snow influenced the leached fraction of PG, as with a high infiltration rate, transport is fast, there is less time for degradation, and thus more PG will leach. In this soil, the effect of the water flow dominates the effect of the degradation parameters on the leaching at 1 meter depth. With increasing depth, the effect of the degradation parameters increases.

6

Synthesis
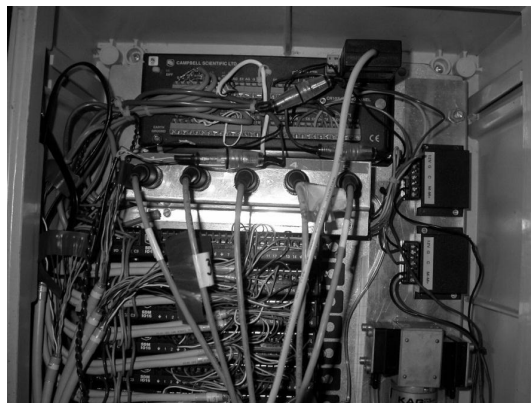
In this thesis, variability in contaminant leaching was discussed, which depends on spatially variable soil properties and transient infiltration rates. Organic degradable contaminants were studied, such as de-icing chemicals (consisting of propylene glycol, PG) and pesticides. In this Chapter, the conclusions from Chapters 2–5 will be summarized by answering the research questions from Chapter 1. Furthermore, an outlook of the results will be given.

6.1   Research questions

- How consistent are preferential flow paths between two seasons with different infiltration rates?

In Chapter 2, a field experiment with a multi-compartment sampler (consisting of 10×10 cells of $3.15 \times 3.15 \text{ cm}^2$ each) was described. This experiment consisted of two parts: one part was done during snowmelt with a high infiltration rate, and the other using irrigation with a lower infiltration rate. The spatial and temporal variability of leaching, and the effect of snowmelt on leaching was quantified, and additionally the leaching of the non-degradable and the degradable contaminant (propylene glycol, PG) was compared.

For both experiments the highest bromide concentrations were found in the same area, thus the preferential flow paths were consistent and independent on the infiltration rate. In the snowmelt experiment a lower exchange between flow paths and its surrounding area was found than in the irrigation experiment. This is caused by the higher infiltration rate during the snowmelt experiment. With low infiltration rates, as in the irrigation experiment, there are more isolated peaks in the bromide leaching than in the snowmelt experiment. The heterogeneous flow in the soil, therefore, is probably caused by small changes in the soil hydraulic properties under different soil moisture contents, and not by macropores. When soil heterogeneity is caused by heterogeneous hydraulic properties under different soil moisture contents, a larger part of the coarse textured soil is highly conductive with a higher infiltration rate. This was observed in the experiment, as the spatial autocorrelation of the leaching of cells was higher with higher infiltration rates. At the scale of the multi-compartment sampler, heterogeneous melting of snow did not influence the heterogeneous flow in the soil.

The highest PG concentrations and the highest bromide concentrations were found in the same areas in the irrigation experiment. Furthermore, the leached masses of the tracer and PG were highly correlated, but the leaching of PG was lower due to degradation. Thus, leaching of a degradable contaminant is similar as of a tracer, but with lower mass.

- How does the infiltration rate determine the spatial distribution and the leached fraction of a degradable contaminant?

The results of the experiment were used in a two dimensional model (Chapter 3), as a random field for a scaling factor for the retention curve was based on the spatial distribution of leaching (Šimunek and Sejna, 1999). This random field was used in a model,

with different transient and steady state infiltration rates. Both the standard deviation and the lateral correlation length determined the spatial distribution of leaching in the model. The correlation length in the direction of flow did not influence the spatial distribution much.

The infiltration rate influences the leaching of a degradable contaminant in two ways. Firstly, the travel time of the contaminant in the soil obviously depends on the infiltration rate. Secondly, the fraction of the soil that contributes to contaminant leaching is influenced by the infiltration rate. As a result, the spatial distribution of contaminant leaching is influenced. With this modelling approach, leaching of a degradable contaminant will be higher than would be estimated with independent stream tubes.

In the field experiment, the weather series were transient due to snowmelt. When this would be approximated with a steady state simulation with an average infiltration rate, the leaching of a degradable contaminant would be underestimated, as the high infiltration rate from the snowmelt is distributed over a longer time. Without snowmelt, a steady state simulation could overestimate the leaching of a degradable contaminant.

- How can the contaminant plume propagation in a layered soil be approximated with average parameters, temporally as well as spatially?

In Chapter 4, the effect of transient and steady state weather on contaminant leaching was also studied in a one dimensional model with a soil that was layered in the adsorption properties (Van Dam et al., 1997). In this study, the contaminant was only degradable in the aqueous phase, not in the adsorbed phase. Besides with the amount of precipitation and evaporation, the climate can influence the leached fraction by seasonality. For a dry climate, seasonal fluctuations in the precipitation and evaporation lead to large differences in travel times in the soil, and thus to large differences in the leached fraction to the groundwater. For a wet climate, the variation in the leached fraction is lower with adsorption than without adsorption, thus a high precipitation surplus diminishes the effect of seasonality.

Besides the weather series, effective transport properties like the average plume velocity and the effective retardation factor were studied for a layered soil and a contaminant that is only degraded in the aqueous phase. The average velocity and the retardation factor were based on moments analysis. In a homogeneous soil with adsorption, the depth of the contaminant plume increases linearly with increasing precipitation surplus. However, in soils that are layered in the adsorption constant, the depth of the center of mass of the contaminant plume depends on the adsorption constant, degradation rate, and dispersivity, if degradation occurs only in the aqueous phase.

The effective retardation factor is usually determined by comparing either the velocities of the center of mass, or the travel times, of non-adsorbing and adsorbing contaminants with each other. The effective retardation factor is shown to depend, besides adsorption, on dispersion and degradation. The effective retardation factor based on spatial moments is time dependent, and the effective retardation factor based on temporal moments depends on the distance travelled in a soil. As a result, it is not possible to derive one effective retardation factor for layered soils.

104

- How does the redox potential in the vadose zone influence contaminant degradation, and how can this be included in a transport model?

In Chapter 5, transport and degradation of de-icing chemical in the vadose zone is described. De-icing chemical (containing PG) can be degraded by micro-organisms. A lysimeter experiment in the field showed that both aerobic and anaerobic degradation pathways of PG occur in the vadose zone. To model transport and degradation of PG, a hydrological and chemical model were combined. The model includes an aerobic mobile zone and an anaerobic immobile zone, to include both degradation pathways. Anaerobic degradation did not occur during snowmelt, with a high soil moisture content, but in the immobile zone, after snowmelt. Then, the MnO_2 concentration decreases in the immobile zone, while in the mobile zone the MnO_2 concentration increases. This is caused by diffusion of dissolved manganese from the immobile to the mobile zone. The application of NO_3^- to enhance biodegradation does not result in a lower leaching of PG, nor in a slower depletion of MnO_2.

Varying the length of the snowmelt and the infiltration rate showed that the mobile zone is always aerobic, also during snowmelt when little oxygen diffusion is possible. Thus, a thick snowcover, and a high meltrate do not result in anaerobic degradation. However, the thickness of the snowcover does influences the leached fraction of PG, as with a high infiltration rate, transport is fast, there is less time for degradation, and thus more PG will leach. In the coarse textured soil, the effect of the water flow dominates the effect on the degradation parameters on the leaching.

6.2 Outlook

6.2.1 Layered soil

In a homogeneous soil, the movement of a contaminant plume can be estimated from the cumulative, stationary, precipitation rate. When the contaminant adsorbs and is degraded with the same rate in the adsorbed and aqueous phase, also the retardation factor should be included to estimate the average depth of the contaminant plume. However, when the contaminant only degrades in the aqueous phase, but not in the adsorbed phase, a retardation factor cannot be determined for a soil that is layered in the adsorption constant. Then, the retardation factor, and thus the movement of the contaminant plume, depends on the dispersivity and the degradation rate, besides the adsorption constant. In a layered soil, this leads to a slower movement of the contaminant plume when the contaminant is only degraded in the aqueous phase, compared to when it is degraded in both phases.

The results can be incorporated in a model that is used to determine the risk of contaminant leaching from the vadose zone to the groundwater on the field scale, which is often based on distributions of the local velocity and dispersion coefficient. For such distributions, approximations with simplified stationary weather series, and homogeneous soil properties, are used. However, in a layered soil, with a contaminant that is only degraded in the aqueous phase, these approximations may lead to too high velocities, and thus in wrong estimations of contaminant leaching. It cannot be concluded beforehand

that a too high velocity results in a too high leached fraction to the groundwater of the contaminant, because also the effective degradation constant (i.e. combined for the adsorbed and aqueous phases) is different for both types of degradation. When a distribution is used for the velocity of a contaminant that only degrades in the aqueous phase, it should be taken into account that the effective retardation factor, and thus the velocity, differs in a layered soil and a homogenous soil. A general relation between the effective retardation factor and the adsorption properties of soil layers might be derived, although this was not found in a steady state analytical approach either.

6.2.2 Preventing leaching of PG

To enhance biodegradation of PG, and to avoid depletion of natural electron-acceptors, electron-acceptors can be added to the soil. It appeared that, in the vadose zone, application of the electron-acceptor nitrate was not effective to reduce PG leaching, or depletion of natural electron-acceptors. In the aerobic part of the vadose zone, sufficient oxygen is available, and in the anaerobic part nitrate is rapidly reduced, and thus not available anymore for degradation. In contrast to the vadose zone, application of electron-acceptors to the groundwater may result in more effective degradation (Cunningham et al., 2001). In the groundwater, transport of oxygen is much slower than in the vadose zone. However, this should be done carefully, to avoid groundwater contamination with for example nitrate.

To minimize the risk of PG leaching from the vadose zone to the groundwater, application of extra electron-acceptors is not successful. Better options to minimize leaching are to avoid contamination of the snow with PG, or to remove contaminated snow from the surrounding of the runways. Then the initial mass and the infiltration rate would be reduced.

6.2.3 Snow and contaminant transport

De-icing chemicals are applied during winter time, and are stored in the snowcover until spring. During snowmelt, PG can infiltrate in the soil with the meltwater, with a high infiltration rate. Thus, infiltration of PG is characterised by high loads in a short period of time, and by fast transport. A thicker snowcover and a higher meltrate of the snow, result in a higher PG leaching, as then the PG plume is transported faster to depths with little microbial activity.

Regarding soil chemistry, the thickness of the snowcover and the meltrate do not influence PG degradation. The soil is aerobic during snowmelt, although the soil moisture content is high and thus oxygen diffusion is low. Apparently, oxygen consumption by degradation does not exceed oxygen transport during snowmelt. This can partly be caused by a relatively inactive biomass during the cold snowmelt period in the beginning of the year. Temperature has an effect on biodegradation, with increasing temperature, degradation rates are higher (Jaesche et al., 2006). As a result of this temperature effect, nearly no degradation is observed in the field during spring. In this model, temperature was ignored, but low degradation during snowmelt was established with a low initial biomass.

106

However, transport of heat can be included in the model. A term for the temperature can be included in the degradation rates. As temperature generally decreases with depth, the degradation rate would decrease with depth. Also microbial biomass decreases with depth, due to smaller availability of carbon (Blume et al., 2002).

Heterogeneous leaching of a tracer and the degradable PG was observed in a coarsely textured soil. The soil heterogeneity was caused by small scale differences in the soil hydraulic properties. With high infiltration rates from the snowmelt, the contaminant leaching was more homogeneous. This is typical for a coarsely textured, stuctureless soil, which is found at Oslo airport. Thus this results is site-specific, at other sites, macropore flow might occur. In a soil where macropore flow dominates, the leaching would be more heterogeneous with high infiltration rates, as then the macropores can be activated. With a high infiltration rate, and thus a higher soil moisture content, a larger part of the coarse textured soil has a high conductivity than with low soil moisture content. Due to the high infiltration rate, the water and contaminant is horizontally redistributed. As a result, the contaminant leaching is higher than it would be in a one dimensional approach. The snowmelt leads to an extreme infiltration event, compared to the remaining of the year, which makes it difficult to estimate an equivalent steady state infiltration rate. Snowmelt is inextricably bound up with infiltration of de-icing chemicals. Therefore, using a one dimensional model with steady state infiltration would result in an erroneous estimate of PG leaching. Snow influences contaminant transport mostly by the high infiltration rate, such that contaminants can be transported rapidly, and that a large fraction of the soil is active in contaminant transport due to the high soil moisture content.

Transport and degradation of de-icing chemical was modelled with a model with a mobile and an immobile zone, which resulted in an aerobic mobile zone, and an anaerobic immobile zone during degradation. In the model, the size of the immobile zone was constant in time, and was estimated from the retention curve. However, the size of the immobile zone probably varies in time. In Chapters 2 and 3 was shown that the spatial distribution of contaminant leaching depends on the infiltration rate. To include this dependence, the immobile zone should change in time. This would only affect the results during wet periods, as then, the zone that is immobile during drier periods can be mobile. In the current model, the breakthrough of contaminants is faster than it actually should be, due to the constant size of the immobile zone. Chemically, a variable size for the immobile zone would not influence the results, as there were no anaerobic soil parts during snowmelt. During drier periods, when anaerobic degradation occurred, the size of the immobile zone would be the same as in the current simulations. Deriving the size of the immobile zone with a field experiment would be a hard task, as the size varies both in time and depth. A two dimensional model could be used to study the size of the immobile zone under transient infiltration. Then, also the possible change of size of the immobile zone with depth can be included. When this is done, aggregates with a variable size can be included in the current model. Now, it is assumed that the oxygen and solutes are mixed instantly and completely over the size of the immobile zone. With more information on the distribution of the aggregate size in time and depth, transport within an aggregate can be included. This would influence the redox regime in the aggregates, as oxygen and so-

lutes will be transported slower inside the aggregates than in the instantly mixed immobile zone.

In the current model, the hydrological and chemical parts (including degradation) are solved separately. However, the soil hydraulic properties can change due to biomass growth. Bielefeldt et al. (2002) observed a decrease in the saturated hydraulic conductivity, and an increase of the dispersivity with an increasing biomass. Therefore, solving both models simultaneously, would lead to slower transport. Probably this effect will be small in the coarse textured soil.

Knowledge of the biomass can improve the parameter estimation for the model. Growth parameters of the biomass could be estimated from observations, as the biomass is important for the degradation rate with Monod kinetics. In this model, decay of the biomass was not included. When depletion of manganese-oxides is studied over several years, decay of biomass should be included.

6.2.4 Transfer to other sites

With experimental results from one site, one of the problems is that conclusions cannot be directly transferred to other sites. In the experiment, contaminant leaching was measured at a high spatial resolution, which can only be done at a small scale. To estimate contaminant leaching at the larger field scale, scaling approaches are needed (Vereecken et al., 2007). The results of the experiment can be used to develop such scaling approaches, which include leaching at different spatial scales. With these general scaling approaches, the results can be transferred to other fields. The small scale heterogeneous leaching measured in this experiment can be included in the prediction for the larger scale, for instance by including the travel time distribution at the small scale.

At scales larger than used in this thesis, heterogeneous infiltration resulting from snowmelt or microtopography may play a role, leading to locally faster transport. Furthermore, at larger depths than investigated here, the spatial distribution of soil properties should be determined, to estimate leaching in heterogeneous soil at larger depth. In this thesis was assumed that the parameters for the random field for the scaling factors were homogeneous in depth. This might not be valid, as the soil can consist of layers with different hydraulic properties, or due to decreasing bioactivity with increasing depth.

Appendix: Semi-analytical solution for layered soil

We present a semi-analytical solution for a two layer soil with degradation in aqueous phase only. The partial differential equations are Laplace transformed. An analytical solution for the backward transformation could not be found, therefore the equations are solved numerically. A practical application of this solution is to determine an effective retardation factor for the two layers.

The convection diffusion equation is used. For the upper layer

$$
\begin{aligned}
&R\frac{\partial c_1}{\partial t} = D_1\frac{\partial^2 c_1}{\partial x^2} - v_1\frac{\partial c_1}{\partial x} - \mu c_1 && t > 0, \quad 0 < x < L, \\
&c_1(x,0) = 0, && 0 < x < L, \\
&c_1(0,t) - \frac{D_1}{v_1}\frac{\partial c_1}{\partial x}(0,t) = C_0 && 0 \le t < t_p, \\
&c_1(0,t) = 0 && t_p \le t
\end{aligned}
\tag{A.1}
$$

and for the lower layer

$$
\begin{aligned}
&\frac{\partial c_2}{\partial t} = D_2\frac{\partial^2 c_2}{\partial x^2} - v_2\frac{\partial c_2}{\partial x} - \mu c_2 && t > 0, \quad L < x, \\
&c_2(x,0) = 0, && L > x, \\
&\frac{\partial c_2(x,t)}{\partial x} = 0, && x = \infty, \quad t > 0,
\end{aligned}
\tag{A.2}
$$

At the interface x=L continuity of the resident concentration (c^r) and flux concentration (c^f) is required ($c^f = c^r - \frac{D}{v}\frac{\partial c^r}{\partial x}$) (Kreft and Zuber, 1978)

$$
\begin{aligned}
&c_1(L,t) = c_2(L,t), && t \ge 0, \\
&c_1(L,t) - \frac{D_1}{v_1}\frac{\partial c_1(L,t)}{\partial x} = c_2(L,t) - \frac{D_2}{v_2}\frac{\partial c_2(L,t)}{\partial x} && t \ge 0,
\end{aligned}
\tag{A.3}
$$

The equations are scaled with (Veling, 1993)

$$\zeta = \frac{v_1 z}{D_1}, \quad \zeta_L = \frac{v_1 x_L}{D_1}, \quad \tau = \frac{v_1{}^2 t}{R D_1}, \quad \tau_p = \frac{v_1{}^2 t_p}{R D_1}, \quad \epsilon = \frac{\mu D_1}{v_1{}^2},$$
$$C_1(\zeta, t) = c_1(x, t), \quad C_2(\zeta, \tau) = c_2(x, t) \tag{A.4}$$

To solve the scaled equations, Laplace transformation is used
$(\overline{C}(\zeta; s) = \int_0^\infty C(\zeta, \tau') exp(-s\tau') d\tau)$. This gives for the upper layer

$$\frac{d^2 \overline{C_1}}{d\zeta^2} - \frac{d\overline{C_1}}{d\zeta} - (s + \epsilon)\overline{C_1} = 0 \qquad\qquad 0 < \zeta < \zeta_L,$$
$$\overline{C_1}(0; s) - \frac{d\overline{C_1}}{\zeta}(0; s) = C_0(1 - exp(-s/\tau_p))/s \qquad \zeta = 0, \tag{A.5}$$

and for the lower layer

$$\frac{D_2}{D_1} \frac{d^2 \overline{C_2}}{d\zeta^2} - \frac{v_2}{v_1} \frac{d\overline{C_2}}{d\zeta} - \left(\frac{s}{R} + \epsilon\right)\overline{C_2} = 0 \qquad \zeta_L < \zeta,$$
$$\frac{d\overline{C_2}(\zeta, t)}{d\zeta} = 0 \qquad\qquad\qquad \zeta = \infty \tag{A.6}$$

At the boundary x=L

$$\overline{C_1}(\zeta_L, s) = \overline{C_2}(\zeta_L, s) \qquad\qquad\qquad\qquad \tau \geq 0,$$
$$\overline{C_1}(\zeta_L, s) - \frac{d\overline{C_1}(\zeta_L, s)}{d\zeta} = \overline{C_2}(\zeta_L, s) - \frac{D_2 v_1}{D_1 v_2} \frac{d\overline{C_2}(\zeta_L, s)}{d\zeta} \qquad \tau \geq 0. \tag{A.7}$$

Solutions of equations A.5 and A.6 have the form

$$\overline{C_1}(\zeta; s) = A exp(\lambda_1 \zeta) + B exp(\lambda_2 \zeta) \tag{A.8}$$
$$\overline{C_2}(\zeta; s) = E exp(\lambda_3 \zeta) + F exp(\lambda_4 \zeta) \tag{A.9}$$

The constants λ_1, λ_2, λ_3 and λ_4 are given by

$$\lambda_{1,2} = \frac{1}{2} \left(1 \pm \sqrt{1 + 4(\epsilon + s)}\right),$$
$$\lambda_{3,4} = \frac{1}{2} \frac{D_1}{D_2} \left(\frac{v_2}{v_1} \pm \sqrt{\left(\frac{v_2}{v_1}\right)^2 + 4\frac{D_2}{D_1}\left(\frac{s}{R} + \epsilon\right)}\right) \tag{A.10}$$

With the abbreviations

$$F_1 = -\lambda_2 + \frac{D_2 v_1}{D_1 v_2} \lambda_3 = \lambda_1 - \frac{D_2 v_1}{D_1 v_2} \lambda_4,$$
$$F_2 = -\lambda_1 + \frac{D_2 v_1}{D_1 v_2} \lambda_3 = \lambda_2 - \frac{D_2 v_1}{D_1 v_2} \lambda_4,$$
$$Q = C_0(1 - exp(-s\tau_p))/s. \tag{A.11}$$

110

A, B and F can be written as (E=0)

$$A = -Q \frac{F_2 exp(\lambda_2 \zeta_L)}{(1 - \lambda_2)F_1 exp(\lambda_1 \zeta_L) - \lambda_2 F_2 exp(\lambda_2 \zeta_L)}, \quad \text{(A.12)}$$

$$B = Q \frac{F_1 exp(\lambda_1 \zeta_L)}{(1 - \lambda_2)F_1 exp(\lambda_1 \zeta_L) - \lambda_2 F_2 exp(\lambda_2 \zeta_L)}, \quad \text{(A.13)}$$

$$C = Q \frac{(F_1 - F_1)exp((1 - \lambda_4)\zeta_L)}{(1 - \lambda_2)F_1 exp(\lambda_1 \zeta_L) - \lambda_2 F_2 exp(\lambda_2 \zeta_L)}. \quad \text{(A.14)}$$

The equations are solved with a numerical inversion algorithm (Hollenbeck, 1998).

Bibliography

R. Ababou, D. McLaughlin, L.W. Gelhar, and A.F.B. Tompson. Numerical simulation of three-dimensional saturated flow in randomly heterogeneous porous media. *Transport in Porous Media*, 4:549–565, 1989.

S.E. Allaire, S. Roulier, and A.J. Cessna. Quantifying preferential flow in soils: A review of different techniques. *Journal of Hydrology*, 378(1-2):179–204, 2009.

S. Attinger, M. Dentz, H. Kinzelbach, and W. Kinzelbach. Temporal behaviour of a solute cloud in a chemically heterogeneous porous medium. *Journal of Fluid Mechanics*, 386: 77–104, 1999.

D.A. Barry and J.C. Parker. Approximations for solute transport through porous media with flow transverse to layering. *Transport in Porous Media*, 2(1):65–82, 1987.

D.A. Barry, H. Prommer, C.T. Miller, P. Engesgaard, A. Brun, and C. Zheng. Modelling the fate of oxidisable organic contaminants in groundwater. *Advances in Water Resources*, 25(8-12):945–983, 2002.

D.S. Bausmith and R.D. Neufeld. Soil biodegradation of propylene glycol based aircraft deicing fluids. *Water Environment Research*, 71(4):459–464, 1999.

J. Bear. *Dynamics of fluid in porous media*. American Elsevier, New York, 1972.

W.H.J. Beltman, J.J.T.I. Boesten, and S.E.A.T.M. van der Zee. Spatial moment analysis of transport of nonlinearly adsorbing pesticides using analytical approximations. *Water Resources Research*, 44(5):W05417, 2008.

C.M. Bethke, R.A. Sanford, M.F. Kirk, Q. Jin, and T.M. Flynn. The thermodynamic ladder in geomicrobiology. *American Journal of Science*, 311(3):183–210, 2011.

S. Beulke, C.D. Brown, C.J. Fryer, and A. Walker. Lysimeter study to investigate the effect of rainfall patterns on leaching of isoproturon. *Pest Management Science*, 58(1): 45–53, 2002.

K.J. Beven, D. Henderson, and A.D. Reeves. Dispersion parameters for undisturbed partially saturated soil. *Journal of Hydrology*, 143(1-2):19–43, 1993.

A.R. Bielefeldt, T. Illangasekare, M. Uttecht, and R. LaPlante. Biodegradation of propylene glycol and associated hydrodynamic effects in sand. *Water Research*, 36(7):1707–1714, 2002.

S. Blagodatsky and P. Smith. Soil physics meets soil biology: Towards better mechanistic prediction of greenhouse gas emissions from soil. *Soil Biology and Biochemistry*, 47: 78–92, 2011.

E. Bloem, J. Vanderborght, and G.H. De Rooij. Leaching surfaces to characterize transport in a heterogeneous aquifer: Comparison between flux concentrations, resident concentrations, and flux concentrations estimated from temporal moment analysis. *Water Resources Research*, 44(10):W10412, 2008.

E. Bloem, F.A.N. Hogervorst, and G.H. De Rooij. A field experiment with variable-suction multi-compartment samplers to measure the spatio-temporal distribution of solute leaching in an agricultural soil. *Journal of Contaminant Hydrology*, 105(3-4): 131–145, 2009.

E. Bloem, F.A.N. Hogervorst, G.H. De Rooij, and F. Stagnitti. Variable-suction multi-compartment samplers to measure spatiotemporal unsaturated water and solute fluxes. *Vadose Zone Journal*, 9(1):148, 2010.

E. Blume, M. Bischoff, J.M. Reichert, T. Moorman, A. Konopka, and R.F. Turco. Surface and subsurface microbial biomass, community structure and metabolic activity as a function of soil depth and season. *Applied Soil Ecology*, 20(3):171–181, 2002.

J.J.T.I Boesten and A.M.A. Van der Linden. Modeling the influence of sorption and transformation on pesticide leaching and persistence. *Journal of Environmental Quality*, 20 (2):425, 1991.

J. Boll, J.S. Selker, G. Shalit, and T.S. Steenhuis. Frequency distribution of water and solute transport properties derived from pan sampler data. *Water Resources Research*, 33(12):2655–2664, 1997.

J.S. Brauner and M.A. Widdowson. Sequential electron acceptor model for evaluation of in situ bioremediation of petroleum hydrocarbon contaminants in groundwater. *Annals of the New York Academy of Sciences*, 829(1):263–279, 1997.

E. Bresler and G. Dagan. Convective and pore scale dispersive solute transport in unsaturated heterogeneous fields. *Water Resources Research*, 17(6):1683–1693, 1981.

A. Brun and P. Engesgaard. Modelling of transport and biogeochemical processes in pollution plumes: literature review and model development. *Journal of Hydrology*, 256(3-4):211–227, 2002.

B. Buchter, C. Hinz, M. Flury, and H. Flühler. Heterogeneous flow and solute transport in an unsaturated stony soil monolith. *Soil Science Society of America Journal*, 59(1): 14–21, 1995.

D.T. Burr, E.A. Sudicky, and R.L. Naff. Nonreactive and reactive solute transport in three-dimensional heterogeneous porous media: Mean displacement, plume spreading, and uncertainty. *Water Resources Research*, 30(3):791–815, 1994.

R.F. Carsel and R.S. Parrish. Developing joint probability distributions of soil water retention characteristics. *Water Resources Research*, 24(5):755–769, 1988.

J.P. Carter, Y.H. Hsaio, S. Spiro, and D.J. Richardson. Soil and sediment bacteria capable of aerobic nitrate respiration. *Applied and Environmental Microbiology*, 61(8):2852–2858, 1995.

C. Chenu and G. Stotzky. Interactions between microooganisms and soil particles: an overview. In P.M. Huang, J.M. Bollag, and N. Senesi, editors, *Interactions between soil particles and microorganisms*, page 19. Wiley, Chichester, 2002.

C.V. Chrysikopoulos, P.K. Kitanidis, and P.V. Roberts. Analysis of one-dimensional solute transport through porous media with spatially variable retardation factor. *Water Resources Research*, 26(3):437–446, 1990.

Council of the European Communities. Directive of the Council of 15 July 1980 relating to the quality of water intended for human consumption. *European Journal of Communication*, L229(Aug 30):11–29, 1980.

J.A. Cunningham, H. Rahme, G.D. Hopkins, C. Lebron, and M. Reinhard. Enhanced in situ bioremediation of BTEX-contaminated groundwater by combined injection of nitrate and sulfate. *Environmental Science & technology*, 35(8):1663–1670, 2001.

G. Dagan and E. Bresler. Solute dispersion in unsaturated heterogeneous soil at field scale: I. theory. *Soil Science Society of America Journal*, 43(3):461–467, 1979.

B.S. Das and G.J. Kluitenberg. Moment analysis to estimate degradation rate constants from leaching experiments. *Soil Science Society of America Journal*, 60(6):1724–1731, 1996.

F. Dassonville and P. Renault. Interactions between microbial processes and geochemical transformations under anaerobic conditions: a review. *Agronomie*, 22:51–68, 2002.

G.H. De Rooij and F. Stagnitti. Spatial and temporal distribution of solute leaching in heterogeneous soils: analysis and application to multisampler lysimeter data. *Journal of Contaminant Hydrology*, 54(3-4):329–346, 2002.

115

F. Delay, G. Porel, and G. de Marsily. Predicting solute transport in heterogeneous media from results obtained in homogeneous ones: an experimental approach. *Journal of Contaminant Hydrology*, 25(1-2):63–84, 1997.

M.W. Denny. *Air and water: the biology and physics of life's media*. Princeton University Press, 1995.

M. Dentz and A. Castro. Effective transport dynamics in porous media with heterogeneous retardation properties. *Geophysical Research Letters*, 36(3):L03403, 2009.

G. Destouni. Applicability of the steady state flow assumption for solute advection in field soils. *Water Resources Research*, 27(8):2129–2140, 1991.

G. Destouni and V. Cvetkovic. Field scale mass arrival of sorptive solute into the groundwater. *Water Resources Research*, 27(6):1315–1325, 1991.

G. Destouni and W. Graham. Solute transport through an integrated heterogeneous soil-groundwater system. *Water Resources Research*, 31(8):1935–1944, 1995.

R. Don Wauchope, S. Yeh, and J.B.H.J. Linders. Pesticide soil sorption parameters: theory, measurement, uses, limitations and reliability. *Pest Management Science*, 58:419–445, 2002.

W. Durner, U. Jansen, and S.C. Iden. Effective hydraulic properties of layered soils at the lysimeter scale determined by inverse modelling. *European Journal of Soil Science*, 59(1):114–124, 2008.

D. Fernàndez-Garcia, T.H. Illangasekare, and H. Rajaram. Differences in the scale dependence of dispersivity and retardation factors estimated from forced-gradient and uniform flow tracer tests in three-dimensional physically and chemically heterogeneous porous media. *Water Resources Research*, 41(3):W03012, 2005.

J. Feyen, D. Jacques, A. Timmerman, and J. Vanderborght. Modelling water flow and solute transport in heterogeneous soils: A review of recent approaches. *Journal of Agricultural Engineering Research*, 70(3):231–256, 1998.

M. Flury. Experimental evidence of transport of pesticides through field soils: a review. *Journal of Environmental Quality*, 25(1):25–45, 1996.

FOCUS. Forum for the co-ordination of pesticide fate models and their use, 2006. *http://focus.jrc.ec.europa.eu/*.

H. French, B. Swensen, J.O. Englund, K.F. Meyer, and S.E.A.T.M. Van der Zee. A lysimeter trench for reactive pollutant transport studies. In J. Soveri and T. Suokko, editors, *Future groundwater resources at risk. IAHS Publications*, volume 222, pages 131–138. Wallingford, Oxfordshire: IAHS, 1994.

H.K. French and S.E.A.T.M. Van der Zee. Field observations of small scale spatial variability of snowmelt drainage and infiltration. *Nordic Hydrology*, 30(3):161–176, 1999.

116

H.K. French, S.E.A.T.M. Van der Zee, and A. Leijnse. Transport and degradation of propyleneglycol and potassium acetate in the unsaturated zone. *Journal of Contaminant Hydrology*, 49(1-2):23–48, 2001.

C. Gallo. *Coupled biodegradation and two-phase flow, a numerical study of interactions and field applications*. PhD thesis, Utrecht Univeristy, 2003.

R.S. Govindaraju and B.S. Das. *Moment analysis for subsurface hydrologic applications*, pages 110, 145. Springer, 2007.

P.M. Groffman, K. Butterbach-Bahl, R.W. Fulweiler, A.J. Gold, J.L. Morse, E.K. Stander, C. Tague, C. Tonitto, and P. Vidon. Challenges to incorporating spatially and temporally explicit phenomena (hotspots and hot moments) in denitrification models. *Biogeochemistry*, 93:49–77, 2009.

L. Guo, R.J. Wagenet, J.L. Hutson, and C.W. Boast. Nonequilibrium transport of reactive solutes through layered soil profiles with depth-dependent adsorption. *Environmental Science & Technology*, 31(8):2331–2338, 1997.

K. Hammel, J. Gross, G. Wessolek, and K. Roth. Two-dimensional simulation of bromide transport in a heterogeneous field soil with transient unsaturated flow. *European Journal of Soil Science*, 50(4):633–647, 1999.

P.J. Hanson, N.T. Edwards, C.T. Garten, and J.A. Andrews. Separating root and soil microbial contributions to soil respiration: a review of methods and observations. *Biogeochemistry*, 48(1):115–146, 2000.

P.A. Holden and N. Fierer. Microbial processes in the vadose zone. *Vadose Zone Journal*, 4(1):1–21, 2005.

P.A. Holden and M.K. Firestone. Soil microorganisms in soil cleanup: how can we improve our understanding. *Journal of Environmental Quality*, 26(1):32–40, 1997.

M. Holder, K.W. Brown, J.C. Thomas, D. Zabcik, and H.E. Murray. Capillary-wick unsaturated zone soil pore water sampler. *Soil Science Society of America Journal*, 55 (5):1195–1202, 1991.

K.J. Hollenbeck. INVLAP.M: A matlab function for numerical inversion of Laplace transforms by the de Hoog algorithm. *http://www.isva.dtu.dk/staff/karl/invlap.htm*, 1998.

K.S. Hunter, Y. Wang, and P. Van Cappellen. Kinetic modeling of microbially-driven redox chemistry of subsurface environments: coupling transport, microbial metabolism and geochemistry. *Journal of Hydrology*, 209(1):53–80, 1998.

P. Jaesche, K.U. Totsche, and I. Kogel-Knabner. Transport and anaerobic biodegradation of propylene glycol in gravel-rich soil materials. *Journal of Contaminant Hydrology*, 85(3-4):271–286, 2006.

N.J. Jarvis. A review of non-equilibrium water flow and solute transport in soil macropores: principles, controlling factors and consequences for water quality. *European Journal of Soil Science*, 58(3):523–546, 2007.

Y. Jia, L. Molstad, A. Frostegard, P. Aagaard, G.D. Breedveld, and L.R. Bakken. Kinetics of microbial growth and degradation of organic substrates in subsoil as affected by an inhibitor, benzotriazole: Model based analyses of experimental results. *Soil Biology and Biochemistry*, 39(7):1597–1608, 2007.

Y. Jin and W.A. Jury. Characterizing the dependence of gas diffusion coefficient on soil properties. *Soil Science Society of America Journal*, 60(1):66–71, 1996.

W.A. Jury and J. Gruber. A stochastic analysis of the influence of soil and climatic variability on the estimate of pesticide groundwater pollution potential. *Water Resources Research*, 25(12):2465–2474, 1989.

W.A. Jury, D.D. Focht, and W.J. Farmer. Evaluation of Pesticide Groundwater Pollution Potential from Standard Indices of Soil-Chemical Adsorption and Biodegradation. *Journal of Environmental Quality*, 16(4):422–428, 1987.

R. Kasteel, T. Pütz, and H. Vereecken. An experimental and numerical study on flow and transport in a field soil using zero-tension lysimeters and suction plates. *European Journal of Soil Science*, 58(3):632–645, 2007.

R. Kasteel, T. Putz, J. Vanderborght, and H. Vereecken. Solute spreading under transient conditions in a field soil. *Vadose Zone Journal*, 8(3):690–702, 2009.

K. Kawamoto, P. Moldrup, P. Schjonning, B.V. Iversen, D.E. Rolston, and T. Komatsu. Gas transport parameters in the vadose zone: Gas diffusivity in field and lysimeter soil profiles. *Vadose Zone Journal*, 5(4):1194–1204, 2006.

E.H. Keating and J.M. Bahr. Reactive transport modeling of redox geochemistry: approaches to chemical disequilibrium and reaction rate estimation at a site in northern wisconsin. *Water Resources Research*, 34(12):3573–3584, 1998.

D.L. Kelting, J.A. Burger, and G.S. Edwards. Estimating root respiration, microbial respiration in the rhizosphere, and root-free soil respiration in forest soils. *Soil Biology and Biochemistry*, 30(7):961–968, 1998.

Kilfrost. Kilfrost df plus (88) material safety data sheet, 2012. *http://www.kilfrost.com/documents/DF88-MSDS.pdf*. Consulted February 24.

J.S. Kindred and M.A. Celia. Contaminant transport and biodegradation: 2. conceptual model and test simulations. *Water Resources Research*, 25(6):1149–1159, 1989.

G.M. Klecka, C.L. Carpenter, and B.D. Landenberger. Biodegradation of aircraft deicing fluids in soil at low temperatures. *Ecotoxicology and Environmental Safety*, 25(3):280–295, 1993.

A. Kreft and A. Zuber. On the physical meaning of the dispersion equation and its solutions for different initial and boundary conditions. *Chemical Engineering Science*, 33 (11):1471–1480, 1978.

A.H. Kristensen, A. Thorbjørn, M.P. Jensen, M. Pedersen, and P. Moldrup. Gas-phase diffusivity and tortuosity of structured soils. *Journal of Contaminant Hydrology*, 115 (1):26–33, 2010.

J.G. Kroes, J.G. Wesseling, and J.C. Van Dam. Integrated modelling of the soil-water-atmosphere-plant system using the model swap 2.0, an overview of theory and an application. *Hydrological Processes*, 14:1993–2002, 2000.

D. Kuntz and P. Grathwohl. Comparison of steady-state and transient flow conditions on reactive transport of contaminants in the vadose soil zone. *Journal of Hydrology*, 369 (3-4):225–233, 2009.

G.M. Laudone, G.P. Matthews, N.R.A. Bird, W.R. Whalley, L.M. Cardenas, and A.S. Gregory. A model to predict the effects of soil structure on denitrification and n_2o emission. *Journal of Hydrology*, 409(1):283–290, 2011.

J.G. Leahy and R.R. Colwell. Microbial degradation of hydrocarbons in the environment. *Microbiological Reviews*, 54(3):305–315, 1990.

P.A. Leffelaar. Dynamics of partial anaerobiosis, denitrification, and water in a soil aggregate: simulation. *Soil Science*, 146(6):427–444, 1988.

P.A. Leffelaar. Water movement, oxygen supply and biological processes on the aggregate scale. *Geoderma*, 57(1):143–165, 1993.

P.A. Leffelaar and W.W. Wessel. Denitrification in a homogeneous, closed system: experiment and simulation. *Soil Science*, 146(5):335–349, 1988.

F.J. Leij and J.H. Dane. Solute transport in a two-layer medium investigated with time moments. *Soil Science Society America Journal*, 55:1529–1535, 1991.

F.J. Leij, M.T. van Genuchten, and J.H. Dane. Mathematical analysis of one-dimensional solute transport in a layered soil profile. *Soil Science Society America Journal*, 55(4): 944–953, 1991.

M. Leistra, A.M.A. van der Linden, J.J.T.I. Boesten, A. Tiktak, and F. van der Berg. PEARL model for pesticide behaviour and emissions in soil-plant systems; descriptions of the processes in FOCUS PEARL v. 1.1.1. Technical Report Alterra-rapport 013; RIVM report 711401009, Alterra; RIVM, Wageningen; Bilthoven, 2001.

B. Lennartz, N.J. Jarvis, and F. Stagnitti. Effects of heterogeneous flow on discharge generation and solute transport. *Soil science*, 173(5):306–320, 2008.

119

E. Lewan, J. Kreuger, and N.J. Jarvis. Implications of precipitation patterns and antecedent soil water content for leaching of pesticides from arable land. *Agricultural Water Management*, 96(11):1633–1640, 2009.

H. Lissner, M. Wehrer, E. Bloem, and K.U. Totsche. Soil heterogeneity strongly affects fate and transport of deicing chemicals. *Geophysical Research Abstracts, EGU 2011*, 13:7529–1, 2011a.

H. Lissner, M. Wehrer, and K.U. Totsche. High degradation efficiency of deicing chemicals affects the natural redox system in airfield soils. *Mineralogical Magazine*, 75(3): 1335, 2011b.

H. Lissner, M. Wehrer, M. Jartun, and K.U. Totsche. Degradation of deicing chemicals threats the natural redox system in airfield soils. *Environmental science and pollution research*, submitted, 2013.

P. Marsh. Water flux in melting snow covers. In M. Y. Corapcioglu, editor, *Advances in porous media*, pages 61–124. Elsevier, Amsterdam, 1991.

K.U. Mayer, E.O. Frind, and D.W. Blowes. Multicomponent reactive transport modeling in variably saturated porous media using a generalized formulation for kinetically controlled reactions. *Water Resources Research*, 38(9):1174–1194, 2002.

G.S. McGrath, C. Hinz, and M. Sivapalan. Modeling the effect of rainfall intermittency on the variability of solute persistence at the soil surface. *Water Resources Research*, 44(9):W09432, 2008a.

G.S. McGrath, C. Hinz, and M. Sivaplan. Modelling the impact of within-storm variability of rainfall on the loading of solutes to preferential flow pathways. *European Journal of Soil Science*, 59:24–33, 2008b.

J.C.L. Meeussen. Orchestra: An object-oriented framework for implementing chemical equilibrium models. *Environmental Science & technology*, 37(6):1175–1182, 2003.

S. Meyer-Windel, B. Lennartz, and P. Widmoser. Bromide and herbicide transport under steady-state and transient flow conditions. *European Journal of Soil Science*, 50(1): 23–33, 1999.

E.E. Miller and R.D. Miller. Physical theory for capillary flow phenomena. *Journal of Applied Physics*, 27(4):324–332, 1956.

R.J. Millington and J.P. Quirk. Permeability of porous solids. *Transactions of the Faraday Society*, 57:1200–1207, 1961.

J.M. Oades. The role of biology in the formation, stabilization and degradation of soil structure. *Geoderma*, 56(1-4):377–400, 1993.

A.V. Ogram, R.E. Jessup, L.T. Ou, and P.S. Rao. Effects of sorption on biological degradation rates of (2, 4-dichlorophenoxy) acetic acid in soils. *Applied and Environmental Microbiology*, 49(3):582–587, 1985.

P. Öhrström, Y. Hamed, M. Persson, and R. Berndtsson. Characterizing unsaturated solute transport by simultaneous use of dye and bromide. *Journal of Hydrology*, 289(1-4): 23–35, 2004.

OSL Airport. Osl and the environment, de-icing, 2013. *http://www.osl.no/en/osl/aboutus/30_Environment/40_Deicing*. Consulted January 6.

J. Øvstedal and B. Wejden. Dispersion of de-icing chemicals to the areas along the runways at oslo airport gardermoen. In *SAE Aircraft and Engine Icing International Conference, Seville, Spain*, 2007.

M. Persson and R. Berndtsson. Water application frequency effects on steady-state solute transport parameters. *Journal of Hydrology*, 225(3):140–154, 1999.

M. Persson, S. Haridy, J. Olsson, and J. Wendt. Solute transport dynamics by high-resolution dye tracer experiments–image analysis and time moments. *Vadose Zone Journal*, 4(3):856–865, 2005.

A. Pierret, C. Doussan, Y. Capowiez, F. Bastardie, and L. Pagès. Root functional architecture: a framework for modeling the interplay between roots and soil. *Vadose Zone Journal*, 6(2):269–281, 2007.

N.N. Poletika and W.A. Jury. Effects of soil surface management on water flow distribution and solute dispersion. *Soil Science Society of America Journal*, 58(4):999–1006, 1994.

V. Pot, J. Šimunek, P. Benoit, Y. Coquet, A. Yra, and M.J. Martínez-Cordón. Impact of rainfall intensity on the transport of two herbicides in undisturbed grassed filter strip soil cores. *Journal of Contaminant Hydrology*, 81(1-4):63–88, 2005.

V.L. Quisenberry, R.E. Phillips, and J.M. Zeleznik. Spatial distribution of water and chloride macropore flow in a well-structured soil. *Soil Science Society of America Journal*, 58(5):1294–1300, 1994.

H. Rajaram. Time and scale dependent effective retardation factors in heterogeneous aquifers. *Advances in Water Resources*, 20(4):217–230, 1997.

C. Rappoldt. The application of diffusion models to an aggregated soil. *Soil Science*, 150 (3):645–661, 1990.

D.M. Revitt and P. Worrall. Low temperature biodegradation of airport de-icing fluids. *Water Science and Technology*, 48(9):103–111, 2003.

M.L. Rockhold, R.E. Rossi, and R.G. Hills. Application of similar media scaling and conditional simulation for modeling water flow and tritium transport at the las cruces trench site. *Water Resources Research*, 32(3):595–609, 1996.

M. Rossi, O. Ippisch, and H. Flühler. Solute dilution under imbibition and drainage conditions in a heterogeneous structure: Modeling of a sand tank experiment. *Advances in Water Resources*, 31(9):1242–1252, 2008.

K. Roth. Steady state flow in an unsaturated, two-dimensional, macroscopically homogeneous, Miller-similar medium. *Water Resources Research*, 31(9):2127–2140, 1995.

K. Roth and K. Hammel. Transport of conservative chemical through an unsaturated two-dimensional miller-similar medium with steady state flow. *Water Resources Research*, 32(6):1653–1663, 1996.

D. Russo and A. Fiori. Stochastic analysis of transport in a combined heterogeneous vadose zone–groundwater flow system. *Water Resources Research*, 45 (doi:10.1029/2008WR007157), 2009.

D. Russo, J. Zaidel, and A. Laufer. Numerical analysis of flow and transport in a three-dimensional partially saturated heterogeneous soil. *Water Resources Research*, 34(6): 1451–1468, 1998.

D. Schotanus, M.J. van der Ploeg, and S.E.A.T.M. van der Zee. Quantifying heterogeneous transport of a tracer and a degradable contaminant in the field, with snowmelt and irrigation. *Hydrology and Earth System Sciences*, 16:2871–2882, 2012.

P. Seuntjens, D. Mallants, N. Toride, C. Cornelis, and P. Geuzens. Grid lysimeter study of steady state chloride transport in two spodosol types using tdr and wick samplers. *Journal of Contaminant Hydrology*, 51:13–39, 2001.

D.P. Shupack and T.A. Anderson. Mineralization of propylene glycol in root zone soil. *Water, Air, & Soil Pollution*, 118(1):53–64, 2000.

J. Šimunek and M. Sejna. *The HYDRUS-2D software package for simulating the two-dimensional movement of water, heat, and multiple solutes in variably-saturated media*. US Salinity Laboratory, Agricultural Research Service, US Dept. of Agriculture, 1999.

J. Šimunek, N.J. Jarvis, M.T. Van Genuchten, and A. Gärdenäs. Review and comparison of models for describing non-equilibrium and preferential flow and transport in the vadose zone. *Journal of Hydrology*, 272(1):14–35, 2003.

G. Stotzky. Soil as an environment for microbial life. In J.D. Van Elsas, J.T. Trevors, and E.M.H. Wellington, editors, *Modern soil microbiology*, page 4. Marcel Dekker, 1997.

J.S. Strock, D.K. Cassel, and M.L. Gumpertz. Spatial variability of water and bromide transport through variably saturated soil blocks. *Soil Science Society of America Journal*, 65(6):1607–1617, 2001.

W. Stumm and J.J. Morgan. *Aquatic chemistry, chemical equilibria and rates in natural waters*. Wiley, New York, 1996.

N. Toride, F.J. Leij, and M.T. Van Genuchten. The CXTFIT code for estimating transport parameters from laboratory or field tracer experiments. version 2.0. *U. S. Salinity Laboratory, USDA, ARS, Riverside, CA*, 137:121, 1995.

A.J. Valocchi. Spatial moment analysis of the transport of kinetically adsorbing solutes through stratified aquifers. *Water Resources Research*, 25(2):273–279, 1989.

W. Van Beinum, J.C.L. Meeussen, A.C. Edwards, and W.H. Van Riemsdijk. Transport of ions in physically heterogeneous systems; convection and diffusion in a column filled with alginate gel beads, predicted by a two-region model. *Water Research*, 34(7):2043–2050, 2000.

J.C. Van Dam. *Field-scale water flow and solute transport: SWAP model concepts, parameter estimation and case studies*. PhD thesis, Wageningen Univeristy, 2000.

J.C. Van Dam, J.M.H. Hendrickx, H.C. Van Ommen, M.H. Bannink, M.T. Van Genuchten, and L.W. Dekker. Water and solute movement in a coarse-textured water-repellent field soil. *Journal of Hydrology*, 120(1):359–379, 1990.

J.C. Van Dam, J. Huygen, J.G. Wesseling, R.A. Feddes, P. Kabat, P.E.V. Walsum, P. Groenendijk, and C.A. Diepen. SWAP version 2.0, theory; simulation of water flow, solute transport and plant growth in the soil-water-atmosphere-plant environment. Technical Report Technical document 45, report 71, Winand Staring Centre, Wageningen, 1997.

M.T. Van Genuchten. A closed-form equation for predicting the hydraulic conductivity of unsaturated soils. *Soil Science Society of America Journal*, 44(5):892–898, 1980.

J. Vanderborght and H. Vereecken. Review of dispersivities for transport modeling in soils. *Vadose Zone Journal*, 6(1):29–52, 2007.

J. Vanderborght, R. Kasteel, and H. Vereecken. Stochastic continuum transport equations for field-scale solute transport overview of theoretical and experimental results. *Vadose Zone Journal*, 5(1):184–203, 2006.

R.H. Veeh, W.P. Inskeep, and A.K. Camper. Soil depth and temperature effects on microbial degradation of 2, 4-d. *Journal of Environmental Quality*, 25(1):5–12, 1996.

E.J.M. Veling. ZEROCD and PROFCD, Description of two programs to supply quick information with respect to the penetration of tracers into the soil, Technical Report nr. 725206009, R.I.V.M., National Institute of Public Health and Environmental Protection, Bilthoven, The Netherlands. *http://www.hydrology.citg.tudelft.nl/veling/zerocd-profcd-doc-new.pdf*, 725206009, 1993.

S. Veltman, T. Schoenberg, and M.S. Switzenbaum. Alcohol and acid formation during the anaerobic decomposition of propylene glycol under methanogenic conditions. *Biodegradation*, 9(2):113–118, 1998.

H. Vereecken, R. Kasteel, J. Vanderborght, and T Harter. Upscaling hydraulic properties and soil water flow processes in heterogeneous soils, a review. *Vadose Zone Journal*, 6(1):1–28, 2007.

P.A. Waldner, M. Schneebeli, U. Schultze-Zimmermann, and H. Flühler. Effect of snow structure on water flow and solute transport. *Hydrological Processes*, 18(7):1271–1290, 2004.

A.W. Warrick, G.J. Mullen, and D.R. Nielsen. Scaling field-measured soil hydraulic properties using a similar media concept. *Water Resources Research*, 13(2):355–362, 1977.

L. Weihermüller, J. Siemens, M. Deurer, S. Knoblauch, H. Rupp, A. Göttlein, , and T. Pütz. In situ soil water extraction: A review. *Journal of Environmental Quality*, 36(6):1735–1748, 2007.

M.A. Widdowson, F.J. Molz, and L.D. Benefield. A numerical transport model for oxygen-and nitrate-based respiration linked to substrate and nutrient availability in porous media. *Water Resources Research*, 24(9):1553–1565, 1988.

P.J. Wierenga. Solute distribution profiles computed with steady-state and transient water movement models. *Soil Science Society of America Journal*, 41(6):1050–1055, 1977.

A.G. Williams, J.F. Dowd, D. Scholefield, N.M. Holden, and L.K. Deeks. Preferential flow variability in a well-structured soil. *Soil Science Society of America Journal*, 67 (4):1272–1281, 2003.

Curriculum vitae

Dieuwke Schotanus, 1 april 1984, Leeuwarden

9-1996	–	6-2002	Christelijk gymnasium Beyers Naudé, Leeuwarden
9-2002	–	8-2005	BSc Bodem, water, atmosfeer, Wageningen Universiteit
9-2005	–	1-2008	MSc Hydrology and water quality, Wageningen Universiteit
9-2006	–	3-2007	Stage, Stockholm University, Zweden
6-2008	–	11-2012	Promotieonderzoek bij de leerstoelgroep Bodemnatuurkunde, Ecohydrologie en Grondwaterbeheer

Netherlands Research School for the
Socio-Economic and Natural Sciences of the Environment

C E R T I F I C A T E

The Netherlands Research School for the
Socio-Economic and Natural Sciences of the Environment
(SENSE), declares that

Dieuwke Schotanus

born on 1 April 1984 in Leeuwarden, The Netherlands

has successfully fulfilled all requirements of the
Educational Programme of SENSE.

Wageningen, 16 September 2013

the Chairman of the SENSE board

Prof. dr. Rik Leemans

the SENSE Director of Education

Dr. Ad van Dommelen

The SENSE Research School has been accredited by the Royal Netherlands Academy of Arts and Sciences (KNAW)

K O N I N K L I J K E   N E D E R L A N D S E
A K A D E M I E   V A N   W E T E N S C H A P P E N

The SENSE Research School declares that **Ms. Dieuwke Schotanus** has successfully fulfilled all requirements of the Educational PhD Programme of SENSE with a work load of 48 ECTS, including the following activities:

SENSE PhD Courses
o Environmental Research in Context
o Research Context Activity: Communicating research to Stichting Retourschip Board and presenting 4 explanatory lessons on soil pollution to high school class
o Uncertainty modelling and analysis

Other PhD Courses
o Eawag Summer School on Environmental Systems Analysis
o PhD Competence Assessment
o Project- and Time Management
o Techniques for Writing and Presenting Scientific Papers
o Career orientation

Management and Didactic Skills Training
o Organizing a workshop on *Ecohydrology* at Wageningen University
o Co-convenor of two conference sessions of the European Geosciences Union (EGU) in 2011 and 2012
o Practical supervision of the BSc courses *Bodem en Water 1 & 2*, *Voortzetting Water*, *Geohydrology*, and *Introductie Omgevingswetenschappen*
o Lecturing for the course *Physical Aspects of Land Management*
o Supervision of one BSc thesis

Oral Presentations
o *Solute transport in a layered soil with adsorption and degradation: an analytical model.* WIMEK-SENSE symposium, 22 February 2011, Wageningen
o *Measurement of contaminant fluxes in the soil during snowmelt at high spatial resolution.* EGU, 3-8 April 2011, Vienna, Austria
o *Modelling transport and degradation of de-icing chemical in soil.* Boussinesq PhD meeting, 20 October 2011, Amsterdam

SENSE Coordinator PhD Education

Drs. Serge Stalpers